PREVENTION OF MICROBIAL AND BIOFOULING ATTACHMENTS IN FOOD PROCESSING APPLICATIONS USING NANOENGINEERED SURFACES

A DISSERTATION SUBMITTED TO THE GRADUATE DIVISION OF THE UNIVERSITY OF HAWAIʻI AT MĀNOA IN PARTIAL FULFILLMENT OF THE REQUIREMENTS FOR THE DEGREE OF

DOCTOR OF PHILOSOPHY
IN
MOLECULAR BIOSCIENCES AND BIOENGINEERING

DECEMBER 2014

By
Natthakan Rungraeng

Thesis Committee:

Soojin Jun, Chairperson
Wei-Wen Winston Su
Tao Yan
Eunsung Kan
Yong Li

© 2014, Natthakan Rungraeng

ACKNOWLEDGEMENTS

This dissertation would not have been possible without help, support and encouragement from my parents, friends, academic advisor, committee members, staff and people around me. I wish to take this opportunity to convey my appreciation to all of them.

I would like to express my gratitude to my academic advisor, Dr. Soojin Jun, for his great guidance, patience and mentorship before and after I started my Ph.D. program. I would like to thank Dr. Yong Li who kindly provided bacterial strains and allowed me to use his lab space and equipment for microbial cultivation and analysis. I would like to extend my deepest appreciation to the rest of my committee members, Dr. Wei-Wen Winston Su, Dr. Tao Yan, and Dr. Eunsung Kan, for their kind words of suggestions and recommendations to the objectives, experimental design as well as the results of this study. I would also like to thank Dr. Chang-Hwan Choi and Mr. Ferdi Hizal at the Stevens Institute of Technology for spending their valuable time for research discussion and cooperation.

In addition, I am also pleased to thank Dr. Il Kyu Cho for the analysis of nanotubes samples, Dr. Marilyn Dunlap and Ms. Tina Carvalho for the use of Biological Electron Microscope Lab. I would like to give special recognition to the staff of the University of Hawai‘i Molecular Biosciences and Bioengineering and Human Nutrition Food and Animal Sciences departments and Mae Fah Luang University for their friendly assistance. Many sincere thanks go out to my previous and current labmates at the Food Engineering Lab for their advice and friendship. I would like to acknowledge the financial support from the USDA TSTAR program (2009-34135-20069) and the Korea Food Research Institute (KFRI).

Last but not least, I greatly acknowledge the support from the Royal Thai Government Scholarship and all Thai people for giving me a remarkable chance of my life to pursue Ph.D. in the United States. Thank you to all of the officers at the Office of Educational Affairs, Royal Thai Embassy in Washington D.C, especially Ms. Somthavil Thongprasert, for their kind help and support since I entered to the Ph.D. program in January of 2010.

ABSTRACT

Due to ever increasing trends in food safety, food manufacturers should take sanitary/ hygienic processes into key consideration. Typically, a routine cleaning-in-place (CIP) procedure is employed to sanitize food contact surfaces in enclosed food processors including plate heat exchangers. Water spraying and disinfectants are, in general, used to sanitize the outer surfaces of food preparation equipment and utensils such as conveyor, knife, and cutting board. The CIP process requires a tremendous amounts of electrical energy, water, and chemicals in use. The economic penalties associated with the CIP also include inevitable production losses caused by frequent process downtimes. It has been estimated that a dairy factory is required to spend 13% of its total energy usage for CIP processes. If not handled properly, most of the chemical disinfectants also cause negative effects to workers and food contact surfaces due to severe corrosion and irritation. Therefore, a series of nanoengineered food contact surfaces including nanoparticulate composite coatings were developed to overcome the intensive uses of water and chemicals in food processing environments by inhibiting the biofouling formulation. The overall goal of this research was to minimize the attachment of biofouling, including milk protein, bacterial cells, biofilms, and liquid food debris, onto a metal substratum using novel surface fabrication techniques based on the nanoscale surface characteristics and anti-fouling mechanism. Three innovative nanoengineered surfaces were designed and fabricated in accordance with a variety of biofoulants found in food processing, such as nanoparticulate composite coatings; an omhiphobic surface; and nanopatterned surfaces using electropolishing and anodization.

The superhydrophobic (SHB) and superhydrophilic (SHL) nanoparticulate composite surfaces were developed and evaluated with milk fouling and bacterial adhesion testing. The fouling occurrence during milk pasteurization was simulated and conducted in a single-channel prototyped plate heat exchanger. The effect of SHB carbon nanotubes (CNTs)-Teflon on the masses of deposited surface foulants was investigated. Water contact angle (WCA) of a stainless steel surface was dramatically increased from 71.2° (uncoated) to 141.1° (CNTs-Teflon coated). After 5 hours of pasteurization, only 30% of milk foulant (18.45 mg/cm^2) was observed on the SHB surface, compared to uncoated steel (62.0 mg/cm^2). For bacterial testing, the SHB (WCA 154.6°) and SHL titanium dioxide (WCA <5°) steel surfaces were exposed to *Escherichia. coli* suspension (3×10^8 CFU/mL) for an hour in both stagnant and dynamic environments. The enumeration of *E. coli* adhering to uncoated, SHB, and SHL steel substrates in stagnant and dynamic flow modes showed that the anti-adhesion effect of SHB was most pronounced after the dynamic test where the lotus effect was in place. As compared to the control, only 20% and 55% of adhering cells were remaining on the SHB and SHL surfaces, respectively. On the other hand, the stagnant test showed that anti-adhesion effect of a hydration layer which would act as a barrier between the cells and the fully wetted surface (SHL) was predominant; thus, 75% and 35% of bacterial cells were found on the SHB and SHL surfaces, respectively. It was, therefore, noted that the anti-adhesion attributes of SHB and SHL surfaces significantly depended on the wall shear rate of liquid medium, and none of these surfaces worked perfectly in both stagnant and flow environments. The lotus effect of the SHB surface seems to require a certain amount of liquid flow to initiate its surface sweeping action. The hydration layer on the SHL might perform best in a stagnant mode and gradually loses its anti-fouling potential as the flow begins.

A new omniphobic (slippery liquid infused porous surface or SLIPS) was developed to overcome the challenge initiated by the SHB and SHL surfaces. The SLIPS fabricated by infusing a low-surface tension liquid (20 mN/m) into the highly porous SHB carbon nanotubes micro/nanostructures was able to create a strong surface tension force (50 mN/m) between the planktonic bacteria in medium and the infused liquid. Therefore, the test bacterial cells (*E. coli* and *Staphylococcus aureus*) and their excreted polymers could rarely penetrate through the developed interface. As a result, the SLIPS surface achieved one log reduction (90% removal) of *E. coli* and *S. aureus* biofilms after 7 days testing, compared to the control surface at the same condition. In addition, the infused liquid also contributed to enhance slipperiness; thus, the omniphobic SLIPS tilted to 5° to 20° readily repelled droplets of syrup, honey, and ketchup without leaving any noticeable debris.

Lastly, the fabricated nanoengineered surfaces include nanosmooth (NS), nanoporous (NR), and nanopillaed (NL) aluminum oxide (AAO) surfaces and nanoporous stainless steel surfaces. The amounts of *E. coli* and *S. aureus* adhering to pristine AAO surfaces (WCA_{NR} <25°; WCA_{NL} <5°) and Teflon coated AAO surfaces (WCA_{NR}:115°; WCA_{NL}:162°) were also compared in both stagnant and dynamic environments for an hour. The most pronounced anti-adhesion effect was found on Teflon-NL surfaces after dynamic tests due to the sharp peak topography of the NL as well as an increase in the surface hydrophobicity. The overall bacterial enumerations averaged in a triplicate were as follows: *E. coli* [NS (2.2×10^4 CFU/cm^2) > NR (2.0×10^3 CFU/cm^2) > NL (4.0×10^2 CFU/cm^2)]; and *S. aureus* [NS (5.4×10^4 CFU/cm^2) > NR (2.1×10^4 CFU/cm^2) > NL (3.4×10^2 CFU/cm^2)].

L. monocytogenes (1.9×10^8 CFU/mL) was used for bacterial adhesion testing of nanoengineered stainless steel surface, which may be more demanding for hygienic food

processing equipment. The NS stainless steel surface was achieved by electropolishing the steel in a mixture of sulfuric and phosphoric acid. For NR stainless steel fabrication, the bare substrates were anodized in a mixture of perchloric acid and ethylene glycol to create two surfaces with two different in nanopore diameters (50 nm and 80 nm), so-called NP_{50} and NP_{80}, respectively. Thereafter, the NS, NR_{50}, and NR_{80} stainless steels were exposed to the *L. monocytogenes* solution in a stagnant environment for four hours. The enumerated average cell counts were 5×10^{3}, 5.0×10^{1}, and 2.8×10^{1} CFU/cm^2 for NS, NR_{50}, and NR_{80}, respectively. The results suggested that regardless of the substratum materials, nanoporous surface finishes could significantly inhibit the adhesion and attachment of *L. monocytogenes*. However, the statistical analysis indicated that the numbers of cells adhering to the 50 nm and the 80 nm nanoporous surfaces were not significantly different. The finding could be because besides the pore diameter, other surface parameters such as peak heights (or pillared magnitudes) and interpore distances might also play an important role on anti-adhesion of *L. monocytogenes.*

TABLE OF CONTENTS

TABLE OF CONTENTS (CONTINUED)

TABLE OF CONTENTS (CONTINUED)

LIST OF TABLES

LIST OF FIGURES

LIST OF FIGURES (CONTINUED)

LIST OF FIGURES (CONTINUED)

LIST OF FIGURES (CONTINUED)

LIST OF ABBREVIATIONS

Ω	ohm
2D	Two dimensional
3D	Three dimensional
A	Aggregated protein
A	Amp
AAO or Al_2O_3	Anodic aluminum oxide
ACNT	Vertically aligned carbon nanotube
AFM	Atomic force microscope
ANOVA	Analysis of variance
A_s	Un-retarded sphere-substrate Hamaker constant in water
b	Bacterium
C_2H_5OH	Alcohol
CA	Contact angle
CDC	Centers for Disease Control and Prevention
CFD	Computational fluid dynamics
CFU	Colony forming unit
C_i	Protein concentration
CIP	Cleaning-in-place
CNT	Carbon nanotube
COOH	Carboxyl group
CVD	Chemical vapor deposition
C_xH_y	Hydrocarbon precursor
D	Deposited protein
d	Separation distance
DAPI	4,6-diamidino-2-phenylindole
D_c	Inter-pore distance
DLC	Diamond like carbon
DLVO	Derjaguin, Landau, Verwey, Overbeek
DNA	Deoxyribonucleic acid
D_p	Pore diameter
EAcAc	Ethyl acetoacetate
E_i	Activation energy
EPS	Extracellular polymeric substance
f	Fraction of the projected area

LIST OF ABBREVIATIONS (CONTINUED)

F	Force
F'	Faraday's constant
f_{CNT}	Fraction of carbon nanotubes
FESEM	Field emission electron microscope
G^{DLVO}	Net interaction energy
G^{EL}	Electrostatic double layer energy
G^{LW}	Lifshitz van der Waals energy
GPa	Gigapascal
h	Distance between two planar plates
h_0	Height of flow path
$HClO_4$	Perchloric acid
HMDS	Hexamethyldisilazane
HTST	High temperature short time
I	Ionic strength of the electrolyte
I'	Electrical current
IPPP	Infinite parallel plane plates
K	Kelvin
k	Spring constant
k_{0i}	Pre-exponential factor
K_{CNT}	Thermal conductivity of carbon nanotubes
K_ε	Effective thermal conductivity of composite
k_i	Kinteics reaction constant
K_m	Thermal conductivity of matrix
l	Liquid medium
M	Number of scans per line
M'	Molecular weight of anode
MoS_2	Molybdenum disulfide
MWCNT	Multiwalled carbon nanotube
N	Native protein
n	Pore density
N	Number of line
n'	Valence of metal ions
Ni	Nickel
N_{RE}	Reynolds number
OD	Optical density
OH	Hydroxyl group

LIST OF ABBREVIATIONS (CONTINUED)

PBS	Phosphate buffer saline
PCA	Plate count agar
PDMS	Polydimethylsiloxane
PHE	Plate heat exchanger
PTFE	Polytetrafluoroethylene
Q	Volumetric flow rate
R	Gas constant
r	Surface ratio
R_a	Arithmetic mean roughness
r_q	Root mean square roughness
s	Flat substratum
SA	Sliding angle
SiF^+	Silicon monofluoride cation
SiO_2	Silicon dioxide
SLIPS	Slippery liquid infused porous surface
SPM	Scanning probe microscope
SWCNT	Single walled carbon nanotube
t	Time
TAF	Amorphous Teflon
TiO_2	Titanium dioxide
TPa	Terapascal
TSB	Tryptic soy broth
Tx	Absolute temperature
U	Unfolded protein
UHV	Ultra high vacuum
V	Voltage
W	Watt
W	Surface free energy
w_0	Width of flow path
WCA	Water contact angle
W_d	Wall thickness
W_{loss}	Mass of removed metal
WSA	Water sliding angle
x	Cantilever deflection
XDLVO	Extended Derjaguin, Landau, Verwey, Overbeek
α	Porosity

LIST OF ABBREVIATIONS (CONTINUED)

β-Lg	Beta-lactoglobulin
γ	Interfacial tension
$\dot{\gamma}$	Wall shear rate
ε_0	Dielectric permittivity in the vacuum
ε_r	Relative permittivity of water
$\eta\ (x_i, y_i)$	Mean height of all the points on the surface
θ	Young contact angle
θ_C	Cassie apparent contact angle
θ_W	Wenzel apparent contact angle
κ	Inverse Debye screening length
λ	Characteristic decay length of AB interactions in water
λ_c	Inter-pore
λ_p	Pore proportionality constant
Φ	Exponential modifying factor
ψ	Surface potential
ω	Resonant frequency

1. INTRODUCTION

1.1. Motivation and Research Background

1.1.1. Significance of biofouling in food processing environment

The term ‘biofouling’ generally refers to undesirable layers of microorganisms (Flemming & Ridgway, 2009) and their metabolitic products and other organic debris as deposits on solid substatra in contact with liquid media (Kumar and Anand, 1998). According to Criado *et al*. (1994) biofouling has many undesirable effects to food industries such as reduction of heat flow across the plate heat exchangers (PHEs) surface, increased frictional resistance at the surface, extra maintenance, higher labor costs, decreased productivity, and increased the corrosion rate at the surface. Furthermore, the fouling of milk in plate heat exchangers can cause the growth of unwanted microorganisms on the corrugated surfaces of the PHEs. After pasteurization, it is difficult to remove the fouling layer from the surfaces manually. Therefore, many liquid food industries have spent a significant amount of time and money on the removal of milk fouling using a conventional protocol, the cleaning-in-place process. As a result, the dairy industry has spent about 13% of the total production costs to clean the processing equipment. It was found that the effort to eliminate the fouling on PHEs costs U.S. industries about $4.2–10 billion/year (Sandu and Singh, 1991).

In the case of another serious surface fouling scenario, bacterial biofilms, the biofilms usually consist of a community of spoilage and pathogenic organisms on the surface of food processing equipment which can potentially cause cross-contamination of processed foods. The contamination of spoilage to the food leads to shorten product shelf-life and, if foodborne pathogens are present, the consumption of contaminated food may possess a health hazard to consumers. For fresh food and fresh produce industry, since the and vegetables are well known to protect human against a wide range of illnesses; however, when contaminated produce is consumed raw or uncooked, it becomes a vehicle that can transmit pathogens as well as bacterial toxins to human beings (Berger *et al*., 2010). A variety of surfaces in food processing

environments whether wet and dry areas are vulnerable to biofilms development. A biofilm is defined as a bacterial community formed by adhering pathogens, from native microflora in raw materials (Liu *et al*., 2013), for prolonged contact time. It is now recognized that 80% of food outbreaks are related to biofilms (Srey *et al*., 2013). Therefore, inhibition of initial adhesion of biofilm-forming pathogenic cells (*Listeria monocytogenes*, *Staphylococcus aureus*, and *Escherichia coli*) on food contact surface in food processing environment is critically needed to minimize foodborne pathogen outbreaks (Hall-Stoodley *et al*., 2004), particularly in fresh produce production facilities. Recent research investigated that cross-contamination between biofilms and fresh fruits and vegetables may occur during entire production steps; therefore, one of the major challenges in the fields of food science and biosafety of fresh and fresh-cut produce is to effectively prevent the formation of biofilms on the surfaces of food processing equipment and in facilities.

It has been known that nanoscale surface patterning and treatment techniques are capable of enabling precise controls of molecular, physical, and biochemical interactions that govern bacterial adhesion to the solid substratum. This research reports and compares different nanoengineered biofouling resistant surfaces for various biofouling scenarios which commonly happen in food processing environments.

1.1.2. Nanoengineered biofouling resistant surfaces

To ensure the consumer safety, food processors should minimize the attachment of microorganisms to food contact surfaces. Kumar and Anand (1998) reported that biofilms can be removed by various techniques including physical methods such as washing, high pressure sprays, super-high magnetic field, ultrasound treatment and high pulsed electric field. Effective chemical methods include uses of hypochlorites, iodophores, and quaternary ammonium compounds. In practice, to apply these biofilms removal techniques, the processing lines should be suspended. By considering the costs of chemicals and process downtime in the economical aspect, the use of self-cleanable surface achieved by applying functional coating material on the surface food processing equipment can be considered as one of the most feasible options.

1.1.2.1. Superhydrophobic and superhydrophilic surfaces

Fabrication of self-cleaning surfaces is one example of most anticipated alternative ways to effectively retard the adhesion rate of bacteria to a solid surface. Recently, many studies have been conducted towards the reduction of bacterial adhesion using extreme surface wettabilites using superhydrophilic (water contact angle or WCA less than 5°) and superhydrophobic (water contact angle or WCA more than 150°) surface finishes. A superhydrophobic surface is normally achieved by roughening a low surface energy material in micro/nanoscale roughness creating a stable air-water interface which contains a number of underlying air pockets with arbitrary shapes and depths. Superhydrophobic surface has an exceptional self-cleaning attribute, so-called 'lotus effect'. Such superhydrophobic surface has been proven to exhibit an outstanding water repellency attribute. A cluster of carbon nanotubes (CNTs) with substantial surface roughness is well regarded as a superhydrophobic material which has been widely used to provide excellent anti-fouling properties as well as other desirable attributes, i.e. strength, flexibility, and thermal/electrical conductivities. On the other hand, extremely water-attractive nanocomposite superhydrophilic surface coated with titanium dioxide (TiO_2) nanoparticles also possesses another anti-fouling performance employing its great superhydrophilicity such that tightly water stretching reactions are able to form a stable bacteria-repelling hydration layer locating near the metal substrate which works great a bacterial barrier in stagnant environment.

1.1.2.2. Slippery liquid infused porous surface or SLIPS

Generally, the slippery liquid infused surfaces are inspired by *Nepenthes* plant that has microscale structures around its surface. The surface features are employed to lock-in a natural lubricating liquid that acts as the repellent surface. Therefore, when the surface tension of the infusing liquid is low enough, the slippery surface is capable of repelling various simple and complex liquids including water, oil, blood, and ice (Boinovich *et al*., 2013) with low hysteresis (Ma *et al*., 2013). Even though the SLIPS and superhydrophobic surfaces share the same porous structure. The principle of the SLIPS is quite different from that of the superhydrophobic surface.

This is due to the fact that the microscale air gaps presenting in SLIPS are filled with a low-surface energy lubricant; thus, creating a stable inert slippery interface.

The SLIPSs are commonly designed based on three main criteria including (i) the lubricating liquid should be able to wick into, wet and stably adhere to the nanostructure, (ii) the solid porous structure must be only wetted by the lubricating liquid not by the liquids that need to be repelled and (iii) the lubricant and test liquid (sliding liquid) should be immiscible. The first requirement is possibly achieved using nanopatterned surface (Anand *et al.*, 2012). In this study a highly porous MWCNTs-PTFE structure which can stably accommodate lubricating liquid inside its microscale features were used as a host-matrix for holding a liquid lubricant. The second and third requirements are satisfied by using a viscous yet low surface energy lubricant provided by Dupont under a commercial name 'Krytox'.

1.1.2.3. Nanopatterned surfaces using surface anodization

In the case of bacterial attachment, it has been known that bacterial adhesion is highly influenced by the substratum topography, i.e. roughness and porosity. Literature data (Mitik-Dineva *et al.*, 2008; Flint *et al.*, 2000; Scheuerman *et al.*, 1998) showed that cells have preferential orientation during the attachment, being more likely to attach onto surface with the arithmetic mean roughness value (R_a) of more than 0.8 μm. Because the cells are able to reside within the rough features, where they are protected from external effects such as shear force, the surface with higher irregularities are harder to clean.

In addition, a rougher surface also provides the increased surface area for bacterial attachment (Verran *et al.*, 2001). However, another study from Woodling and Moraru (2005) reported that controlling of surface roughness alone is not enough for minimizing microbial attachment because the flat metal surface prepared by electropolishing treatment (i.e., nanosmooth stainless steel) was also attractive to bacterial cells. This is due to the fact that bacterial cells tend to align themselves in various ways to maximize contact area between their surfaces and the substratum during the attachment process. Hsu *et al.* (2013) fabricated and

compared the amounts of bacterial cells (*E. coli* and *Pseudomonas fluorescens*) attached to various alumina substrata including nanosmooth and nanoporous surfaces (20 and 200 nm in pore diameters). For most time points, *E. coli* ATCC 25922 adhesion results showed more attachment of the bacterial cells on the nanosmooth (control surface) than on the 20 nm and 200 nm pore size membranes; these differences were most pronounced at 96 h, the time point at which a mature biofilm was formed.

2. RATIONALE AND OBJECTIVES

The overall goal of this dissertation was to fabricate and test the developed nanoengineered surfaces for minimizing biofouling attachments including milk protein adsorption and adherences of microorganisms and their biofilms to stainless steel substratum. Specific research objectives addressed in this project are as follows:

Objective 1. Develop and Optimize Superhydrophobic Carbon Nanotubes-Polytetrafluoroethylene Nanocomposite Coating for Milk Fouling Reduction in Plate Heat Exchanger.

Rationale: Whey protein, beta-Lactoglobulin (β-Lg) denatures during the heat treatment of milk including pasteurization plays a major role in the formation of surface foulant (de Jong 1997; Visser 1997; Visser and Jeurnink 1997). When influenced by high-processing temperature, whey protein chains (native) unfold, resulting in a formation of protein aggregation and deposit attached to the surface of plate heat exchangers (PHEs). Also, the material properties like roughness, wettability and charge density of the PHE surfaces play critical roles in determining the fouling rate and protein adsorption of skim milk. Most of all, it is known that hydrophobic surface coating materials reduce the interfacial energy between PHE surfaces and milk deposits, which could minimize the fouling rate effectively (Santos *et al*. 2004). Surface treatments for PHEs could be divided into two classes, i.e., hydrophobic and hydrophilic, based on the water contact angles (WCAs) (Klein *et al.* 2003; Chiang and Lu 2011). Superhydrophobic coating materials that have the WCAs of 150° or above are still far from being applied to PHEs which is generally exposed to harsh operation conditions such as high temperature and long operation time (Lau *et al*. 2003; Huang *et al*. 2005; Li *et al*. 2010; Luo *et al*. 2010; Men *et al*. 2010). Therefore, in the recent past, various types of surfaces suitable for food grade have been tested for minimizing milk fouling (Santos *et al*. 2004; Rosmaninho and Melo, 2006; Rosmaninho *et al*. 2007; Balasubramanian and Puri 2009a, 2009b;).

A superhydrophobic surface such as multiwalled carbon nananotubes (MWCNTs)-Teflon (PTFE) nanocomposite coated stainless steel would potentially reduce the risk of under-processed milk and decrease the frequency of the routine cleaning-in-place (CIP) program. The PHE unit requires the surface nature of high durability because of its harsh operating environment associated with high temperature and pressure. A long operation period with minimal downtime of CIP processes is preferred from industrial standpoints. To meet such demands, this study was aimed (i) to develop and optimize MWCNTs-PTFE nanocomposite coating on the heat transfer surface and (ii) to minimize the foulant mass on test plate heat exchanger surface during high temperature short time (HTST) pasteurization process of milk. PTFE and MWCNTs-PTFE nanocomposite coatings were applied to a test PHE unit for fouling simulation at the initial step of milk pasteurization process. The surface nanomorphology was explored using a field emission scanning electron microscopy (FESEM).

Objective 2. Develop and Optimize Superhydrophobic and Superhydrophilic Nanocomposite Surface Coatings for Removal of Bacteria Adhering to Solid Substratum Under Different Fluid Flow Conditions.

Rationale: A number of recent studies have shown that both superhydrophobic and superhydrophilic coatings potentially minimize microbial adhesion to solid substrates; however, a comprehensive investigation of both extreme surface characteristics is not available to date. Therefore, this study was aimed to test and compare the amounts of bacteria adhered to superhydrophobic and superhydrophilic nanocomposite surfaces under different fluid flow conditions. A superhydrophobic surface which possesses micro/nanoscale roughness has its unique self-cleaning attribute, so called 'lotus effect'. However, the lotus effect of a superhydrophobic surface requires a flow stream of liquid (Patel *et al*., 2010). On the other hand, extremely water-attractive nanocomposite surface coated with TiO_2 nanoparticles; for example, also has another anti-fouling attribute i.e., surface superhydrophilicity.

Escherichia coli is a group of hazardous biofilm-forming pathogenic bacteria which can cause several foodborne illnesses including diarrhea and hemolytic uremic syndrome (HUS),

leading to severe kidney failure (Montville and Matthews, 2008). Contaminations and outbreaks caused by *E. coli*, specifically O157:H7 strain, have been recently reported in various food products, such as vegetable juices, dairy products, sausages, and nuts (Lu and Jun, 2012).To ensure the consumer safety, the food processor should control the adherence of microorganisms to food contact surfaces. The attachment of microbial cells to a supporting surface is associated with two key surface characteristics such as micro/nano roughness and chemical heterogeneity of solid surface. Investigation of both parameters is usually performed at a micro/nanoscopic level which can be determined by atomic force microscopy (AFM) or field emission scanning electron microscopy (FESEM). The study of surface roughness includes the wettability and repellency of surfaces. The wettability can be noticed when water is brought into contact with a solid surface. Water may readily spread on the superhydrophilic substrate with a contact angle less than 5°. On the other hand, the superhydrophobic substrate repels water with a contact angle greater than 150°. Therefore, the wettability can be determined by measuring the contact angle of a water drop resting on a solid substrate (Erbil, 2006; Neumann *et al*., 2010). There have been several studies reported accounting for fouling preventions on solid substrates using hydrophobic or hydrophilic surface modifications (Crick *et al*., 2011; Lai *et al*., 2012; Nosonovsky and Bhushan, 2009; Su *et al*., 2010).

Superhydrophobic surfaces are capable of reducing down the attachment of biofouling including bacterial cells due to the lotus effect in association with the stream of liquid such as water; however, to the contrary, it would promote bacterial adhesion in a stagnant condition, due to the disruption of surface microstructure (Epstein *et al*., 2012). On the other hand, superhydrophilic surfaces are able to develop a thin water layer that is fully adsorbed onto the substrate so that additional biofouling contact will be isolated from the surface (Kobayashi *et al*., 2012; Tiraferri *et al*., 2012). Most food processors are filled with liquid flow or dried powders and often paused for stops; thus, the anti-biofouling performance of the surface, either superhydrophobic or superhydrophilic, should be limited depending upon its environmental conditions.

To our knowledge, there have been no studies for comprehensive investigation of extreme surface characteristics for effective inhibition of bacterial adhesion, further biofilms formation in food applications. Therefore, the objective of this activity was to test and compare the amounts of adhered bacteria on superhydrophobic and superhydrophilic nanocomposite surface coatings under static and dynamic environments. The flow conditions included a stagnant flow with the wall shear rate close to zero and a dynamic flow with the sheared hydro-boundary layer. A parallel-plate flow pattern was selected as a case study due its several advantages, for instance, facile fabrication of highly uniform nanocomposite coatings on test surfaces as well as rapid determination of bacteria adhered to the surface using a fluorescence staining technique which is preferable for on-site assessment of the bacterial cells adhering to the food processing equipment.

Objective 3. Develop and Optimize Slippery Liquid-Infused Porous Surface (SLIPS) for Removals of Liquid Food Debris and Bacterial Biofilms.

Rationale: Food debris and foulants are ample sources of water and nutrients for microorganisms presenting in a food food-processing plant to grow and multiply. Microorganisms that come with raw materials may continuously contaminate and attach to the surfaces of poorly sanitized processing equipment, utensils, packaging, conveyors and other food contact materials (Chmielewski and Frank, 2003). Prolonged bacterial attachment on the fouled substratum would result in the development of hard-to-remove extracellular polymers-mixed bacterial community complex or 'biofilms'. A biofilm is a dense aggregation of microorganisms attached to each other and a supporting surface via extracellular polymeric substances (EPSs) of their own secretion. The EPS serves several beneficial purposes to microorganisms; especially, sheltering them from drastic environmental conditions including changes in temperature, nutrients, light exposure and hazardous chemicals (Flemming and Wingender, 2010). The presence of biofilms on surfaces is problematic; major negative effects of biofilms are the possibilities to increase the surface friction, accelerate corrosion on metal surface, cause food spoilage and; more importantly, contribute the infection as well as foodborne illnesses to human (Kociolek, 2009). Biofilms are also recognized as the source of persistent infections. Biofilms

invasions and biofilms-induced infections are often difficult or impossible to remedy through the use of biocides, antibiotics, or host defenses. It is now recognized that approximately 80% of food outbreaks are related to biofilms (Srey *et al*., 2013). Therefore, dual-preventive technique for controlling both surface debris (active prevention) and biofilms (passive prevention) on the food contact surface in food processing environment is urgently needed to minimize foodborne pathogen outbreaks.

Self-cleaning characteristic of 'bio-inspired' surfaces such as superhydrophobic, superoleophobic, and superhydrophilic has been broadly employed towards the prevention and removal of biofouling, microbial attachment and biofilms on solid surfaces in many research activities (Nishimoto and Bhushan, 2013). One of these self-cleaning surfaces is the well-known superhydrophobic surface comprising significant amount of micro/nano-scale air gaps within its hierarchical roughness structures to render 'lotus effect' showing high water contact angle (more than 150°) and low contact angle hysteresis (less than 10°). The superhydrophobic surface can potentially cause water and other watery liquids to roll over, pick up and carry away dirt, dust and other water-insoluble particles from the surface. Nevertheless, the effectiveness of the lotus effect is likely to be significantly limited in particular circumstances; especially, when the superhydrophobic surface is subjected to repel low-surface tension and complex liquids; for instance, hydrocarbon liquid including oils, alcohol, blood, and bacterial biofilms. This is due to the fact that low-surface energy liquid can readily 'wet' and permeate into the micro/nano-scale rough features and likely to be permanently trapped inside the grooves of the superhydrophobic surface. Another interesting example of bio-inspired surfaces is the 'omniphobic'(Yao *et al*., 2013) slippery liquid-infused porous surface (SLIPS). The SLIPS is inspired by *Nepenthes pitcher* plant or monkey cup. The most important self-cleaning characteristic of the pitcher plant is high-level slipperiness of its inner surface. Therefore, the surface is capable of repelling wider range of liquids compared to the superhydrophobic surface. Because the synthetic omniphobic surface was designed to retain a stable layer of lubricating film that locates between solid substrate and liquid needs to be repelled (oil, bacterial suspension, etc.). The most commonly used configuration to fabricate such slippery environment is the combination of highly porous solid surface (i.e., most of superhydrophobic surfaces are qualified for this requirement) and a

low-surface energy lubricant. In this combined environment, the solid substrate with micro/nano-scale porous structure can store the lubricant in place within its topographies resulting in a formation of steady lubricating film covering entire areas of the developed omniphobic surface. Hence, the ideal repellant should have significant low-surface tension, so that it can rapidly wet and firmly attach to the prepared porous structure, and immiscible with organic liquids. According to these needs, there has been observed that a group of high-performance high-boiling point low-surface energy perfluoropolymers on market such as Dupont Krytox, commonly known as perfluoroalkylether or PFPE oils (boiling point: 180-295°C and surface tension: 16-20 mN/m), showed an exceptional liquid repellency when they were used as a repelling lubricant. Regarding the choice of the porous platform to hold the repellant, utilizations of both ordered and random alignments of micro/nanomaterials can be seen in the literatures; for instance, exopy-resin composite and polytetrafluoroethylene membrane (Wong *et al*., 2011; Epstein *et al*., 2012), polypyrole (Kim *et al*., 2012) and butyl methacrylate-ethylene dimethacrylate (Xiao *et al*., 2013). However, these surface treatments require a considerable amount of specialty equipment including clean room, electropolishing system, and electrospray deposition as well as diligent procedures towards their fabrication.

Teflon AF is a group of amorphous fluoropolymers which was developed to exhibit a number of unique features including electrical and chemical resistances, high optical transmission and glass transition temperature, hydrophobic, exceptional mechanical properties, soluble in selected commercial solvents (e.g., Fluorinert family developed by 3M). More importantly, the Teflon AF solution can be firmly attached to micro/nano-scale structure with minimal affected to the topography of the substrate (Wu *et al*., 2011). Herein, we introduce a development of biofouling resistant omniphobic SLIPS using scalable coating procedure. In this work, the highly porous hierarchical-structure superhydrophobic prepared from multi-walled carbon nanotubes (MWCNTs)-Teflon AF (TAF) composite was used as an underlying porous material for holding the food-grade liquid lubricant (Krytox, Dupont). The developed SLIPS can be directly applied on the surface of stainless steel where the soil, debris, and bacterial biofilms are commonly found in food processing plant. To the best knowledge, no food contact surface has been developed and confirmed to significantly repel a wide variety of food debris as well as

bacterial biofilms in food processing environment. Therefore, this research was aimed to study and compare self-cleaning performance of the SLIPS and conventional stainless steel surface using commonly found liquid foods covering both single-phase (i.e., water, ethanol and vegetable oil) and complex (i.e., ketchup, honey and bacterial biofilms).

Objective 4. Develop and Optimize Nanoscale Patternings on Aluminum and Stainless Steel Surfaces for Prevention of Bacterial Adhesion

Rationale: This pioneering surface fabrication is designed through processes that exhibit fundamental control over the physical attribute of nanoscale structure in relation to bacterial interaction. Thus, the designed nanoporous and nanopillared surfaces characteristics was applied on a small specimen of stainless steel substrate for reduction of substratum-cells interactions leading to significantly limit the adhesion and attachment of bacterial cells to the steel surface. The bacterial adhesion mechanism is considerably complex and many factors can affect adhesion scenarios. Although, many techniques have been tried to minimize the surface contamination resulting from bacterial adhesion. The effects of nanoscale surface patterns with modulated surface wettability to the bacterial adhesion was investigated. Prevention of attachment of bacterial cells onto solid substrates is one of the effective methods to inhibit biofilms formation. Cell adhesion *in vivo* is a three-dimensional (3D) phenomenon that is distinct from the interaction on two-dimensional (2D) surfaces *in vitro*. The attachment of bacterial cells is associated with various cells-surface interactions including hydrodynamic force, porosity, surface energy and roughness. Recent advancement in fabrication has yet made it possible to create well-organized nanofeatures (i.e. nanoporous and nanopillared) uniformly over a large surface area of a metal specimen (Jeong & Choi, 2014). However, it has not been studied systematically yet how such well-regulated nanofeatures affect the adhesion of bacteria and the formation of biofilms in various surface wetting conditions as well as hydrodynamic flow conditions. In particular, the adhesions of *S. aureus*, *E. coli*, and *Listeria monocytogenes* bacteria on the nanoporous and nanopillared surfaces in hydrophilic and hydrophobic surface wetting conditions during stagnation and dynamic adhesion scenarios.

3. LITERATURE REVIEW

3.1. Introduction

This chapter includes theoretical backgrounds of biofouling formation and removal. Characteristics of the nanomateials used for surface fabrication are shown. In addition, a variety of preventive and removal methods of biofouling in food contact surface and food processing environments using nanoengineered surfaces are also discussed.

3.2. Literature Review

3.2.1. Formation and removal of milk protein foulant in plate heat exchanger

Indirect-type heat exchangers such as plate and tubular heat exchangers are usually employed as heating equipment for food products. During heating, the liquid foods continuously flow in contact with hot heat exchanger surfaces. Besides the bacterial inhibition, the applied heat treatment also simultaneously leads to cause many undesirable side reactions of food components including solidification fouling on the surfaces. For example, milk fouling which is caused by denaturation and deposition of whey protein β-Lactoglobulin, β-Lg, at temperature less than 90°C (especially 70-74°C) due to the unfolding of its protein structure. Adsorbed layer of fouling on the heat exchanger surface significantly interferes the heat transfer rate of liquid foods, results in an insufficient pasteurization problem (Jun and Puri, 2005a; 2005b; 2006a; 2006b). Another drawback of surface fouling in plate heat exchangers is increase in pressure drop within the heating chambers thus affecting the economy of processing plants (Bansal and Chen, 2006).

A four-phase milk fouling model is commonly employed to describe the chemical reactions that take place within the milk (i.e., unfolding and denaturation rates of native whey protein β-Lg) as well as a surface reaction (i.e., deposition rate of unfolded protein on plate heat

exchanger). The dynamic relationship between four main β-Lg species in four-phase reaction model is shown in Eq. (3.1):

$$\begin{array}{l} N \rightarrow U \rightarrow A \\ \quad\downarrow \\ \quad D \end{array} \tag{3.1}$$

where *N*, *U*, *A* and *D* are native, unfolded, aggregated and deposited β-Lg species, respectively. Kinetics equations for each of the species are as follows:

$$\frac{\partial C_N}{\partial t} = -k_U C_N \tag{3.2}$$

$$\frac{\partial C_U}{\partial t} = -k_U C_N - k_A C_U^2 - k_D C_U \tag{3.3}$$

$$\frac{\partial C_A}{\partial t} = -k_A C_U^2 \tag{3.4}$$

$$\frac{\partial C_D}{\partial t} = -k_D C_U^2 \tag{3.5}$$

where C_i is the protein concentration, t is time, and k_i is the reaction constant related to absolute temperature according to the Arrhenius equation as follow:

$$k_i = k_{0i} \exp\left(-\frac{Ei}{RT_K}\right), i = U, A \text{ and } D \tag{3.6}$$

where E_i is the activation energy, R is the gas constant, T_K is the absolute temperature and k_{0i} is the pre-exponential factor.

Although surface foulant can be eliminated by routine clean-in-place (CIP) program in which the considerably amounts of chemicals, water and electrical energy are required. The costs of productivity loss due to frequent equipment shutdown for cleaning including water and

chemical expenses are approximately $5 billion annually (Balasubramanian and Puri, 2009a). It is known that hydrophobic coating is one of the effective surface treatments to reduce the biological fouling on heat exchanger surface (Santos *et al*., 2004; Rosmaninho *et al*., 2007; Balasubramanian and Puri, 2009b; Ozden and Puri, 2010). The hydrophobic surface can be categorized into two classes based on their water contact angle (WCA) values. A hydrophobic material usually refers to any surfaces having the WCAs greater than 90° while a superhydrophobic, or hyperhydrophobic refers to ones which have the WCAs greater than 150°.

The superhydrophobic surface is basically a combination of a hydrophobic surface integrated with micro- and/or nano-scale roughness on its surface. Because the wettability of superhydrophobic surfaces are extremely low, the utilization of hydrophobic and superhydrophobic surface coatings on plate heat exchangers (PHEs) for liquid foods including milk and other dairy products have been recently elucidated by a number of researchers. Beuf *et al*. (2003) investigated that the fouling rate on an uncoated stainless steel 316 during milk product pasteurization was not significantly different from surfaces that were modified by eight different hydrophobic surface coatings including Diamond Like Carbon (DLC), Silica, SiO_2, Ni–P–PTFE, Excalibur, Xylan, and ion implantations (SiF^+, MoS_2).

However, they found that surface energy and surface roughness of coatings played the important roles on the cleaning efficiency of fouled surfaces. Rosmaninho *et al.* (2007) also confirmed that fouled PHE surfaces caused by calcium phosphate, β-lactoglobulin (β-Lg) and milk-based fluids of were easily cleaned on a Teflon-based hydrophobic Ni–P–PTFE surface coating. Balasubramanian and Puri (2009b) investigated that food-grade hydrophobic polymer-based coatings including Ni–P–PTFE, Lectroflour, and AMC148 could significantly diminished surface deposition and thermal energy consumption rates of PHE system for milk pasteurization. Ozden and Puri (2010) found that the mass of foulants on test PHE surfaces on superhydrophobic CNT-coated stainless steel was much lower than control and other hydrophobic coated surfaces i.e., Ni–P–PTFE, TM117P and AMC148.

Many other researchers (Lau *et al*., 2003; Santos *et al*., 2004; Huang *et al*., 2005; Li *et al*., 2010; Luo *et al*., 2010; Men *et al*., 2010) have also reported that the superhydrophobicity could be obtained by growing vertically aligned carbon nanotubes (ACNTs) onto the metal substrate directly. However, the growth of a ACNTs could not be achieved when the size and shape of the substrate are large than the size of the chamber of nanotubes synthesizer. Therefore, a randomly aligned carbon nanotubes network is more preferable for large-scale surface coating.

3.2.2. Hazard and prevention of bacterial biofilms in food processing

Biofilms are surface-adherent communities of microorganisms enclosed in their own water-rich matrix. The cells in the communities are sheltered within sticky extracellular polymeric substances (EPSs) consisting of many microbial metabolites such as polysaccharides, lipids, and proteins. The biofilms can be readily formulated in nature wherever water is present. In the water industry, biofilms formation is beneficial in some circumstances such as bio-filtration and biodegradation. In general, a biofilm, however, is the unwanted deposition of microorganisms such as pathogens and spoilages and their EPSs on solid surfaces. Prevention of biofouling and its adverse effects on performance and efficiency of machine in water systems is one of the major challenges in many steps (Dror-Ehre *et al*., 2010).

The consumption of fresh produce such as fruit and vegetable is an increasing trend. The produce is a good source of minerals and fiber for human (Olaimat and Holley, 2012). Despite the fact that demand of fresh produce has been increasing over the past years due to their high nutritional values, data collected by the Centers for Disease Control and Prevention (CDC) during 2006-2014 show that considerable amounts of foodborne outbreaks linked to the cross-contamination of pathogenic bacteria such as *E. coli* O157:H7, *Listeria monocytogenes*, and *Salmonella* spp. were found in fresh fruits and vegetables (Warriner *et al*., 2009). These pathogens are well known to cause serious illnesses in human if they are present in food (Bermúdez-Aguirre *et al*., 2013), especially when the food is consumed raw or uncooked. Bacterial biofilms present in food processing environment are suspected to be main sources of

cross-contamination in a wide variety of fresh produce such as sprouts, lettuce, fennel, cilantro, cantaloupes, orange juice, tomatoes, melons, mango, celery and parsley (Lapidot *et al*., 2006).

The cross-contamination of biofilms-related pathogens from a contaminated surface in fresh produce can be involved in various processing stages including wash-water-mediated transfer (i.e., washing and rinsing steps) or direct contact with the infected surface (Liu *et al*., 2014). In general, ready-to-eat fruits and vegetables such as leafy greens are not subjected to any major microbial inactivation process such as pasteurization, cooking, boiling or steaming. As a result, it is nearly impossible to entirely eliminate all pathogens from the infected produce after the cross-contamination occurs because bacteria on the produce surface can be internalized through vegetable tissues (Gómez-López *et al*., 2014).

Conventional surface cleaning methods only allow the removal of 90% of adherent bacterial from surfaces without killing them. Moreover, the detached bacteria may re-attach to other surfaces to form a biofilm. Although, conventional antimicrobial agents can be used to reduce microbial population; however, the effectiveness of disinfectants is limited by the presence of organic materials commonly found in food (e.g., fat and carbohydrates), pH, temperature, and contact time (Srey *et al*., 2013). Additionally, microorganisms in a biofilm develop a tolerance to the cleaning procedures, and a mature biofilm is relentless and difficult to completely eliminate. Importantly, periodic cleaning is costly and can leave scratches and crevices on the metal surfaces. Some of the oxidative disinfectants may also promote the formation of biofilms by providing biodegradable organic substances that can be utilized by microorganisms; thus, inducing the formation of bacterial biofilms (Dror-Ehre *et al*., 2010).

3.2.3. Nanomaterial and nanotechnology for biofouling prevention

3.2.3.1. Growth and functional properties of carbon naotubes

Carbon nanotubes (CNTs) were discovered by a Japanese physicist, Sumio Iijima in 1991. Since then number of studies towards the properties and applications of CNTs have been

investigated and reported. Carbon nanotubes are apparently elongated fullerenes having either single or multiple hexagonal rolled up sheets of carbon atoms (graphene) as the walls with capped end (Xie *et al.*, 2005). Single-walled carbon nanotubes (SWCNTs) and multi-walled carbon nanotubes (MWCNTs) are commonly known as the common types of carbon nanotubes. Specifically, a SWCNT has only single layer of graphene-sheet wall located around a central hollow core (tube).On the other hand, MWCNTs are generally composed of more than one graphene shells coaxially located along the tube. Diameters of nanotubes are in the range of 1-10s nm, depending on number of walls, with high length-to-diameter ratio (generally more than 1000). Typical field emission scanning electron microscopic (FESEM) image of a network of MWCNTs are shown in Fig. 3.1. CNTs are traditionally produced by thermal degradation of carbon source in the presence of a metal catalyst using laser ablation or arc discharge approaches. The limitations of these methods are widely reported; specifically, the laser ablation is not applicable for large-scale production while the CNTs produced by the arc discharge process contain high-level contaminations of carbonaceous impurities as well as metal catalyst (Meyyappan *et al*., 2003).

Kumar and Ando (2010) reported that the synthesis of CNTs by chemical vapor deposition or CVD method has been widely employed. The benefits of CVD technique are low capital cost, high production yield, easy to scale-up and high versatility of production. The CVD system can be designed to fabricate CNTs in various forms such as powder, film, aligned and entangled tubes, depending on the configurations of metal catalyst and substrate. Process parameters of CNT growth in CVD are type of hydrocarbon precursors and catalysts, temperature, pressure, flow rate, deposition time and reactor's dimension. The simplified configurations of CVD system is shown in Fig. 3.2. The growth of CNTs by CVD system in continuous system is achieved by flowing a vapor of select hydrocarbon precursor (C_xH_y) i.e., methane, ethylene, acetylene, benzene, xylene and carbon monoxide over a substrate containing metal catalyst on its surface in a cylindrical reaction chamber. The temperature within the reactor is typically controlled to be 600 to 1200°C using an electronic temperature source with a controller.

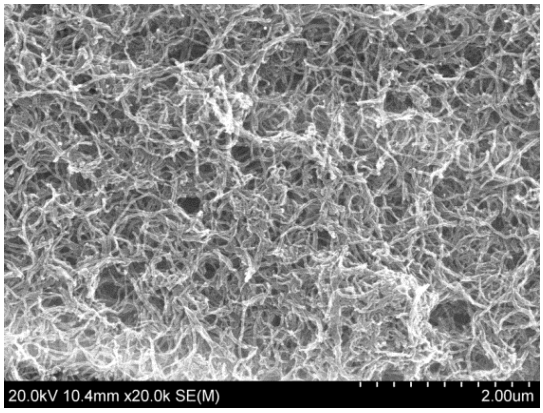

Figure 3.1. FESEM micrograph of mutiwalled carbon nanotunes

At this step, the decomposition of hydrocarbon vapor occurs when it reacts with metal catalyst at high temperature producing carbon and hydrogen species within the chamber. The hydrogen is not involved and passing through the outlet of the reactor while carbon is readily dissolved into the metal catalyst.

The formation of nanotubes occurs when the concentration of dissolved carbon specie within the catalyst exceeds the maximum solubility limit. As a results of the formation of cylindrical network of carbon atoms that are growing out from the surface of catalyst. The growth models of CNTs can be categorized into two main cases namely "tip-growth model" and "base-growth model". As shown in Fig. 3.3 (a), the first case happens when interfacial interaction between catalyst and substrate is weak. Therefore, a CNT is growing from the catalyst-substrate interface and pushing the catalyst particle away from the substrate. The elongation of nanotube continues from its tip where the metal catalyst is located. On the other hand, the latter model is used to describe the CNT growth takes place when the interaction of catalyst-surface is stronger than the force produced by the CNT precipitation. Therefore, a CNT precipitates out from the top of the catalyst and extends its length by forming a tube from the bottom (Fig. 3.3 (b)). Size of metal catalyst for growing SWCNT is typically in the range of a few nanometers while the size of a few tens nanometers is needed for growing a MWCNT.

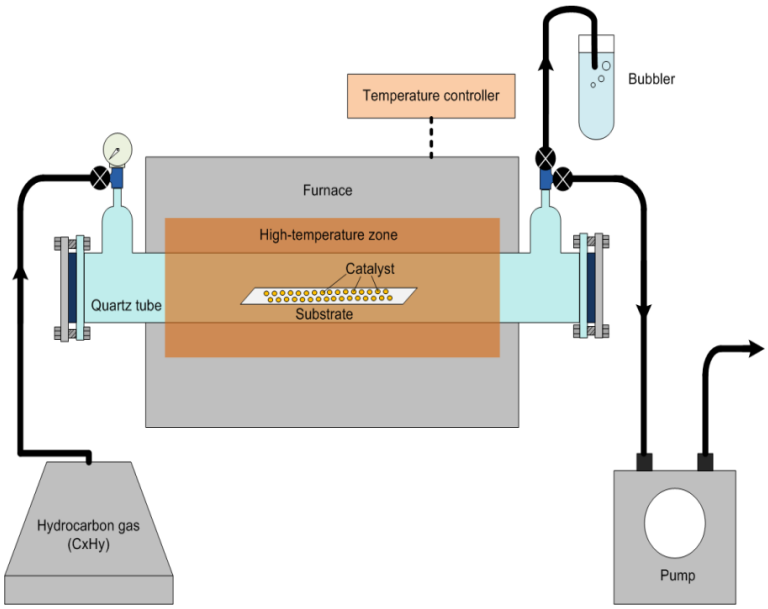

Figure 3.2. Schematic diagram of simplified CVD system for growing CNTs.

Both SWCNTs and MWCNTs have the exceptional mechanical, thermal, chemical magnetic, optical and electrical properties. Some of these CNTs properties are shown in Table 3.1. According to the data shown in the table, the tensile strength of CNTs are found to be hundred times that of steels with approximately one order of magnitude of steel density. Therefore, CNTs are well-known as lightweight yet high-performance materials that are suitable for a wide range of applications ranging from biosensors to space exploration.

Recently, fabrications of CNT-polymer composites have been intensively studied in order to expand the availability of CNTs. However, aggregation of CNT particles is a challenging task confronting the fabrications of CNT-polymer composites. The formations of bundles and ropes occur during the production of CNTs due to van der Waals attraction among nanoparticles. This problem results in the limited exhibition of CNTs potential. Therefore, the proper pretreatments are needed to appropriately disintegrate and disperse individual nanotubes before mixing in order to enhance uniformity of CNTs in the surrounding polymer matrix.

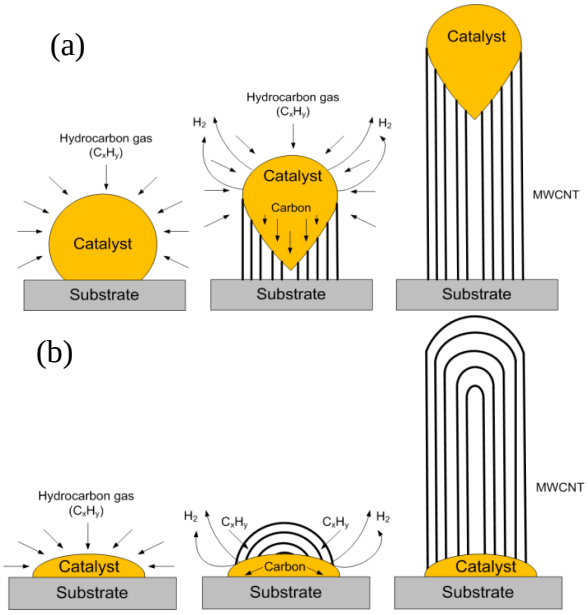

Figure 3.3. Growth mechanisms of CNTs in CVD system (a) tip-growth model and (b) base-growth model.

Dispersion of CNTs in the matrix of polymer

The most commonly used techniques to disperse CNTs in polymer matrices include physical blending, chemical fictionalization, and in situ perimerization. The principles and applications of these methods are shown as follows (Xie *et al*., 2005);

- *Physical blending*

High power disaggregation methods are required to properly disperse nanofillers such as CNTs in a polymer matrix. Ultrasonicator and high shear mixer are commonly employed to achieve such fabrication requirements. The ultrasonic waves generate cavitations in a CNT suspension and subsequently disaggregate CNT bundles to form individual nanotubes. However, excessive use of ultrasonication might shorten both SWCNTs as well as MWCNTs. Although the shortening mechanism of CNTs is still unclear, it was found that shortening is more likely to

occur near the center of mass (CoM) of CNTs which generally happens to the shortening of polymers during ultrasonication (Pagani *et al*., 2012). In addition, re-aggregation of both SWCNTs and MWCNTs will occur after ultrasonication is removed (Lahelin *et al*., 2011). Therefore, surfactants or heat may be applied to enhance the dispersion stability of CNTs in a polymer matrix.

Table 3.1 Select properties of carbon nanotubes

Property	**CNTs**
Specific gravity	0.8 g/cm^3 for SWCNT;
	1.8 g/cm^3 for MWCNT (theoretical)
Elastic modulus	approx. 1 TPa for SWCNT; 0.3–1 TPa for MWCNT
Strength	50–500 GPa for SWCNT; 10–60 GPa for MWCNT
Resistivity	5–50 μΩ cm
Current density	> 10^8 A/cm^2 (Zhong *et al*., 2012)
Thermal conductivity	3000 W m^{-1} K^{-1} (theoretical)
Thermal expansion	Negligible (theoretical)
Thermal stability	>700°C (in air); 2800°C (in vacuum)
Specific surface area	10–20 m^2/g
Aspect ratio	up to 132,000,000:1

- *Chemical functionalization*

This chemical functionalization is typically recognized as a promising method to magnify the mechanical properties of CNT-based composites. The method is also called "grafting to" approach. Generally, a polymer matrix is allowed to react with oxidized or pre-functionalized CNTs. As-grown CNTs may contain other undesirable impurities, which impart the quality of CNTs, such as fullerenes, nanocrystalline graphite as well as metallic catalysts (Feng *et al*., 2003). Therefore, removal of these impurities should be done before functionalization process.

Linking of carboxyl group (-COOH) or hydroxyl group (-OH) on the surfaces of CNTs is the primary step of CNT functionalization. Because these groups can be further replaced by various number of other functional groups that can provide homogeneous dispersion for high-performance CNTs-polymer composites. Furthermore, it was found that the dispersibility of COOH-functionalized in water and other organic solvents is better than pristine CNTs. In addition, acids used in this process also increase the purity of CNTs by removal any remaining metal catalyst from nanotubes. To obtain COOH functionalized CNTs, nanotubes are typically treated with concentrated organic acids including nitric acid, sulfuric acid and also a mixture of both acids. Afterwards, sonication is then applied to the mixture for few hours before being agitated at high temperature for several hours.

- *In situ polymerization*

The *in situ* method is also called "grafting from" approach, is an effective way to uniformly disperse nanocomposite throughout polymer matrix. The method is faster and also less expensive than chemical functionalization of nanomaterials including CNTs. Therefore, it is the most practical way to process CNT-polymer composite in large production scale. In particular, the emulsion/suspension polymerization method (Lahelin *et. al*, 2010). This polymerization technique consists of several steps including immobilizing the sidewalls and the edges of CNT particles with monomer in the presences of surfactant and initiator. Subsequently, the CNT-polymer mixture is polymerized to create uniformly distributed CNT-polymer composites at high level of CNT loadings.

3.2.3.2. Use of Teflon as polymeric matrix for nanocomposite coating

Typically, polytetrafluoroethylene (commonly known as PTFE or Teflon) is a thermoplastic polymer $(F_2C\text{-}CF_2)_n$ which is synthesized by the polymerization of tetrafluoroethylene monomers, $n{\cdot}F_2C{=}CF_2$. The C-F bond presents in PTFE has exceptionally high bonding energy, typically more than 100 kg/mole, resulting in a very low surface free energy of PTFE (18 mN/m, Lau *et al*., 2003). Because the melting point of PTFE is

approximately 327°C; therefore, it is commonly employed as an inert coating on the surface of various type of materials including plastics and metals. The PTFE is commercially introduced into food processing equipment as a non-stick cookware coating which enables minimum adhesion of biological fouling layer to the PTFE coated surface. In addition, PTFE coating also provides an excellent easy-to-clean attribute to the surface of frying pan. However, the applications of PTFE coating are restricted by its own several limitations i.e., poor thermal conductivity as well as high wear rate. Therefore, PTFE composites are developed by conjugation PTFE with other materials, either a filler or a matrix, in order to improve the ware resistance of PTFE. Chen *et al*. (2003) reported that wear rate and friction coefficient of MWCNTs-PTFE composites was dramatically decreased when the CNTs content was increased. The lowest wear rate of developed composite was only 1/290 that of pristine PTFE when the 20% vol. of CNTs were introduced and conjugated into the PTFE matrix.

Other than the improvement in wear rate, the conjugation of CNTs nanocomposite within a PTFE matrix also utilized to develop a self-cleaning superhydrophobic surface in many applications. The term hydrophobic surface typically used to describe any surface having a water contact angle (WCA) greater than 90°. Water contact angle of superhydrophobic surface is generally more than 150° and water sliding angle (WSA) less than 10°. The unique attribute of superhydrophobic surface is self-cleaning which is also called "lotus effect" caused by the formation microscale roughness of material, i.e. CNTs that allows air to be trapped within its rough structures; thus, preventing the direct contact between water on the superhydrophobic surface and the underlying substrate. Therefore, water stream flowing on top of the superhydrophobic surface would quickly picks up dust and other solid impurities away from the superhydrophobic surface.

Due to its chemical inertness and high melting temperature, PTFE has been commonly used for non-stick cookware and often times as filler and matrix. As a matrix, it has been successfully filled with nanoparticles such as alumina and CNTs. Interestingly, the wear resistance of Al_2O_3–PTFE nanocomposite as surface coating was reported to be 600 times higher than unfilled PTFE (Sawyer *et al*., 2003). Similar improvements of the wear resistance for CNT-

PTFE nanocomposite coating have been observed and reported (Burris *et al*., 2007; Chen *et al.*, 2003). The wear rate of 5–20% v/v CNT-PTFE nanocomposite is reported to be more than 100 times lower than pristine PTFE (Chen *et al*., 2003).The development of uniform CNT-PTFE nanocomposite film can be fabricated by ultrasonic wave and high temperature annealing applications (Show and Takahashi, 2009).

3.2.3.3. Development of nanopattern on metal surfaces via anodization

Anodization process is one of the electro-chemical treatments commonly used to protect metals from corrosion. Two-step anodization has been heavily employed to develop highly ordered hexagonal porous structures on metals when they were served as anodes in anodizing system. Recently, anodic aluminum oxide (AAO) or alumina has been engineered for used as templates to develop size-controllable surface in nanotechnology fields. Simplified experimental equipment used for fabrication of a porous AAO surface is shown in Fig. 3.4. It is noted that high purity of aluminum specimen (purity of 99.99%) is commonly used as an anode to achieve an array of uniform porous oxide layer on aluminum substrate. Oxalic, phosphoric, and sulfuric acid are typically used as electrolytes for creating nanopores of between 10 and 240 nm in diameter (Poinern *et al.*, 2011). Formation of nanoporous on an alumina is complex and has not been fully understood. However, it can be explained using dissolution reactions presented as follows (Poinern *et al.*, 2011);

$$2\mathrm{Al}+3H_2O \rightarrow Al_2O_3 + 3H_2 \tag{3.7}$$

Such oxidation process occurs above the bottom of the nanopore; therefore, oxide material grows perpendicular to the aluminum surface. This formation of the oxide layer results in development of columnar structure with high aspect ratio. The channel extends from the base of the pore towards the surface of the oxide layer.

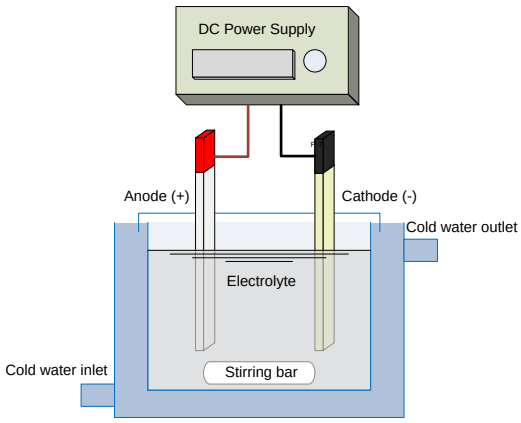

Figure 3.4. Schematic of main components required to produce porous aluminum oxide layer on aluminum substrate.

Fig.3.5 shows the schematic of pores on an AAO. A set of equations that can be used to predict pore diameter (*D*p) and interpore distance (*D*c) of the AAO surface under potentiostatic conditions are as follows (Poinern *et al.*, 2011);

$$\text{Pore diameter } (Dp) = \lambda_P U$$
$$\text{Inter pore distance } (Dp) = \lambda_P U \tag{3.8}$$

where λp is the pore proportionality constant = 0.9 nm per volt and λc is inter-pore proportionality constant = 2.5 nm per volt. Wall thickness (W_d) of circular pore can be calculate by:

$$\text{Wall thickness } (Wd) = \frac{1}{2}(D_c - D_p) \tag{3.9}$$

Porosity (α) and pore density (n) are expressed below:

$$\alpha = \frac{\pi}{2\sqrt{3}}\left(\frac{D_p}{D_c}\right)^2$$
$$n = \frac{2.10^6}{\sqrt{3}\ D_c^2} = \frac{2.10^6}{\sqrt{3}\ U^2\lambda_c^2} \tag{3.10}$$

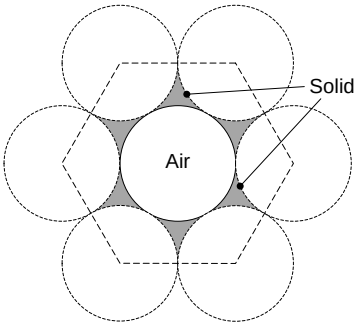

Figure 3.5. Schematic of a group of hexagonally packed pore array

3.2.4. Physics and mechanics of bacterial adhesion and attachment to solid substratum

Bacterial attachment and nucleation are prerequisites for colonization and subsequent transmission of pathogens when the contaminated fruits and vegetables are consumed. In fact, once the attachment is successfully done, it is very difficult to remove the attached pathogens from contaminated produce by washing (Berger *et al*., 2010). There are two types of mechanism for the bacterial attachment to solid substratum, which are: (a) two-step (Marshall *et al*., 1971), and (b) three-step processes (Busscher and Weerkamp, 1987) (Fig. 3.6). For the two-step process, including reversible and non-reversible stages, the bacteria transports close enough to the surface so they can be adsorbed onto the surface. This is recognized as a reversible process because attached bacteria can be removed by simply washing. Once the cells are adsorbed, they will start to produce the EPS which is consider time dependent and involves the material that anchors the bacteria to the contaminated solid surface.

For the three-step process, the attaching process depends on the distance of the bacteria from the surface. At the long distance between them (more than 50 nm) only long-range forces operate and the adhesion is reversible. At the medium distance (about 20 nm) both long-range and electrostatic interactions are operating; thus, this process is initially reversible but over the time it becomes non-reversible. The last step occurs when the distance is less than 15 nm. At this point, bacteria can produce reinforcing substances such as adhesive polymers leading to

irreversible attachment. These bacteria-excreted polymers are called extracellular polymeric substances (EPS). They help in anchorage of the cells to the surface and stabilizes the colony from the fluctuations of the environment (Characklis and Marshall, 1990).

In addition, the EPS layer also helps in protecting the cells from the effect of antimicrobial agents (Kumar and Anand, 1998). Besides the cell-surface distance, other factors affecting the attachment of bacterial cells to solid include motility or gravitational transportation of the planktonic (free floating), diffusion or shear force of the surrounding fluid phase. Surface properties including surface topography, surface charge, hydrophobicity, and nutrients also play important roles in attachment of bacterial cells. For example, surfaces that are found to be vulnerable to microbial attachment and biofilm development include plastic, glass, metal, wood, and food products (Srey *et al*., 2013). Although the cell-substratum interaction is complex, a significant number of mathematical models for describing the interaction have been successfully developed. Among these concepts, DLVO (Derjaguin, Landau, Verwey, Overbeek) theories e.g. classic DLVO and extended DLVO (also known as XDLVO) have been broadly used as models for qualitative and quantitative estimations of adhesion energy involved in bacterial adhesion and aggregation as functions of separation distance between the interacting surfaces (Bayoudh *et al*., 2009).

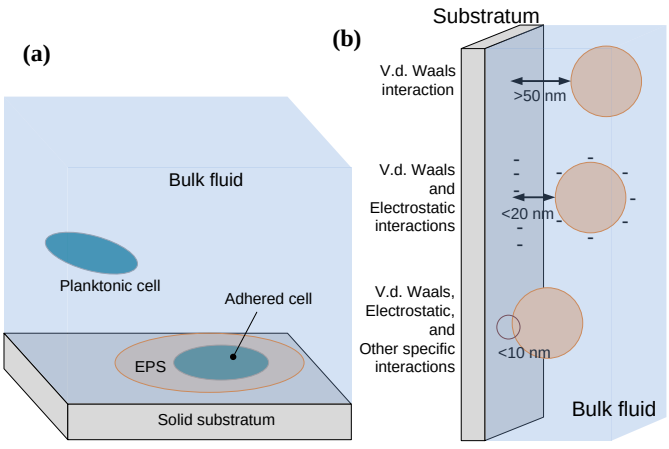

Figure 3.6. Schematics of different bacterial adhesion processes (a) two-step and (b) three-step.

According to recent reports, the XDLVO theory enables more accurate prediction for bacterial adhesion than the classic DLVO theory for hydrophobic and hydrophilic substratum surfaces. As described by Bayoudh *et al*. (2009), in the classical DLVO theory, the net interaction energy (G^{DLVO}) needed to bring a bacterium (*b*) into contact with a flat substratum surface (*s*) immersed in aqueous medium (*l*) is the balance between two additive interaction energies: the attractive Lifshitz van der Waals energy (G^{LW}) and the repulsive or attractive electrostatic double layer energy (G^{EL}). The total interaction or adhesion energy as a function of the separation distance (*d*) between a bacterium (sphere) and a substratum (flat plane) surfaces is therefore can be written as:

$$G_{slb}^{DLVO}(d) = G_{slb}^{LW}(d) + G_{slb}^{EL}(d) \tag{3.11}$$

Later, Van Oss *et al*. suggested that the acid–base energy (G^{AB}), arising from hydrogen bonding between two surfaces immersed in a polar solvent (e.g., water), must be accounted in addition to LW and EL interaction energies. The inclusion of the polar interaction energy (GAB) resulted in the XDLVO approach, in which the total interaction energy (GXDLVO) may be written as:

$$G_{slb}^{DLVO}(d) = G_{slb}^{LW}(d) + G_{slb}^{EL}(d) + G_{slb}^{AB}(d) \tag{3.12}$$

From thermodynamic point of view, an adhesion or attraction between two interacting surfaces occurs when the total energy G^{XDLVO} is negative, and repulsion occurs when G^{XDLVO} is positive. Since the total interaction energy is evaluated as a function of the separation distance (*d*) between the interacting surfaces, therefore the interaction energy profile illustrates the type of interaction (attraction or repulsion) as the microbial particle approaches a substrate surface. Free energy per unit area between two infinite planar surfaces brought into close contact with each other (distance, *h*) must be used to calculate XDLVO interaction energy between surfaces of a sphere and a flat plane. According to Derjaguin approximation, the interaction energy is calculated as the sum integral of the corresponding plate–plate free energy per unit area along the separation distance, *d*, and the actual LW, AB and EL interaction energies between a sphere (bacterium) and a flat surface immersed in a liquid are expressed as follows:

$$G_{slb}^{LW}(d) = -\frac{A_s a}{6d}$$

$$G_{slb}^{AB}(d) = 2\pi a\lambda\Delta G_{d0}^{AB} exp\left(\frac{d_0 - d}{\lambda}\right)$$

$$G_{slb}^{EL}(d) = \pi\varepsilon_r\varepsilon_0 a\left[2\psi_b\psi_s \ln\left(\frac{1+e^{-kd}}{1-e^{-kd}}\right) + \psi_b^2 + \psi_s^2(\ln 1 - e^{-2kd})\right] \quad (3.13)$$

where A_s is the un-retarded sphere (bacterium)–substrate Hamaker constant in water, λ (i.e., 0.6 nm) is the characteristic decay length of AB interactions in liquid medium e.g., water, and a is the radius of a sphere, ε_0 (i.e., 8.854×10^{-12} $CV^{-1}m^{-1}$) is dielectric permittivity in the vacuum, ε_r (i.e., 79 in vale) is the relative permittivity of water, κ (i.e., 3.28×10^{9} $I^{1/2}$ m^{-1}, where I is the ionic strength of the electrolyte in terms of molarity) is the inverse Debye screening length, and ψ_b and ψ_s are the surface potentials of the bacterium and the substrate. The total XDLVO adhesion energy is the summation of the three components at a given distance between a sphere and substrate (Bayoudh *et al*., 2009).

3.2.5. Principles and measurements of surface topography and chemistry

3.2.5.1. Estimation of surface free energy of ideal solid surface using Yong's equation

The study of energy of solid surface is beneficial for understanding of wettability and adhesion characteristics of surface. However, the solid surface energy, or surface tension, is difficult to measure directly (Tavana and Neumann, 2007). Several indirect approaches, both experimental and theoretical, have been developed. Static contact angle measurement with different liquids is one of the most common methods. According to Young's equation, the estimation of solid surface tensions from contact angles is based on the principle of mechanical equilibrium under the action of three interfacial tensions (Fig. 3.7).

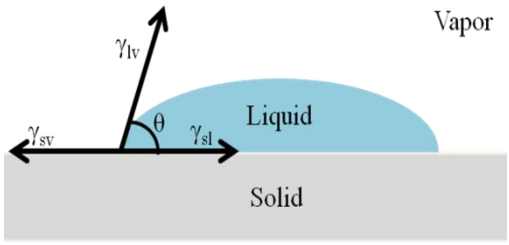

Figure 3.7. A schematic diagram of a sessile water drop, contact angle (θ), and the three interfacial tensions (γ^{lv}: liquid–vapor, γ^{sv}: solid–vapor, and γ^{sl}: solid–liquid).

The equilibrium relation between the forces and contact angle is known as Young's equation as given by:

$$\cos\theta = \frac{\gamma_{sv} - \gamma_{sl}}{\gamma_{lv}} \tag{3.14}$$

where θ is the Young contact angle and γ represents the interfacial energy.

Since, the only measurable quantities in Young's equation are γ_{lv} and θ. Therefore, to obtain γ_{sv} and γ_{sl}, an additional relation is required. By utilizing the geometric mean combining rule, Girifalco and Good (1957) approximated the free energy of adhesion of a solid–liquids system (W_{sl}) in terms of the free energy of cohesion of the solid (W_{ss}) and free energy of cohesion of the liquid (W_{ll})

$$W_{sl} = \sqrt{W_{ll} W_{ss}} \tag{3.15}$$

Knowing that $W_{ss} = 2\gamma_{sv}$ and $W_{ll} = 2\gamma_{lv}$, the above equation is written as

$$W_{sl} = 2\sqrt{\gamma_{lv}\gamma_{sv}} \tag{3.16}$$

By the definition $W_{sl} = \gamma_{lv} + \gamma_{sv} - \gamma_{sl}$, the above relation becomes

$$\gamma_{sl} = \gamma_{lv} + \gamma_{sv} - 2\sqrt{\gamma_{lv}\gamma_{sv}} \tag{3.17}$$

Combining this relation with Young's equation yields

$$\cos\theta = -1 + 2\sqrt{\frac{\gamma_{sv}}{\gamma_{lv}}} \tag{3.18}$$

In the 1950s, a modifying factor known as "Good's interaction parameter, Φ" was established, as given by

$$\gamma_{sl} = \gamma_{lv} + \gamma_{sv} - 2\Phi\sqrt{\gamma_{lv}\gamma_{sv}} \tag{3.19}$$

The researchers quantified Φ for various systems using the molar volumes of the two phases in contact. In the early 1990s, an exponential modifying factor $e^{-\beta(\gamma_{lv}-\gamma_{sv})^2}$ was formulated as the value of Φ

$$\gamma_{sl} = \gamma_{lv} + \gamma_{sv} - 2\sqrt{\gamma_{lv}\gamma_{sv}}\, e^{-\beta(\gamma_{lv}-\gamma_{sv})^2} \tag{3.20}$$

Combining Eq. (3.20) with Young's equation yields

$$\cos\theta = -1 + 2\sqrt{\frac{\gamma_{sv}}{\gamma_{lv}}}\, e^{-\beta(\gamma_{lv}-\gamma_{sv})^2} \tag{3.21}$$

3.2.5.2. Effect of surface roughness to apparent contact angle

It is well known that the surface energy of ideal solid surface (microscopically smooth) can be estimated using the balance of interfacial forces established by Young (1805). The

magnitudes of these forces can be quantified by measuring the contact angle of a liquid droplet on solid surface (Kwok & Neumann, 1999). On the other hand, the apparent contact angle obtained from non-ideal, heterogeneous surfaces including nanocomposite coatings and nanopatterned surfaces can be described using the two classical models namely Wenzel model (surface is entirely wetted by liquid droplet, Fig. 3.8 (a)) and Cassie model (air pockets appear underneath liquid droplet and the surface is partially wetted, Fig.3.8 (b)) as follows:

Wenzel model

$$\cos\theta_W = r\cos\theta \tag{3.22}$$

where θ_W is the Wenzel apparent contact angle and r is the surface area ratio (ratio of the actual area of the solid surface to the projected area on the horizontal plane).

Cassie model

$$\cos\theta_C = f\cos\theta + f - 1 \tag{3.23}$$

where θ_C is the Cassie apparent contact angle and f is the fraction of the projected area to the solid surface that is wetted by liquid. Note that surface roughness and fraction play important roles in both Wenzel and Cassie models.

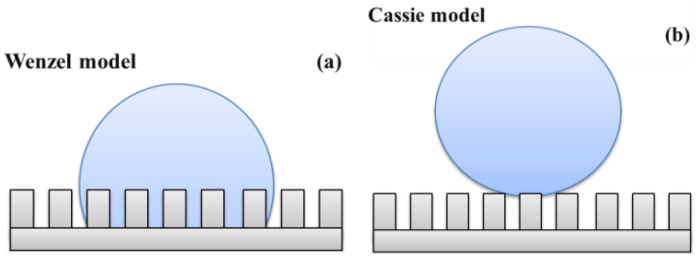

Figure 3.8. Schematic of liquid droplets on non-ideal surface: (a) Wenzel model and (b) Cassie model.

Factors *r* and *f* shown in Eqs. (3.22) and (3.23)) are mathematically correlated to degree of roughness of solid surface (Ma *et al*., 2012). The roughness values are measurable factors obtained using surface topography analyzers such as contact profilometers and atomic force microscopes (AFMs). For roughness values estimation using an AFM, the arithmetical mean roughness, r_a, and root mean square roughness, r_q are calculated using the following equations:

$$r_a = \frac{1}{MN}\sum_{j=1}^{N}\sum_{i=1}^{M}\left|\eta\left(x_i, y_i\right)\right| \tag{3.24}$$

$$r_q = \sqrt{\frac{1}{MN}\sum_{j=1}^{N}\sum_{i=1}^{M}\left|\eta^2\left(x_i, y_i\right)\right|} \tag{3.25}$$

where, *M* and *N* are the number of samples per line and the number of lines, respectively. η (x_i, y_i) is the mean height of all the points on the surface.

3.2.5.3 Principle of atomic force microscopy (AFM)

AFM is one of the scanning probe microscopy (SPM) techniques which is commonly used to study chemistry and morphologies of both electrically conductive and non-conductive surfaces. An AFM usually consists of six main components including a probe (sharp tip, with the radius less than 10 nm), a flexible cantilever, a piezoelectric actuator, a laser source, a feedback controller with a data processor, and a position-sensitive laser detector. All of these components are shown in Fig. 3.9. AFM acquires tip-sample forces at a very close working distance, normally between 0.2-10 nm, by detecting the cantilever deflection while the tip gently touches the surface of the sample. The correlation between the degree of tip deflection and tip-surface force can be explained using Hooke's law:

$$F = -kx \tag{26}$$

where *F* is force; *k* = spring constant; and *x* is cantilever deflection. The spring constant of the cantilever vary between 0.1 to 200 N/m. typically, there are three main operating modes in AFM

namely contact mode (probe-surface distance is less than 0.5 nm), intermittent or tapping mode (working distance is between 0.5 and 2 nm), and non-contact mode where the working distance in a range of 0.1 to 10 nm.

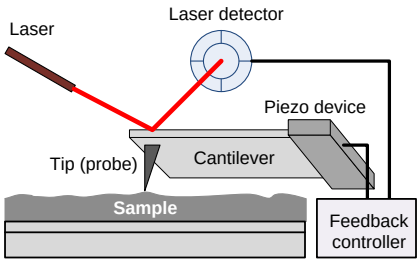

Figure 3.9. Basic components of an AFM

When the AFM is operated in contact mode, the degree of cantilever deflection is fixed at a constant value determined by a feedback control mechanism, as a result the forces between the probe and the sample remain constant. Fast scanning rate and higher image resolution are the major advantages of contact mode; however, the tip may deform or destroy the surface of the soft samples. In tapping and non-contact modes, the cantilever oscillates (raster scans) at near-resonant frequency (ω) excited by a piezoelectric element. While being operated in the tapping mode, the tip lightly taps the surface of the sample. Because the contact time is much shorter than that of the contact mode; thus, the lateral force is significantly reduced. Therefore, the tapping mode is normally used for imaging soft samples such as polymers, carbon nanotubes, and thin films (De Oliveira *et al*., 2012).

Whereas, the non-contact mode allows the tip to oscillate above the surface without touching it. The topography of the surface is calculated based on the changes in amplitude of the oscillation at a constant resonant frequency (ω). Despite the fact that the forces applied on the sample are relatively low (at the magnitude of 10^{-12}N) which does not affect the soft structure of the measuring surface, the resolution obtained from non-contact mode is significantly lower than that of the other two methods. Additionally, the topographic data is possibly distorted where contaminant layer i.e., water is present. However, this problem is generally solved when the

measurement is carried out under ultra-high vacuum (UHV) environment. For food safety applications, AFM was utilized to rapidly detect and quantify the presence of pathogenic microorganisms such as *E. coli* on solid substratum (Yang and Wang, 2008).

4. MATERIALS AND METHODS

This chapter explains methods and materials used for designing, fabrication, optimization, and evaluation of anti-biofouling performances of the developed nanoengineered surfaces. Depending on the types and targeted bioflouing, five different biofouling resistant surfaces were utilized in this study. These nanoengineered surfaces include (i) superhydrophobic multiwalled carbon nanotubes (MWCNTs)-polytetrafluoroethylene (PTFE or Teflon) composite and PTFE coatings for minimizing the formation of milk foulant on plate heat exchanger surface during pasteurization; (ii) superhydrophobic (MWCNTs-Teflon) and superhydrophilic (Titanium dioxide, or TiO_2) surfaces for prevention of microbial adhesions in dynamic and stagnant environments; (iii) slippery liquid infuse surface (SLIPS) for reduction of complex food debris and bacterial biofilms; (iv) nanoporous and nanopillared aluminum oxide (Al_2O_3 or AAO), and (v) nanoporous stainless steel surfaces for controlling bacterial attachments to solid substrata. Table 4.1. shows the summary of major materials used for all nanoengineered surfaces.

Table 4.1. List of main materials used for individual nanoengineered surfaces

		Surface				
Material	**Specifications**	**#1**	**#2**	**#3**	**#4**	**#5**
Aluminum	99.9995%				■	
Nanotubes	MWCNTs	■	■	■		
Stainless steel 316	Finish #4	■	■	■		
Stainless steel 316	Finish #8					■
Teflon	PTFE-30	■				
Teflon	AF-1600		■	■	■	
Titanium dioxide			■			

Remarks: *#1 superhydrophobic MWCNTs-Teflon composite coating for minimizing the formation of milk foulant on plate heat exchanger surface during pasteurization; #2 Superhydrophobic MWCNTs-Teflon and superhydrophilic TiO_2 surfaces for prevention of microbial adhesions in dynamic and stagnant environments; #3 SLIPS for reduction of complex food debris and bacterial biofilms; #4 nanoporous and nanopillared AAO surfaces, and #5 nanoporous stainless steel surfaces for controlling bacterial attachments to solid substrata.*

4.1. Materials

The following materials and chemicals were used during nanoengineered surface designs and fabrications:

4.1.1. Food samples

Three samples of each liquid including homogenized pasteurized cow milk, vegetable oil, ketchup, and honey were purchased from a local store (Honolulu, HI). Then, the representative test liquids were obtained after mixing equal portion of three collected samples using a mechanical blender.

4.1.2. Bacterial strains and culture media

Frozen stocks of *Escherichia col*i K-12, *Staphylococcus aureus*, and *Listeria monocytogenes* were kindly provided by Dr. Yong Li (Food Microbiology Lab, University of Hawaii at Manoa, Honolulu, HI). BD Bacto peptone, BD BBLTM trypticase soy broth, and BD Difco plate count agar were procured from VWR (West Chester, PA).

4.1.3. Metal substrates

Super-corrosion-resistant type stainless steel 316 plates with surface finish #4 or satin finish (for plate heat exchanger surface, superhydrophobic, superhydrophilic, and SLIPS coatings) and finish #8 or mirror-like finish (for nanoporous steel surface) were supplied from McMaster-Carr (Chicago, IL). According to specifications provided by the manufacturers, the plates were designed in accordance with ASTM A240, ASTM A167 and MIL-S-5059 (suitable for food processing, handling and drastic CIP process). The compositions of the stainless steel were 16-18% chromium; 10-14% nickel; 0-0.08% carbon; 0-2% manganese; 0-0.75% copper; 0-3% molybdenum; 0-1% silicon; 0.03% sulfur; 0-0.045% phosphorous; 0-0.1% nitrogen; and iron

makes up the remaining percentage. High purity aluminum (99.9995%) and platinum foils (99.99%) were manufactured by ESPI Metals (Ashland, OR).

4.1.4. Nanomaterials and coating substances

Chemical vapor deposition (CVD) grown MWCNT, (>95% nanotubes, 1–2 μm long, 10–30 nm in an outer diameter) was purchased from SES research (Model number 900–1201-5G, Houston, TX). Tetra-n-butyl titanate solution for titanium dioxide coating was obtained from Sigma-Aldrich (St. Louis, MO).

Water-based PTFE emulsion (PTFE-30, Fuel Cell Earth LLC, Boston, MA) containing 60% w/w of 0.2–0.5 μm PTFE particle was used for plate heat exchanger experiment only. The amorphous Teflon or TAF resin used for the rest of the surface coatings (Poly[4,5-difluoro-2,2-bis(trifluoromethyl)-1,3-dioxole-co-tetrafluoroethylene] or Teflon AF-1600) was purchased from Sigma-Aldrich (St. Louis, MO). Liquid lubricant or Krytox GPL 105 (manufacturer specs: boiling point 200°C; surface tension 17 mN/m; kinematic viscosity 800 cP; NSF certified H-1 food grade lubricant) was purchased from McMaster-Carr (Elmhurst, IL). Polydimethylsiloxane (PDMS; Sylgard 184 silicone elastomer curing agent and base) was ordered through Dow Corning (Midland, MI).

4.1.5. Other chemicals

Acetone (95-100%), ethyl acetoacetate (EAcAc, >99%), ethyl alcohols (95% and 99.5%), ethylene glycol (anhydrous, 99.8%), fluorinert (FC-40), hexamethyldisilazane (HMDS, 99.9%), oxalic acid (99.999%), perchloric acid (70%), phosphoric acid (85%), and sulfuric acid (99.999%) were supplied from Sigma-Aldrich (St. Louis, MO). Excepted as described otherwise, all chemicals were ACS grade. All chemicals were used as received without any further purification.

4.2. Methods

4.2.1. Fabrications of nanoengineered surfaces and fouling chambers

4.2.1.1. Superhydrophobic MWCNTs-PTFE coating for milk pasteurization

- Superhydrophobic 5%w/w MWCNTs-Teflon PTFE-30 coating using spin coating technique

Water-based PTFE emulsion (PTFE-30) was used as a polymer matrix for heat exchanger coating. The MWCNT nanoparticles were well introduced and disintegrated into the PTFE solution by ultrasonication for 30 min (Branson Digital Sonifier 450, 400 W, Danbury, CT). The final concentrations of MWCNTs in PTFE solution were controlled to range from 0 to 5% CNTs (w/w). The prepared CNT-PTFE nanocomposite solution was spin-coated on a cleaned and degreased stainless steel surface. A uniform MWCNTs-PTFE film on stainless steel surface was obtained by two-step processes: the plate was constantly held at 100°C for 10 min to allow the water in the mixture to completely evaporated. Thereafter, the plate was kept in a furnace at 360°C for an hour to melt down all PTFE content onto the surface. The nanomorphologies of the developed coating film was determined using a FESEM (Hitachi S-4800, Biology Department University of Hawaii at Manoa). The average thickness of coating film measured by digital micrometer (Mitutoyo electronic outside micrometer, accuracy ± 0.001 mm, Aurora, IL) was 11 ± 0.03 μm.

- Test plate heat exchanger unit

The homogenized pasteurized cow milk was warmed to room temperature before pasteurization using a custom-designed test PHE unit was performed. A 2×5 inch stainless steel 316 plate was used as a heat exchanger surface. The plate was coupled with a plexiglass sheet and round rubber gasket to build up a single channel PHE unit (Fig. 4.1.) that could hold 20.5 ml of milk and permitted the flow rate of 52.7 ml min^{-1}. Inlet and outlet temperatures of pasteurizing milk were measured and recorded by a data acquisition unit (Agilent 39704A, Agilent

Technologies, Inc., Palo Alto, CA). Heat-treated milk was cooled down to room temperature for recirculation process. The cooling process was performed using a custom-made tubular heat exchanger. To simulate the initial heating section of the industrial milk pasteurization process, the heat flux for the heat transfer surface was controlled to be constant and consequently the surface temperature was fixed at 72°C. The constant surface temperature was obtained by adjusting input voltages for an array of six resistive heaters (Wirewound Resistors 50 W 330 ohms, Vishay Intertechnology, Inc., CT) using a variable transformer (Fig. 4.1b). The measured inlet and outlet temperatures of milk during heating process were 20 ± 2.5 and 60 ± 0.7°C, respectively.

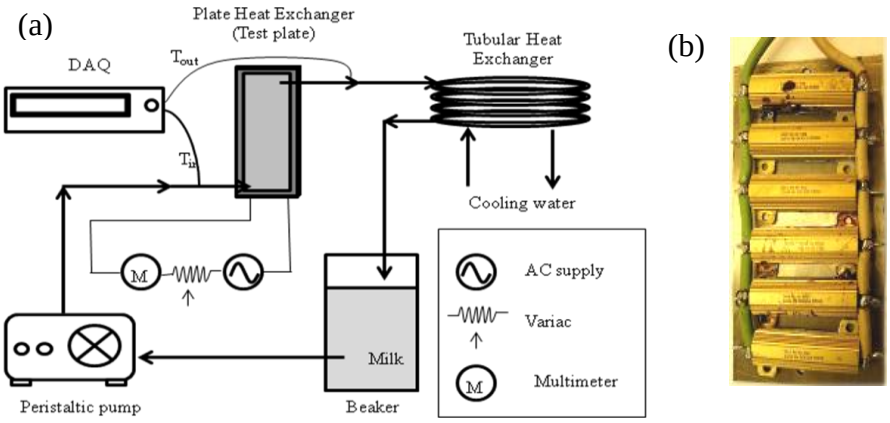

Figure 4.1. (a) Schematic diagram of custom-designed PHE unit and (b) array of resistive heaters on the test plate.

- *Quantification of milk foulant on PHE surface*

Weights of milk foulants on uncoated, PTFE-coated, and MWCNTs-PTFE with 5% MWCNTs (w/w) coated stainless steel surfaces during the heating process were compared. After the first hour of the pasteurization process, the test stainless steel plate was carefully dissembled from the array of heating elements on the back side and its round rubber gasket on the front side. The plate with milk deposits accumulated on its surface was immediately brought to an analytical balance to weigh mass differences. After weighing was done in triplicate, the test plate

was reassembled with the heat resources and the gasket to further undergo a continuous pasteurization. The weighing process for different surface coatings was carried out under the same protocol. In addition, the microstructure of foulant was investigated using FESEM imaging technique.

4.2.1.2. Superhydrophobic MWCNTs-PTFE and superhydrophilic TiO_2 surfaces for microbial adhesion tests

Super-corrosion-resistant type stainless steel 316 plates with surface finish #4 were used as control (uncoated) and substrates for superhydrophobic and superhydrophilic coating. The test steel plates (125 mm×50 mm×1 mm) were prepared and ultrasonically cleaned with acetone, ethanol and distilled water for 10 min, respectively. After dried in the air, plates were separated into three groups including control (uncoated steel), carbon nanotubes–polytetrafluoroethylene (MWCNTs–Teflon PTFE-30) nanocomposite coating (superhydrophobic) and TiO_2 nanocomposite coating (superhydrophilic).

- *Superhydrophilic TiO_2 coating*

The deposition of TiO_2 nanocomposites onto a stainless steel surface was carried out using a sol–gel method which was slightly modified from the work of Shen *et al*. (2005). In brief, 20 mL ethanol was mixed with 1 mL ethyl acetoacetate (EAcAc) at room temperature; 4 mL of tetra-n-butyl titanate was added to the mixture and kept stirring for an hour. 0.2 mL of deionized water was gently added to the solution for hydrolysis. After aging for 24 h, the aged titanium dioxide solution was spin-coated on the prepared steel plate at a rotational speed of 200 rpm. The wetted stainless steel surface was primarily heated at 150°C for 15 min to completely evaporate water from the surface. The surface coating and primary drying steps were repeated three more times in order to create the desired thickness of TiO_2 layers on the surface.

The dried steel plate was further brought to the final drying step, annealing, in an electronic furnace at 450°C for 30 min, where the superhydrophilic feature of the stainless steel

plate was achieved by the oxidation process of the deposited TiO_2 particles. In addition, the TiO_2 coated plate was further hydrothermally treated by submerging into boiling water for 10 min followed by reheating at 450°C for 10 min in order to prevent TiO_2 carrier, i.e., EAcAc, from cracking on the surface. The plate was cooled down in the air until it reached room temperature before being rinsed with deionized water to wash away excessive TiO_2 particles from the surface.

- *Superhydrophobic MWCNTs-Teflon PTFE-30 via spray coating*

The protocol to fabricate the superhydrophobic surface was modified from the method developed by Wang *et al*. (2010). The process started by mixing 0.1% wt of MWCNTs in 95% ethanol in a sonicating bath for 2 h. The MWCNTs dispersion was continuously sprayed onto PDMS-coated stainless steel plate, which was placed on a hot plate while being held at the temperature of ca. 90°C, until the desired thickness was achieved (thickness of MWCNTs was ca. 5 µm). To optimize the hydrophobicity of the porous MWCNTs layer, the deposited MWCNTs film on PDMS surface was cured in a furnace at 150°C for 1 h. In order to enhance the durability of the superhydrophobic surface, water-based PTFE suspension (Teflon, PTFE-30) was then spin-coated on the top of the CNT coating layer at 500 rpm for 1 min. The developed MWCNTs–PTFE nanocomposite was kept inside the furnace at 360°C for 1 h to completely melt cure Teflon in the composite. The WCA value of the MWCNTs–PTFE coated stainless steel was 154.6 ± 6° (superhydrophobic). Superhydrophobic effect of such developed MWCNTs–PTFE composite would be mainly due to entangled orientation of hydrophobic MWCNTs that contained micro-scale air pockets incorporated with low-surface energy fluorine-containing group of PTFE.

- *Bacterial adhesions test chamber*

All three test stainless steel 316 plates (125 mm×50 mm×1 mm) were individually coupled with an acrylic sheet and rubber gaskets to build up a parallel flow channel holding 20.5 mL of bacterial suspension (Fig. 4.2. (a) and (b)). Bacterial adhesion tests in static and dynamic

conditions were performed using the same flow chamber with different flow rates. Estimations of wall shear rate ($\dot{\gamma}$) and Reynolds number (N_{RE}) for rectangular liquid flow channel, i.e. duct or infinite parallel plane plates (IPPP) can be calculated based on the relation of channel's geometry and flow rate (Busscher and van der Mei, 2006), given by

$$\dot{\gamma} = \frac{3Q}{2(h_0/2)^2 w_0} \tag{4.1}$$

$$N_{RE} = \frac{\rho Q}{(w_0 + h_0)\eta} \tag{4.2}$$

where Q is the volumetric flow rate of the bacteria suspension (200 mL/min or 3.33×10^{-6} m^3/s in dynamic conditions), h_0 and w_0 are height and width of cross-sectional flow path ($h_0 = 3.3\times10^{-3}$ m and $w_0 = 5.0\times10^{-2}$ m), ρ is the solution density (1025 kg/m^3), and η is the solution viscosity (1.25×10^{-3} kg/m s). For proposed dynamic tests, the flow pattern inside the flow chamber was simulated using COMSOL Multiphysics software (COMSOL 4.1, COMSOL, Inc., Palo Alto, CA), which the program codes were similar to our previous computational fluid dynamics (CFD) study (Choi *et al*., 2012).

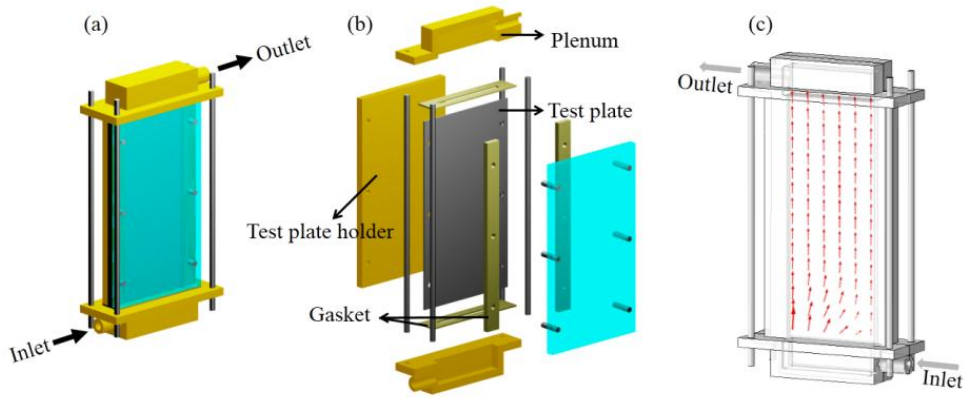

Figure 4.2. Schematic representations of test unit: (a) flow chamber,(b) exploded view and (c) simulated velocity profile-COMSOL data.

As a result of CFD simulation, the uniform velocity profile of the suspension flowing at 200 mL/min inside the flow chamber was clearly observed (average fluid velocity was 1.6×10^{-2} m/s), indicating that the laminar flow scheme was developed from the rectangular opening (Fig. 4.2 (c)). The calculated shear rate and Reynolds number in the dynamic flow environment were 37 s^{-1} and 51.3 (less than 2000, laminar flow regime), respectively.

4.2.1.3. Design and fabrication of slippery liquid infused porous surface (SLIPS)

- Krytox-infused MWCNTs-amorphous Teflon (Teflon AF-1600) composite

The fabrication method of a superhydrophobic MWCNTs porous structure used in this section was similar to the method previously described in section 4.2.1.2. However, in order to preserve the porosity of the nanotubes structures, the MWCNTs coating was reinforced using a thin layer of hydrophobic polymer i.e., Teflon AF-1600 polymer instead of Teflon PTFE-30.

The Teflon AF-1600 coating was carried out through a three-step process. First, adhesive hydrophobic layer of hexamethyldisilazane (HMDS) was promoted on the MWCNTs by spin-coating at 3000 rpm for 30 s followed by heating at 112°C for 10 min. Second, 0.2% wt of Teflon AF-1600 in FC-40 solvent (dissolving time was 4 days) was by spin-coated on the nanotubes at 1000 rpm for 60 sec followed by heating at 165°C for 5 min. Finally, the coating was sintered at 330°C for 15 min using a Thermolyne furnace (model FB1415M, Thermo Scientific, Dubuque, IA).

After air-cooling to room temperature, microporous structure of prepared MWCNTs-Teflon AF composite was infused with a lubricating liquid, perfluoroalkylether (i.e., Krytox 105), by applying droplets of lubricant to the porous coating layer. Afterward, the lubricating liquid was left on the microstructure at least 10 hours for completing the infusion process, then the excess amount of lubricant was removed by tilting the infused surface vertically for 4 hours (Xiao *et al*., 2013). The SLIPS fabrication steps are summarized and shown in Fig. 4.3.

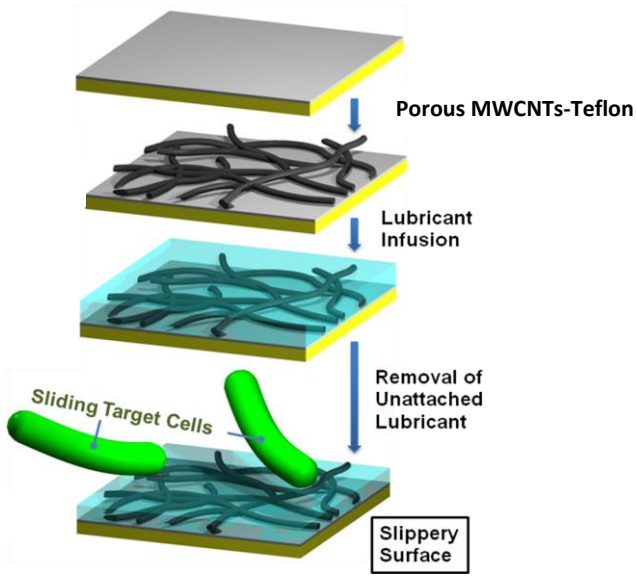

Figure 4.3. Schematic of SLIPS coating process on stainless steel.

4.2.1.4. Nanosmooth, nanoporous and nanopillared aluminum oxide surfaces

The fabrication of nanoporous and nanopillared alumina samples was carried using the following steps (Hizal *et al*., 2014). High purity (99.995%) aluminum foils were cut into 10 ×20×1 mm (width×height×thickness) cleaned and degreased in acetone, ethanol and deionized water by an ultrasonic cleaner for 10 min, respectively. Subsequently, the surface irregularities on each aluminum specimen was removed using electropolishing where a mixture of perchloric acid and 99.5% ethanol ($HClO_4/C_2H_5OH$ = 1:4 v/v) was used as an electrolyte. The process was continued in a stirred two-electrode glass jacketed beaker (250 mL) under an applied potential of 20V for 2 min. The temperature of the electrolyte was kept at 7°C by a circulation cooling water bath.

Thereafter, the electropolished specimen (nanosmooth) was used as a working electrode (anode), and a platinum foil was employed as a counter electrode (cathode) in an electropolishing/anodizing system shown in Fig. 4.4. The two electrodes were separated by a distance of 5 cm. The same experimental setup for electropolishing was also used for the surface

anodization; however, the solution temperature was kept at 15°C and 0.3M oxalic acid was now used as an electrolyte. The electrical voltage of 45V was continuously applied on both electrodes for 15 min to develop approximately 1μm-thick porous aluminum oxide (Al_2O_3 or AAO) layer on the surface of the anode.

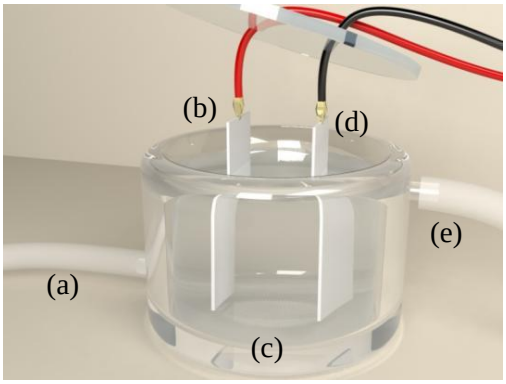

Figure 4.4. Schematic of surface electropolishing/anodizing apparatus (a) water inlet, (b) anode (aluminum or stainless steel), (c) 250 mL jacketed beaker, (d) counter electrode or cathode and (e) water outlet.

In order to fabricate the pillared alumina structures, the porous sample was then etched in 5% wt. phosphoric acid for 35 min. Fig. 4.5 shows a schematic comparison of all aluminum surfaces used in this study. As can be seen in the schematic, the pillared alumina surface was achieved after rapid drying of the carpet-like structure in the air. For the hydrophilic surface condition of the nanoporous and nanopillared samples, the hydrophilicity of both aluminum oxide surface was used without any further modification.

For hydrophobic surface treatment, the fabricated surface samples were coated with a thin layer of hydrophobic polymer, i.e. Teflon AF-1600. The samples were spin-coated with 0.1% of Teflon AF-1600 in FC-40 solution at a 1000 rpm with a ramp of 500 rpm in 30 s which followed by an annealing at 330°C for 15 min. The resulting surfaces with a uniform hydrophobic Teflon coating with less than 10 nm in thickness were obtained. Finally, the

samples were rinsed by 95% ethanol and water for 5 min and then dried in air for 1 day before used.

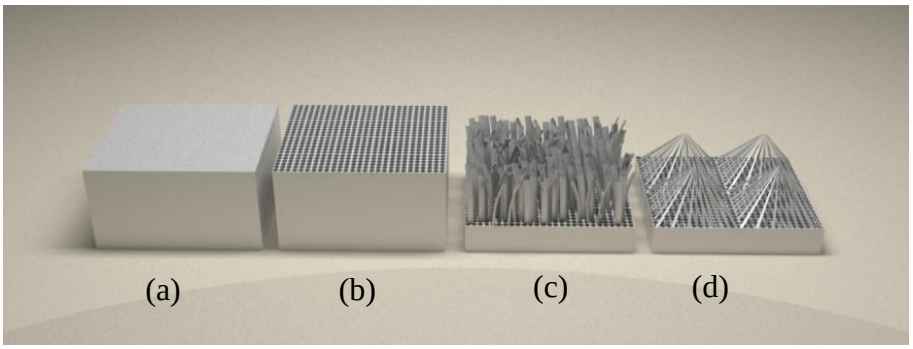

Figure 4.5. Schematic of aluminum surfaces (a) nanosmooth surface (control) obtained after electropolishing, (b) nannoporous surface porous aluminum oxide layer achieved after anodization, (c) carpet-like surface:this type of aluminum oxide structure was developed after the nanopores were widened in 5% wt phosphoric acid and (d) pillared surface: bundlled aluminum oxide carpets induced by capillary force exerted during rapid drying.

4.2.1.5. Nanosmooth and nanoporous stainless steel surfaces

Stainless steel plates 316 with a surface finish #8 (i.e., mirror-like) on one side were cut into 15×30×1 mm (width×height×thickness). The samples were cleaned and degreased by ultrasonicating in acetone, ethanol, and deionized water for 10 min, respectively. After cleaning, steel specimens were separated into two groups for further electropolishing and anodization treatments. The electropolishing process was accomplished in following steps (Lafiti *et al.*, 2013): the cleaned and dried specimen was etched in a mixture of phosphoric acid and sulfuric acid (60%:40% volumertic ratio). Electropolishing was conducted in a glass jacketed beaker (250 mL). During electropolishing, the steel plate served as an anode (working electrode) while a sheet of platinum foil was used as a cathode (counter electrode).

The working electrode was partially submerged into the electrolyte to keep the total etching area of 2×1 cm^2 (including back and front sides of the specimen). The space between the

two electrodes was fixed at 6 mm. The electrochemical process was completed in 10 min at a constant electrolyte temperature of 80°C at a fixed applied voltage of 3.5V without agitation for 10 min. Thereafter, the electropolished sample was rinsed with 95% ethanol and deionized water and subsequently dried under a stream of compressed air. The counter electrode was also rinsed with 95% ethanol and deionized water and stains, if any, on its surfaces was removed using a bunsen burner.

Nanoporous stainless steel was fabricated by anodizing the degreased specimen in a 5% vol. of perchloric acid in anhydrous ethylene glycol. At this step, the back side (unpolished surface) of the specimen was covered with a water resistant tape to prevent the effect of surface irregularities on the intensity and direction electric field. After that, the taped specimen was served as an anode and a platinum foil was used as an anode. The applied voltage and anodization time were varied to obtained different pore diameters. In order to obtain 50 and 80 nm in pore diameters, the anodizing voltage and time combinations were 40V for 10min and 50V for 35min, respectively.

4.2.2. Surface characterizations

4.2.2.1. Contact angle and sliding angle measurements

Static contact angle (CA) and sliding angle (SA) (degree of surface tilting required to initiate the movement the test liquids e.g., water, food debris or bacterial suspensions) of the surfaces were measured using an FTA-1000 contact angle goniometer (First Ten Ångstrom, Portsmouth, VA). The CA was determined using 5µL sessile droplet test that was previously reported in the literature (Wang *et al*., 2010). To determine the slipperiness of the SLIPS, the plate was placed on a horizontally leveled platform of the goniometer. Then, a 5 µL of each sample was introduced to the surface using a liquid dispenser. The platform was gradually tilted until the resting liquid started to slide. The tilting angle of the goniometer platform was recorded using a digital camera and used as SA data. The CA and SA were presented in the average values of five readings (n=5) performed on different spots along the prepared surfaces.

4.2.2.2. Surface morphologies study using field emission scanning electron microscope (FESEM) and atomic force microscope (AFM)

A field emission scanning electron microscope or FESEM (Hitachi S-4800, Biological Electron Microscope Facility, University of Hawaii at Manoa) and two atomic force microscope (AFMs) namely N-Tracer Scanning Probe Microscope which was equipped with carbon nanotube tip (10–30 nm in diameter and <1 μm in length, NanoFocus, Inc., Korea) and tapping mode using Nanosurf NaioAFM (Nanosurf, Inc., MA) with silicon tip coated with reflective aluminum coating (Budget Sensors, Model no. Tap 190Al-G, resonant frequency 190 Hz, cantilever spring constant 48 N/m) were used to visualize the micro/nanoscale surface morphologies and determine surface roughness of the developed surfaces (measured areas in the rage of 1x1 μm^2 to 10x10 μm^2).

Average roughness (r_a) and root mean square roughness (r_q) of each sample were analyzed from the corresponding AFM micrographic data using WSxM (V.5.0) software developed by Horcas *et al*. (2007). In some cases, the AFM images were also analyzed using Gwyddion (Nečas and Klapetek, 2012) or SPIP (Trial version, Image Metrology, Hørsholm, Denmark) software packages.

4.2.3. Preparation and quantification of surface adhering bacteria and biofilms

4.2.3.1. Bacteria preparation

In this research, the laboratory strains of *E. coli* K-12 and *S. aureus* and *L. monocytogenes* were used as bacterial models for evaluating the anti-bacterial attachment attributes of developed nanocomposite surfaces during stagnant and dynamic adhesion tests. Frozen stocks of both *E. coli* K-12, *S. aureus* and *L. monocytogenes* cells were separately activated grown in tryptic soy broth (TSB) at 37°C for 24 h twice before testing. Thereafter, bacterial cell pellets were collected after the TSB suspension was centrifuged at 4500 rpm for 5 min, washed with sterile deionized water and suspended in 100 mM phosphate buffer saline

(PBS) at a pH of 7.1–7.3 (Li and Logan, 2004). The initial concentrations of bacteria in PBS solution enumerated by plate count agar were in the range of $1.9-3.2\times10^{8}$CFU/mL, depending on the types of the strains and varied among experiments.

4.2.3.2. Bacteria quantification

To perform the stagnant adhesion test, the prepared bacterial suspension was held inside a pre-cleaned test chamber. Otherwise, the bacterial suspension was used for dynamic adhesion test where the suspension was continuously pumped through the chamber at the flow rate of 200 mL/min. The sterile silicone tubes and beakers were used in all adhesion protocols and both experiments were controlled to run for an hour. Subsequently, loosely adherent bells on the surface of the test plate were gently rinsed off and discarded by rinsing with 1 mL of sterile deionized water.

Rinsed plates were dried in the air then a droplet of fluorescence stain namely 4,6-diamidino-2-phenylindole (DAPI) and a glass cover slip were placed on the surfaces in order to make bacterial cells easily observed under the fluorescence microscope (Olympus BX 51, with 10X 20X and 40X (object lenses) and 10X (eyepieces) in magnifications, Biological Electron Microscope Facility, University of Hawaii at Manoa). The DAPI droplet was allowed to completely penetrated and stained cells by keeping the stained samples in the dark environment for at least 5 min before observation was performed. The corresponding fluorescence intensity (FI) of each surface was determined by ImageJ software (National Institutes of Health, Bethesda, MD) with Edge Ratio macro plug-in (V.1.1.1). Standard aerobic plate count of bacteria on the surfaces using plate count agar (PCA) were also performed.

For PCA method, the bacterial cells adhered to the surfaces were gently removed by applying sonication. This method was slightly modified from the work previously reported by Zhao *et al.* (2008) which the adhered plate was placed in a sterile beaker containing 500 ml of sterile peptone water. The beaker and sample were subsequently put in an ultrasonic bath and sonicated for 10 min. The temperature of distilled water in the beaker was monitored by

thermocouple and did not exceed 25°C. Thereafter, 100 µL of ultrasonicated suspension and its serial dilutions (10^{-1}, $10^{-2}$and 10^{-3}) were plated on PCA in duplicate, and incubated overnight at 37°C. Aforementioned adhesion assays and measurements were done in a triplicate.

In order to evaluate the anti-biofilm performance of the SLIPS, bacterial suspensions were separately inoculated on test surfaces e.g., stainless steel (control), and the slippery surface for 7 days at room temperature in sterile polystyrene petri dishes. Thereafter, bacterial suspensions and their biofilms were removed from the test plates by tilting the plates vertically for 2 min, followed by rinsing the tilted plates with 5 mL of sterile deionized water and followed by air-drying. Subsequently, the dried specimens were separated into two groups for different characterization purposes e.g., (i) the remaining surface adherent bacterial cells were observed using a fluorescence microscope and (ii) the biofilm residuals were quantified using spectrophotometric method. The former samples were stained with a droplet of DAPI. For the latter samples, substrata were carefully rinsed with PBS, followed by 0.1% w/v crystal violet solution for 20 min. Then, the elution of crystal violet on each stratum was performed using 4 mL of 99.5% ethanol. The amounts of eluted bacterial biofilms were measured using a spectrophotometer (Genesys 20 Visible spectrophotometer, Thermo Electronic, Waltham, MA) at 590 nm or OD 590 (Epstein *et al.*, 2012). The measured absorbance values were used to indicate the concentration of the remaining bacterial cells and biofilms in the eluents, and the results were reported as an average value of three readings.

4.3. Statistical Analysis

Three replications were performed for each experiment (n=3). The statistical differences were determined using a one-way analysis of variance (ANOVA) method followed by a Duncan's multiple range test. The values reported are mean values with standard deviation. The resulting statistical analyses with significantly difference/similar were presented with superscript letters when the probability was less than 0.05 (95% confidence level).

5. RESULTS AND DISCUSSION

5.1. Effects of Superhydrophobic multiwalled carbon nanotubes (MWCNTs)-polytetrafluoroethylene (PTFE) coating on Milk Foulant on Plate Heat Exchange Surface (Objective 1)

Cleaning of milk fouling on plate heat exchanger surface causes intermittent downtime to milk processing industry. Fouling occurs during milk pasteurization potentially reduces the heat transfer rate of plate heat exchangers (PHEs), leading to serious energy deficiency. The morphologies and micro/nanostructures of PTFE and MWCNTs-PTFE nanocomposite coated surfaces were illustrated by FESEM. A FESEM image of PTFE coating (Fig. 5.1 (a)) shows that the melting condition was completed because the PTFE coating layer was smooth and uniform. The ultrasonicating and annealing processes played crucial roles in uniform distribution of MWCNT nanoparticles into the PTFE matrix. These preparation steps successfully built a hybrid nanocomposite surface which possesses high wear resistance as well as high hydrophobicity. Fig. 5.1 (b) shows that well-regulated MWCNT nanoparticles were partially anchored with PTFE leaving some parts uncovered by the matrix. The PTFE-merging parts of the nanotubes significantly strengthened the overall durability of the composite coating while the unconcealed parts increased the micro/nanoscale surface roughness leading to the development of superhydrophobicity regime of the composite. Typically, MWCNTs have high Young's moduli (1.8 TPa, Chen *et al*., 2003), and thermal conductivity (600 W $m^{-1}K^{-1}$, Moisala *et al*., 2006). Therefore, the addition of the MWCNTs into the PTFE matrix enhanced mechanical properties of the resulting composite The estimation of thermal conductivity of the uniformly blended MWCNTs-PTFE coating can be estimated using the following correlation previously provided by Moisala *et al.* (2006);

$$\frac{K_e}{K_m} = 1 + \frac{fK_{CNT}}{3K_m} \tag{5.1}$$

where K_ε = effective thermal conductivity of composite, $K_m = K$ of matrix (0.25 W m^{-1} K^{-1}, Xie *et al.*, 2005), $K_{CNT} = K$ of nanotubes (600 W m^{-1} K^{-1}) and f_{CNT} = mass fraction of filler).

According to this estimation, the MWCNTs-PTFE composite contains 5% CNTs is 10.25 W m^{-1} K^{-1}. It can be noted that the thermal conductivity of MWCNTs-PTFE nanocomposite is closer to that of food grade stainlesssteel (16.3 W $m^{-1}K^{-1}$), compared to the unfilled PTFE.

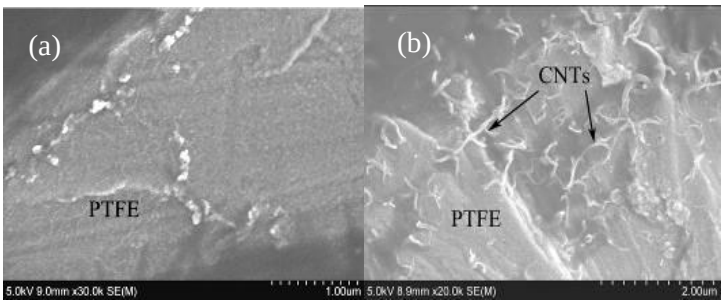

Figure 5.1. FESEM images of (a) PTFE and (b) 5% w/w MWCNT-PTFE nanocomposite films on stainless steel 316 surface.

FESEM image of the dried milk protein foulant (Fig. 5.2) shows a high porosity structure of denatured milk protein. These pores might decrease the heat and mass transfer coefficients of milk during pasteurization process. The surface foulant potentially initiates the adhesion of bacteria on fouled heat exchanger surface by accommodating a shelter from heat and shear force (Murray and Deshaires, 2000) which eventually contaminates into food, questioning food safety

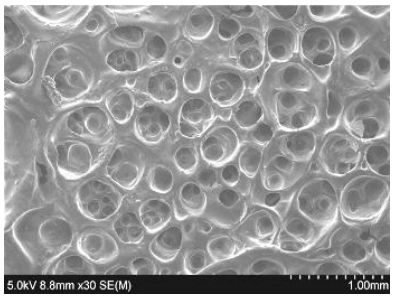

Figure 5.2. FESEM image of milk foulant on heat exchanger surface.

Fig. 5.3 compares the behaviors of a water droplet on the developed MWCNTs-PTFE nanocomposite surface and the control. It can be seen that the nanocomposite coating can prevent the water droplet from being adsorbed to the surface. The water repellent phenomenon

observed in a nature, which is so called ‘‘lotus effect’’, led to the development of a self-cleaning surface which the surface impurities will be swept away from surface by mean of flowing water. Self-cleanability of the targeted surface was achievable when the WCA value approaches 140−150° and more. The water droplet falling on the MWCNTs-PTFE nanocomposite coated surface actually had sufficient momentum to leave the surface, making several more bounces, eventually bounced off without ever coming to rest on the surface (Fig. 5.3 (a)). On the other hand, no bouncing of water droplet found on the control surface (Fig. 5.3 (b)).

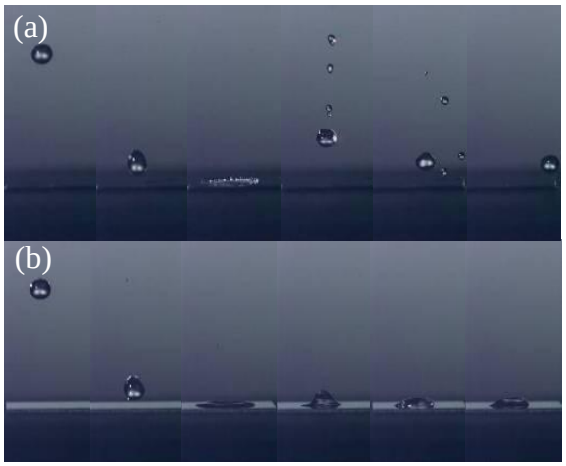

Figure 5.3. Snapshots of a water droplet falling on (a) MWCNTs-PTFE nanocomposite, and (b) control surfaces.

WCAs were measured from sessile droplets of deionized (DI) water of uncoated, PTFE coated and 5% w/w MWCNTs-PTFE coated surfaces were 71.2, 119.6 and 141.1°, respectively (Fig. 5.4.). The superhydrophobicity of the composite coating was due to the fact that MWCNT particles in the dispersed phase dramatically improved micro/nanoscale roughness of base PTFE surface by creating numerous voids which acted as a boundary layer between water and PTFE surface. These voids limited the chance of water surface to come into contact with both base PTFE and stainless steel substrate, resulting in magnification of the water-repellent and self-cleaning surface properties (Xie *et al*., 2005; Nosonovsky and Bhushan, 2009). It should be noted that the nanocomposite coating with 5% MWCNTs (w/w) significantly switched the wettability of the steel substrate from hydrophilic to superhydrophobic, which was only

achievable by aligned MWCNTs coating technique in the past. Integration of superhydrophobic MWCNTs into hydrophobic PTFE matrix made a contribution to an increase in total surface roughness, leading to the extreme non-wettable surface, compared to unfilled PTFE.

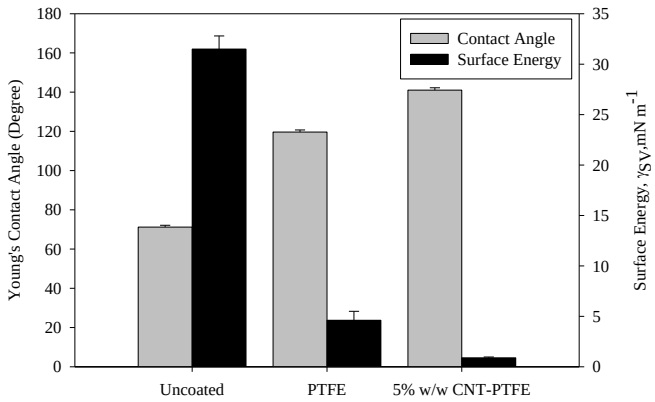

Figure 5.4. Young's contact angles and surface energy values, γ^{SV} , of heat exchanger surfaces with different coating materials.

The surface deposition of milk is mainly caused by the natural milk whey protein namely beta-lactoglobulin (β-Lg). In general, the concentration of β-Lg in cow milk is 0.32–0.37% (de Jong *et al.*, 2002; Bansal and Chen, 2006). During milk pasteurization using the test PHE unit, milk foulant on the surface was a soft-white solid that tended to accumulate at low-flow areas such as corners and gasket over the heating time (Fig. 5.5). The foulant mass per unit area on the control surface after the first hour run was 23.41 mg/cm^2. During the continuous pasteurization, it was found that the weight of the total foulant increased linearly to reach 43.71 and 62.00 mg/cm^2 after 3 and 5 h of pasteurization, respectively (Fig. 5.6).

It can be noticed that the developed PHE unit demonstrated a single channel heating section; therefore, the pressure drop across the heat transfer surface between inlet and outlet was considerably negligible. In addition, this test unit was not a pressurized system which could be normally found in the industrial scale PHEs. As a result, the pattern and weight of the foulants seen on the test surfaces in this study might be different from the larger PHE commonly found in dairy industry. The calculated velocity and Reynolds number of the milk stream during the test

trials were 0.0054 m/s and 170.84, respectively. Since the flow behavior of milk was laminar-type, the mass of the foulants would be higher than industrial PHEs operating at turbulent flow profiles. However, the fouling deposition rates were reduced down when using the coated surfaces, depending on their hydrophobicities. For PTFE coating, the masses of milk deposits collected after a continuous flow of milk for 1, 3 and 5 h were 18.29, 27.44 and 35.34 mg/cm^2, respectively.

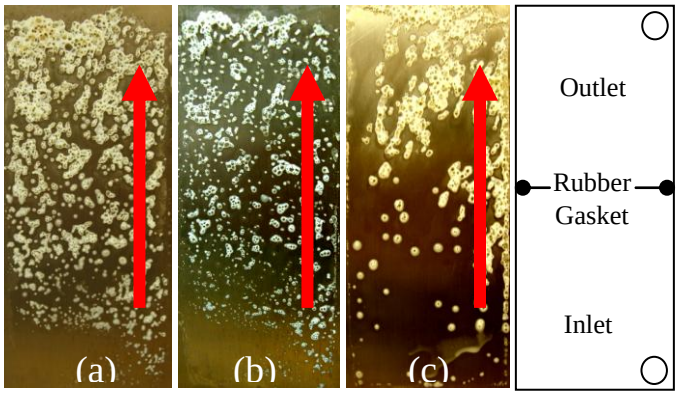

Figure 5.5. Foulants on the test plates after 6 hours of pasteurization (a) control, (b) unfilled PTFE, (c) MWCNTs-PTFE and (d) schematic diagram. Arrows represent the flow direction of milk.

For the foulant on the MWCNTs-PTFE nanocomposite surface, the attachment of protein nucleation on the MWCNTs-PTFE composite was weaker than those onto uncoated and PTFE coated surfaces due the sweeping action caused by the lotus effect on superhydrophobic surface. Therefore, the shear force of milk stream exerted on the surface could sweep away the deposited protein molecules from the surface, resulting in a lower foulant nucleation rate compared to both uncoated and the PTFE coated surfaces when the same pasteurization time was applied. After 1, 3, and 5 h of pasteurization the accumulate foulants on the nanocomposite surfaces were 4.96, 16.74 and 18.45 mg/ cm^2, respectively.

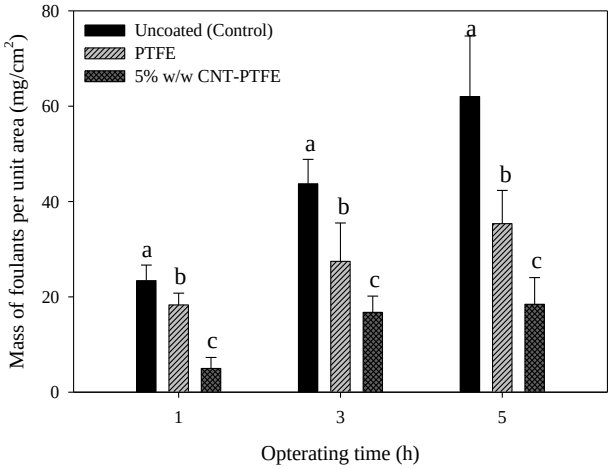

Figure 5.6. The amounts of surface foulants on the test PHE unit collected after different operation times (significant differences ($P<0.05$) within data at the same time indicated by dissimilar letters).

According to the estimation of thermal conductivity of the nanocomposite, the heat transfer rates of the test PHE unit were possibly enhanced by an increased MWCNTs-PTFE thermal conductivity; thus, the estimated total energy consumption of the nanocomposite-PHE was approximately 2844 kJ which was only 89% of the total energy required to heat the milk at the same condition using the uncoated PHE surface, 3168 kJ. It could also be explained that the increased total energy consumption found on the control experiment was affected by the development of milk foulant itself. The foulant was found to significantly impair the overall heat transfer between milk and the heating source during the pasteurization process; as a result, the fouled PHE typically needs 8% in extra energy compared to the clean PHE to achieve the same lethality level to the treated milk product (Balasubramanian and Puri, 2009b). It can be concluded that the amounts of energy required for pasteurization was possibly depended on the milk deposits accumulated on heat exchanger surfaces. There were decreases in the total heat energy consumption required to accomplish milk pasteurization for a period of 5 h by 3.4–10.2% when PTFE and MWCNTs-PTFE nanocomposite coated surfaces were applied. The use of superhydrophobic surface could save the energy consumption for thermal processes by lowering the nucleation and accumulation rates of milk deposits on the PHE surface.

5.2. Effects of Superhydrophobic MWCNTs-PTFE and Superhydrophilic TiO_2 Surfaces on *Escherichia Coli* K-12 Attachment to Stainless Steel Surfaces in Stagnant and Dynamic Environments (Objective 2)

According to the surface wettability and morphologies results, the sensile drop water contact angles (WCAs) of the fabricated surfaces with two different surface wettabilities along with the control (uncoated) stainless steel sample were illustrated compared in Fig. 5.7 (a) to (c). According to the results, the wettability of naturally hydrophilic uncoated stainless steel (WCA 71.2°) was dramatically switched to superhydrophobic (WCA > 150°) and superhydrophilic (WCA < 5°) regimes after coating with titanium dioxide (TiO_2) and multiwalled carbon nanotubes-Teflon (MWCNTs-PTFE) composite, respectively. The morphologies and micro/nanostructures of the control stainless steel plate, superhydrophobic MWCNTs–PTFE and superhydrophilic TiO_2 nanocomposite coated surfaces were illustrated by FESEM and AFM images (Fig. 5.8 (a) to (d). FESEM images of untreated stainless steel and treated with MWCNTs–PTFE coating show that most of the surface crevices appeared on unmodified stainless steel were replaced by a highly entangled MWCNTs layer in conjugation with thin connective PTFE sheets between their structures. The developed MWCNTs and PTFE matrix improved both surface roughness originating from the MWCNTs and wear resistance contributing from the connective PTFE polymeric sheets.

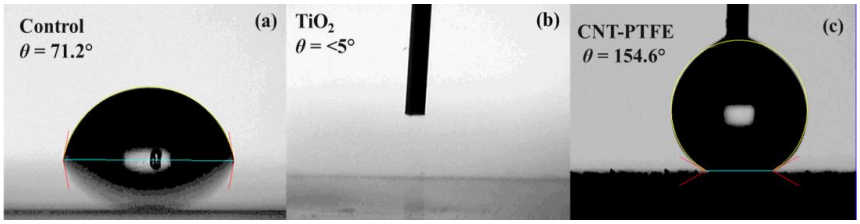

Figure 5.7. Shape of water droplets on test surfaces (a) untreated stainless steel, (b) TiO_2 coated plate and (c) carbon nanotubes-Teflon coated plate.

According to the AFM micrographs and the calculated roughness (r_a and r_q) of all the surfaces (Table 5.1), it can be noted that air could be trapped into entangled nanocomposite structure (average size ranging between 0.1 and 0.2 μm, FESEM estimated) during the adhesion test, while larger particles including bacteria were less likely to reside on the surface when a sufficient amount of liquid flow was continuously applied.

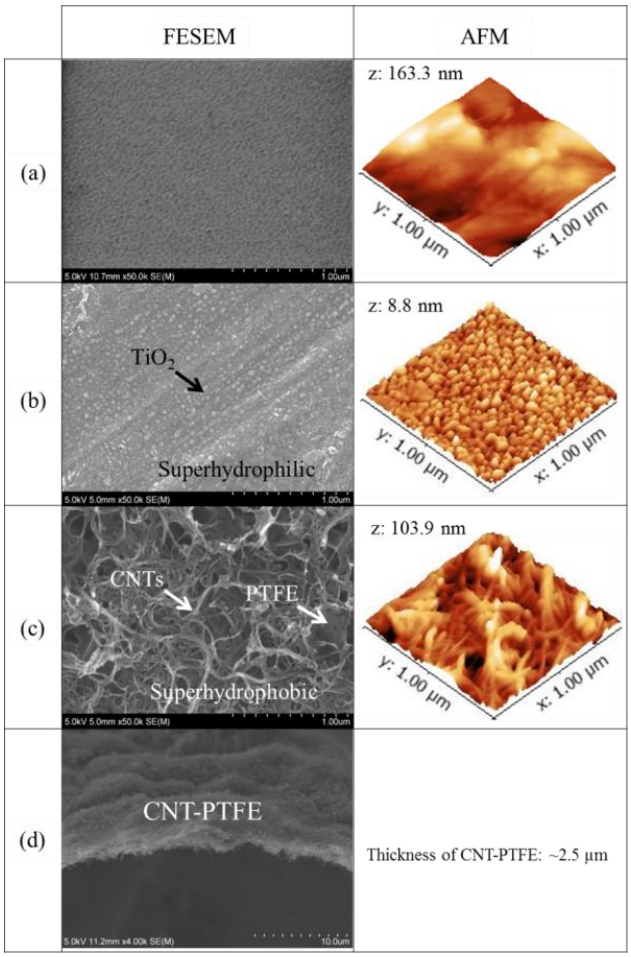

Figure 5.8. FESEM and AFM micrographs of samples (a) control stainless steel, (b) TiO_2 coated plate, (c) MWCNTs-PTFE-coated plate and (d) three dimensional micrograph of MWCNTs-PTFE coating.

For TiO_2 coated surface, it can be seen that the titania nanoparticles was tightly aligned on the steel surface, resulting in the formation of highly uniform superhydrophilic

nanoparticulate matrix. Average particle sizes of TiO_2 composites were approximately 20–30 nm (estimated from another close-up FESEM image, data not shown), leading to the creation of many tiny structures around groups of agglomerated TiO_2 which are so-called 'micropapillae'. Therefore, these three-dimensional structures accommodated water to instantly spread onto TiO_2 coated surface mainly due to the water surface tension and capillary effects, resulting in the formation of tightly bound water layer near superhydrophilic surface (Song *et al*., 2008).

Table 5.1. Calculated roughness values of test plates obtained from AFM measurements.

	Control	**Superhydrophilic**	**Superhydrophobic**
$\boldsymbol{R_a}$ **(nm)**	11.34 ± 3.75	1.07 ± 0.06	13.38 ± 1.07
$\boldsymbol{R_q}$ **(nm)**	14.00 ± 4.91	1.36 ± 0.05	17.01 ± 1.29

Fig. 5.9 (a) shows the adhesions of bacteria to the three test surfaces, namely control, superhydrophilic, and superhydrophobic surfaces which were subjected to two different flow conditions, i.e. static and dynamic. Adherent and aggregation of bacterial cells on each surface became visible with DAPI staining when determined under fluorescence microscope at the magnification level of 1000X. Fig. 5.9 (b and c) illustrate the typical anti-adhesion mechanisms of superhydrophobic and superhydrophilic surfaces.

Due to the extremely low water contact angle reading from the superhydrophilic surface implied that water was readily spread out and fully wetted the thin layer of TiO_2 coating. Since TiO_2 has abundant hydroxide ions (–OH groups) around its surface which have a strong affinity for water molecules in aqueous solution, tightly bound water layers near TiO_2 surface were formed (Fig. 5.9 (b)) (Advincula *et al*., 2006). The developed hydration layer, also called 'lubricating liquid film' or 'water shield', was capable of lessening attractive electrostatic interactions between foulants, i.e., bacterial cells, and solid surface (Tiraferri *et al*., 2012). For superhydrophobic surface, which usually has WCA > 150°, water was not adsorbed or spread (wet) over the surface; thus, water dynamics can keep its underlying surface clean by sweeping away solid materials such as dust and microbial cells. (Fig. 5.9 (c)).

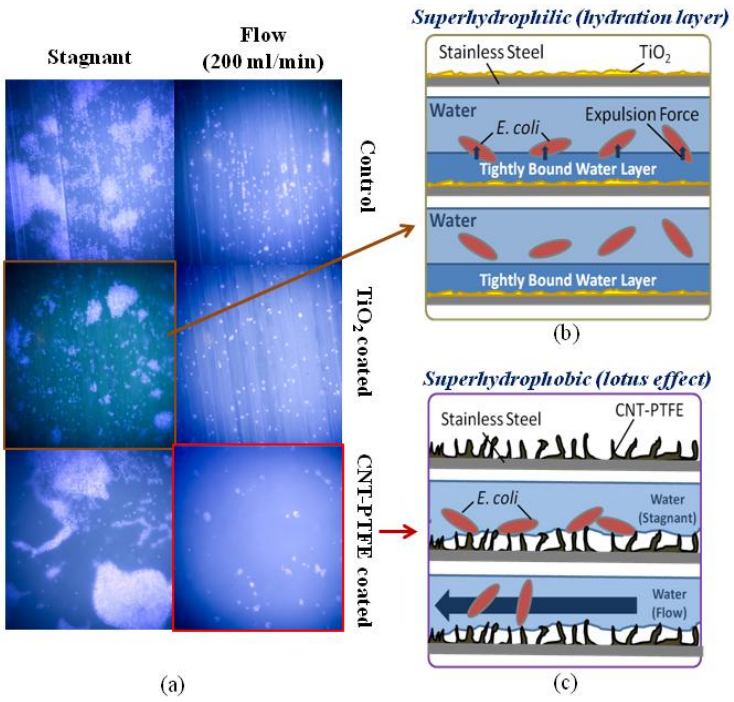

Figure 5.9. Bacterial adhesions on nanocomposite surfaces (a) fluorescence microscopic images of bacteria adhered to six surfaces after DAPI staining, (b) schematic of anti-adhesion effect of superhydrophilic TiO_2 coating and (c) schematic of anti-adhesion effect of superhydrophobic MWCNTs-PTFE coating.

Fig. 5.10. also confirms that attachment of *E. coli* cells to the test surfaces was significantly affected by both the wall shear rate and hydrophobicity/ hydrophilicity of the surface. At different flow conditions, it is noted that an increase in the flow rate significantly decreased the numbers of bacteria adhering to all surfaces. The measured fluorescence intensity values of all adhered surfaces were in a good agreement with the data obtained from aerobic plate counting for quantifications of *E. coli c*ells. The numbers of bacterial cells adhered to the TiO_2 plate estimated using the FI value and plate counting was significantly lower than the other surfaces in the stagnant environment (approximately 65% lower than control).

This result indicated that the hydration layer (approximately 10 Å, Mamontov *et al*., 2007) would most effectively inhibit the bacterial adhesion in a stagnant environment. However,

a significant decrease in the hydration thickness could happen due to an increase in the shear rate in the parallel plate flow chamber (Leng and Cummings, 2006). Therefore, anti-bacterial adhesion of the superhydrophilic surface was approximately 45% lower, compared to that of control after the sheared test; however, the superhydrophobic surface was superior to the superhydrophilic and control plates by eliminating up to 80% of adhering cells during the dynamic adhesion test. On the other hand, in stagnant environment, the amounts of *E. coli* cells on the superhydrophobic plate were found to be slightly lower than the control plate, but significantly higher than the superhydrophilic surface. The possible reason behind this phenomenon may include the irreversible change from superhydrophobic Cassie's state to Wenzel's state which is less hydrophobic (Bormashenko *et al*., 2007; Nosonovsky and Bhushan, 2007).

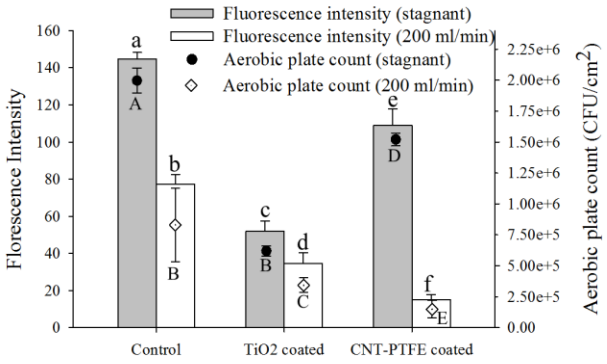

Figure 5.10. Fluorescence intensities reflecting number of adhered bacteria to test plates after DAPI staining compared to total number of microorganisms quantified using aerobic plate count method (significant differences within data obtained from fluorescence intensity and aerobic plate count measurements were indicated by dissimilar lowercase and uppercase letters, respectively ($P<0.05$)).

The cell adhesion results obtained from superhydrophobic surfaces were consistent with the observation by Ozden and Puri (2010) reporting that vertically aligned carbon nanotubes (ACNTs) coated on plate heat exchanger surface significantly prevented the accumulation of milk foulants during the heating process. The mass of milk foulants after heating for 6 h was

reduced by 90%, as compared to the control. Milk foulants were swept away from the surface because of the superhydrophobic MWCNTs-PTFE composite coating.

5.3. Effects of Extreme Slipperiness on Removals of Liquid Food Debris and Bacterial Biofilms from Stainless Steel Surface. (Objective 3)

This work demonstrated the fabrication and anti-adhesion attributes of a self-cleaning surface 'SLIPS' by modifying the surface of stainless steel which is most commonly used in food industry. The developed surface consisted mainly of a network of randomly aligned multiwalled carbon nanotubes (MWCNTs), thin films of amorphous Teflon−as a wear resistant enhancer, and a low-surface tension liquid lubricant (Krytox) or an infusing liquid. The degree of slipperiness of the developed SLIPS was measured using an estimation of the sliding angles measured from 500 µL droplets of deionized water as well as oil, ketchup and honey droplets. To evaluate the anti-biofilm performance of the slippery nanocomposite surface, *Escherichia coli K-12* and *Staphylococcus aureus* (2×10^8 CFU/mL both) biofilms were separately grown on stainless steel (control) and the SLIPS composite for 7 days.

The four main fabrication steps of the SLIPS were developed. The first two steps were mainly aimed to develop the extremely porous surface to properly accommodate the lubricating liquid after infusion step to create a stable lubricating film around the SLIPS. The last step was used to eliminate the excess amounts of the Krytox from SLIPS before performing tests using liquid foods and microbial biofilms. The measured WCAs of stainless steel (control), stainless steel with Krytox lubricant, MWCNTs composite coated steel, MWCNTs-Teflon AF (amorphous Teflon) coated steel, and SLIPS are shown in Table 5.2.

It was clearly seen that, wettability of stainless steel changed upon various surface treatments. Typically, stainless steel 316 has been used in food industry as a food contact surface because of its adequate mechanical and corrosion-resistance properties; however, the surface is also known to have high surface energy (i.e., hydrophilic surface with the CA<90°). As a result, the surface is considered as an attractive surface to liquid food debris as well bacterial biofilms.

According to the results, the WCA of the unmodified steel was 68.24°. This value suggested that the surface was prone to adsorb debris, bacterial cells, and other contaminants from the surroundings.

Table 5.2 Characteristics of stainless steel, superhydrophobic, and SLIP surfaces.

	Water contact angle (CA, °)		**Remarks**
	mean	**SD**	
Stainless steel	68.24	0.22	Control
Stainless-Krytox	91.74	0.55	Time < 2s
Stainless-Krytox	66.21	0.61	Time = 30 mins
MWCNT coated	153.82	1.19	Superhydrophobic
MWCNT-TAF coated	154.91	1.37	Superhydrophobic
MWCNT-TAF-Krytox	91.72	0.64	SLIPS (Time = 30 mins)

Nonetheless, the WCA of the steel surface could be temporary raised from 68.24° to 91.74° after the plate was coated with a layer Krytox lubricant. It was seen that, the shape and CA of water droplet resting on the steel-Krytox surface critically changed after a few seconds because the underlying Krytox was vastly repelled by the droplet due to polar (water)-nonpolar (Krytox) repulsive interaction. After 30 mins of experiment, the droplet on the steel-Krytox surface significantly returned to its original state (WCA = 66.21); hence, further surface modification step should be developed and implemented to lock the liquid lubricant in its place. Therefore, a stable porous layer of sponge-like microporous solid should be developed on the steel surface to overcome the liquid instability problem. The omniphobic SLIPS was developed by integrating a layer porous MWCNTs-Teflon AF topography with the liquid lubricant, Krytox. The MWCNTs, Teflon AF, and Krytox played important roles in prevention the attachment of a set of liquid food samples and two bacterial biofilms to the SLIPS. MWCNTs are a multiple hexagonal rolled-up sheets of graphene, a 2-dimensional (2D) carbon network. Due to its extraordinary properties, MWCNT has been widely used in many fields including sensors,

micro- and nano-elctromechanical systems (MEMS and NEMS), superhydrophobic surface, and oil absorbing material (Dong *et al*., 2012; Wu *et al*., 2014).

Despite the fact that a porous network of MWCNTs can be developed on solid substrate using simple methods such as spray coating, micro/nanoscale features of the coating may not be able to withstand mechanical stress. The chemical structures of Teflon AF and Krytox lubricant are shown in Fig. 5.11 (a) and (b), respectively. Even though Teflon AF is solid while Krytox is liquid at room temperature, both of these chemicals share main important characteristics. Their chemical structure mainly consists of a long chain of fluorinated carbon atoms in strong covalent C-F bonding configurations. Hence, both Teflon AF and Krytox are generally considered chemically inert, highly thermal- and chemical-resistant, and low-surface energy (or surface tension) materials.

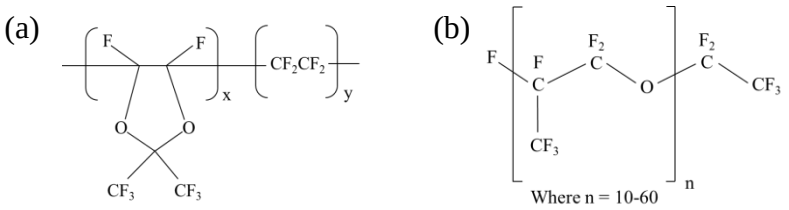

Figure 5.11. Chemical structures of SLIPS components (a) amorphous Teflon or Teflon AF and (b) Krytox lubricant.

Fig. 5.12 shows the comparison of the developed porous MWCNTs structures before (Fig. 5.12 (a) and after (Fig. 5.12 (b)) Teflon AF coating. As confirmed by SEM shown in Fig. 5.12, a layer of Teflon AF was firmly deposited and fully covered the porous MWCNTs structures. It can be seen that, the Teflon AF also generated polymer cross-linkages between individual pieces of nanotube to essentially improve the mechanical robustness of as-prepared MWCNTs layer. More importantly, the WCAs of as-prepared MWCNTs and MWCNTs-Teflon AF coatings were very similar to each other (153.82° and 154.91°, respectively) suggesting that both surfaces possessed highly degree of superhydrophobicity (CA>150°) and these phenomena can be described using the Casie-Baxter equation (Cassie and Baxter, 1944). In addition, the

presence of thin TAF layer did not compromise the micro/nanoscale roughness and porosity of MWCNTs because the upper insets of Fig. 5.12 (a) and (b), also show that water droplets resting on both MWCNTs and MWCNTs-Teflon AF were in sphere-like shape. More importantly, the lower insets of Fig. 5.12 (a) and (b) show excellent oil absorbing function of both MWCNTs and MWCNTs-TAF when the surfaces were infused with the Krytox lubricating oil. The oil droplets readily penetrated and were absorbed into porous structure of both surfaces confirming that surfaces were extremely porous. After Krytox infusion, the contact angle of water droplet on the MWCNTs-Teflon AF-Krytox or SLIPS showing in Table 5.2 was 91.72° and remained constant for over 30 mins. The results showed that the SLIPS had greater ability to lock in the Krytox lubricant compared to unmodified stainless steel.

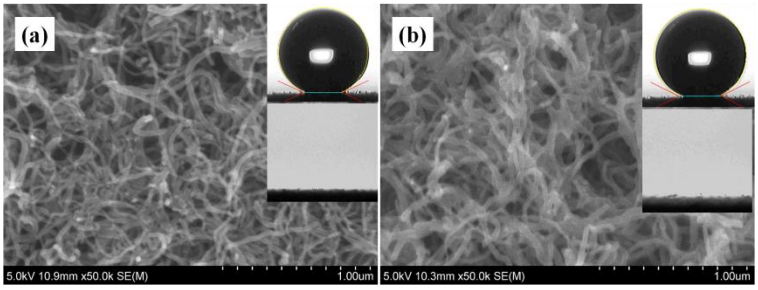

Figure 5.12. Porous MWCNT features (a) before, and (b) after Teflon AF coating

Fig. 5.13 illustrates that the miscibility behavior of Krytox lubricant with other liquids. As shown, regardless of the types of the liquid samples, it was always noticed that the Krytox was insoluble with all samples including the simple liquids (e.g., water, EtOH, and cooking oil) or the complex liquids (e.g., honey, and ketchup) when the tests were performed at room temperature and pressure environment for 1 h. Such superior property of the Krytox as compared with other lubricants is due to strong chemical interaction (e.g., covalent bonding) between highly electronegative fluorine atoms and a long-chain carbon skeleton. This C-F bond is generally regarded as one of the strongest bond in organic chemistry. According to this reason, the Krytox lubricant is insoluble in water, acidic and alkaline solutions, as well as most of the organic solvents; however, there are some possibilities to dissolve the Krytox if it is exposed to highly fluorinated or some supercritical fluids such as CO_2 (Casimiro *et al*., 2005).

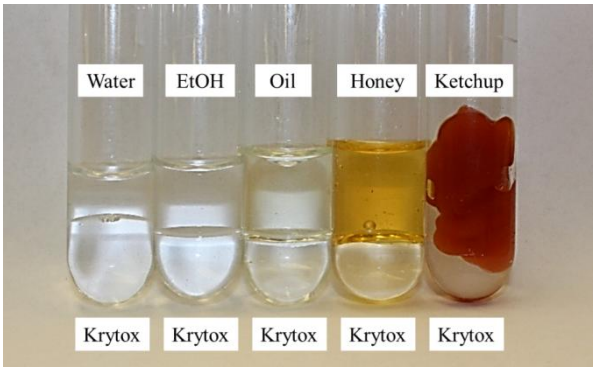

Figure 5.13. Photograph showing miscibility of Krytox oil with test liquids.

Table 5.3 shows the sliding angle or SA of liquid samples obtained from goniometer readings. The SA of most liquid foods (all food samples except ketchup) including bacterial suspensions were approximately 5°. Unlike other liquid samples, ketchup's sliding angle was approximately 20° due to its high viscosity (more resistance to flow) and special flow behavior (non-Newtonian: Bingham plastic) which the initial force was required to initiate the flow. However, 500 µL of ketchup started to slide-off the SLIPS without leaving any noticeable debris after the plate was tilted more than 45°.

Fig. 5.14 shows the remarkable ability of the developed SLIPS in prevention of biofilms attachments. The lubricating liquid (Krytox) in this setup was infiltrated into a porous MWCNTs-TAF substrate presenting as a uniform liquid–liquid interface to bacteria. Due to a large difference in surface tension, greater than 50 mN/m (surface tensions of water and Krytox are 72.8 mN/m and 20 mN/m, respectively), so that bacterial cells were not able to penetrate across the Krytox-water interface (Eipstein *et al*., 2012). As a results, bacterial cells and their biofilms suspended in watery biofilms phase locating outside SLIPS structure.

Table 5.3 Sliding angles of liquid food samples and bacterial biofilms on the SLIP surface.

	Average	Standard Deviation
Water	1.24	0.13
Honey	2.03	0.19
Ketchup	20.68	1.12
Vegetable oil	1.40	0.22
Bacterial suspensions	1.49	0.34

For microbial tests, the difference in amounts of adherent bacterial cells (e.g., *E. coli* and *S. aureus*) on control and SLIPS were clearly visualized under fluorescence microscope. The fluorescence dye, DAPI, is very specific to bacterial DNA. Because the dye can form a fluorescence complex when attaches to A-T sequences of the DNA (Kapuscinski, 1995). Therefore, the dye can be used to stain both gram-positive (i.e., *S. aureus*) and gram-negative cells (i.e., *E. coli*). As shown in Fig. 5.14 (a) to (d), the stained bacterial cells clearly appeared in bright blue with a dark background, so that their population on the control and the SLIPS can be estimated and compared. The remaining bacterial cells, shown in bright blue, on the control surfaces (Figures 5a and c) were much more that of the SLIPS (Fig. 5.14 (b) and (d)) after 7-day of on-surface microbial growths.

The results suggested that the attachment of both bacterial biofilms to SLIPS surface was significantly low compared to the control surface. Additionally, it can be also noticed that the slipperiness and other anti-adhesion attributes of the SLIPS were not notably changed over the time. Quantification of biofilms (cells-EPS matrix) was also performed using absorbance measurement at 590 nm (OD 590). As reported in previous works (Burton *et al*., 2007; Díez-García, *et al*., 2012), crystal violet has ability to bind to both bacterial cells and EPS. In addition, the crystal violet essay can be used to quantify large numbers of bacterial strains with reproducible results. The correlation between optical density of crystal violet and the amounts of bacterial biofilm biomass was already verified (Izano *et al*., 2008; Peeters *et al*., 2008). It can be seen in Fig. 5.14 (e) and (f) that the SLIPS repelled approximately 90% or one-log reduction of

E. coli and *S. aureus* biofilms after 7-day growth. Because of the fact that majority amounts of the biofilms biomass were slid-off the SLIPS very rapidly when the plate was tilted with 1.49° (shown in Table 5.2). The observed prevention level was consistent with the vigorous surface cleaning method commonly employed in food industry (i.e. high-pressure water spray), which also allowed the removal of 90% of adherent bacterial from the infected surfaces (Gibson *et al*., 1999). It is suggested that applying SLIPS fabrication technique on the surface of food processing facilities could permit the same sanitary level without high-pressure water spraying aid.

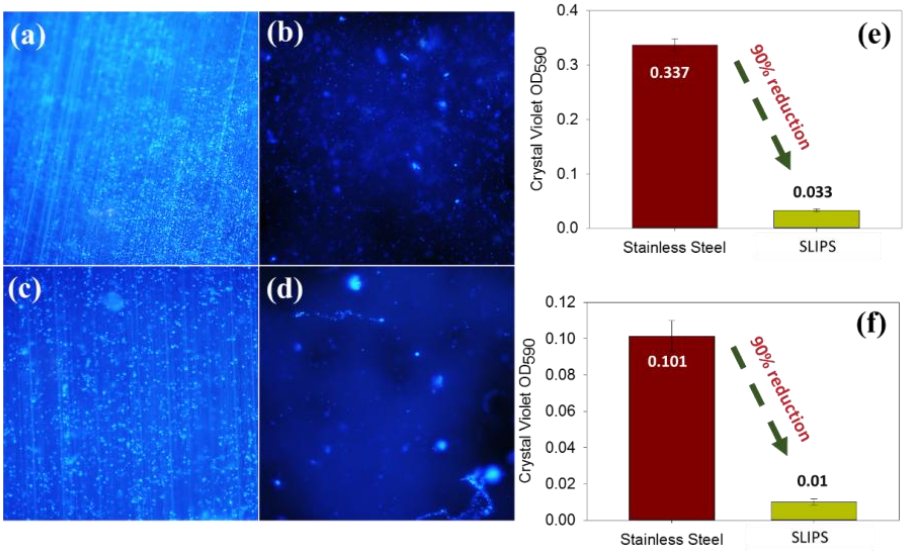

Figure 5.14. Comparison of remaining bacterial cells or biofilms on control and SLIPS after 7-day growth. Fluorescence images of bacterial cells on different surfaces (a) *E. coli* on control, (b) *E. coli* on SLIPS, (c) *S. aureus* on control, and (d) *S. aureus* on SLIPS. Absorbances (OD 590) of bacterial biofilms stained with crystal violet on stainless steel plates compared to that of slippery surfaces after 7 days: (e) *E. coli*, and (f) *S. aureus.*

5.4. Effects of Hydrophobicity of Nanoporous and Nanopillared Aluminum Oxide Surfaces on Bacterial Adhesions in Static and Dynamic Environments. (Objective 4)

Generally, electropolishing is referred to a diffusion-controlled etching of metal surface using a concentrated acidic electrolyte which removes surface irregularities. As a result, the process yields a reflective and planar surface to the etched metal (Takhistov, 2004). In this research, electropolisihing process was applied to high purity aluminum specimens to make a control (nanosmooth) surface for bacterial adhesion tests (Fig 5.15. (a)). The FESEM micrograph of the electropolished shows that the surface was free-from cracks, defects, and other irregularities. For anodizing process, the method is commonly referred to a process that produces a hard oxide film at the metal surface caused by the partial dissolution of the metal in electrolyte as well as the development of oxygen gas at the cathode during anodization. (Takhistov, 2004). There have been investigated that, voltage, time, types of electrolytes, pH and temperature are main affecting factors on the size and depth of the resulting porous oxide layer formed on aluminum. Most common acidic electrolytes used for developing porous oxide layer include sulfuric, oxalic, phosphoric, and chromic acids.

The fabricated porous aluminum oxide surface anodized in oxalic acid is shown in Fig. 5.15. (b). The figure clearly shows that a uniform array of nanoporous structure was successfully fabricated using the developed anodization recipe where 0.3M oxalic acid was used as an electrolyte with a constant applied voltage of 45V for 15 min. The diameter of the developed nanopore was determined by a distance measuring tool in the SEM imaging software. It was found that the average pore and interpore distances were ca. 30 and 50 nm, respectively. Fig. 5.15. (c) shows the self-bundled nanopillared array.

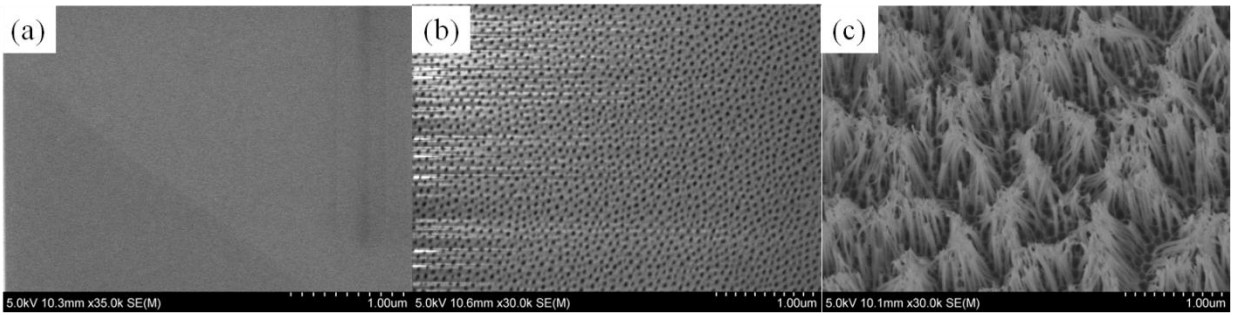

Figure 5.15. FESEM micrograph of nanoengineered aluminum surfaces (a) nanosmooth, (b) nanoporous and (c) nanopillared specimens.

The schematic diagram of the formations of nanosmooth, nanoporous and nanopillared is illustrated in Fig 5.16 (a) to (d). As can be seen in first three steps, the pore size on the steel surface was continuously widened over etching time. The pore-widening was limited at the third step where the side walls of the pores were mostly dissociated in electrolyte leaving the triple points of hexagonal intersections undamaged. The nanoscale triple points were so-called nanowires or nanocarpets which eventually self-bundled to become the three dimensional nanopillared features after drying using compressed air.

The wettability of fabricated nanoengineered surfaces was also evaluated using a goniometer. The water contact angles (WCAs) of the porous surfaces were 10−25°, while those of the nanopillared surfaces were close to 0° (superhydrophilic). The water droplet spread and permeated readily on the unmodified nanopillared features, suggesting that the three dimensional pillared nanostructures significantly affected the water spreadability by stretching water within its structures. However, when the nanoporous and nanopillared surfaces were subsequently coated with a thin layer of hydrophobic coating such as amorphous Teflon polymer, the WCAs of both surfaces were increased, depending on the morphology of surfaces. In the case of nanoporous surfaces, the WCAs were increased to be ca.115^{o}. The increase of the WCAs on the Teflon-coated three-dimensional nanopillared surfaces was more pronounced, ca.162^{o} which was superhydrophobic (WCA > 150°). The significant increases of WCAs on the Teflon-coated hydrophobic surfaces indicated that their wetting states should be in the Cassie-Baxter state, where gas (air) should be trapped between water and the surface nanostructures and the water

should partially contacted to the solid surface. The apparent WCA increases with a decrease of the solid fraction. The sharp-conical nanopillared surface resulted in the significant decrease of the wetted solid fraction with the Teflon coating, showing the higher value of the measured WCA than the two-dimensional nanoporous surface. Such a decrease of the wetted area of the hydrophobic surfaces, especially the nanopillared surface, would also result in the minimized bacteria interactions and adhesions on the solid surfaces.

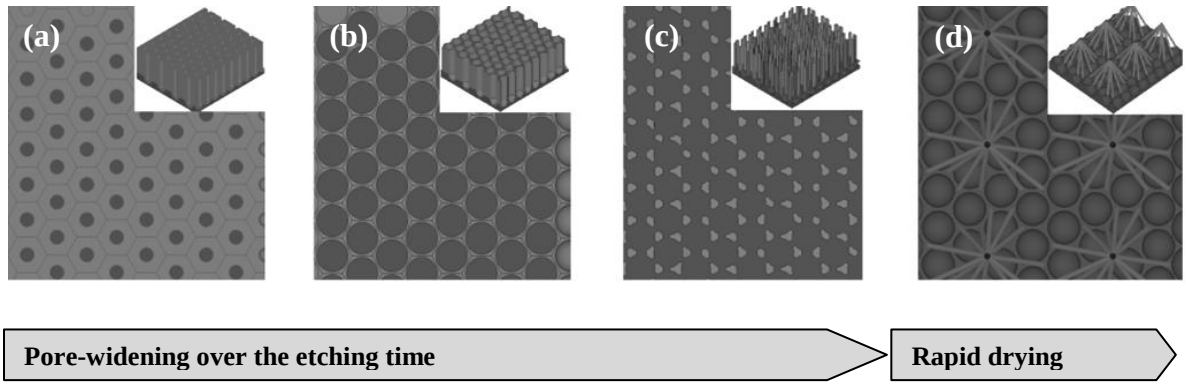

Figure 5.16: Schematic of the fabrication process to transform nanoporous structures of anodic aluminum oxide (AAO) to nanopillared structures (a) initial nanoporous AAO pattern, (b) nanoporous AAO pattern with widened pore size, (c) triple points or nanocarpets, (d) nanopillared AAO pattern obtained after drying.

The quantification of viable bacterial cells adhering to the test surfaces in both static and dynamic environments is shown in Fig. 5.17. The bacterial cells were aggregated together in case of the static adhesions, whereas more individual bacterium was observed in the dynamic flow condition. The amounts of adhering bacterial cells in the dynamic condition were less than that of the static condition. This was attributed to the lack of ability of the bacteria to anchor to the surface because of magnitude of the shear force locating near the surface. Similar results were observed on hydrophobic nanoporous surfaces. It could be described that the bacteria formed small islands of clusters in a static condition. Another reason for this formation could be the growths and multiplications of bacteria after the prolonged attachment (adhesion time was 1 h in this study). On hydrophilic nanopillared surfaces, no significant difference was observed between

static and dynamic conditions. The wall shear effect that was apparent on the hydrophilic nanoporous surfaces was not evident on the nanopillared surfaces. This is attributed to the three-dimensional surface morphology and the more extreme wettability i.e., superhydrophilicity of the pillared surfaces, where the bacteria suspension fully wetted the surface and bacteria reach and adhere everywhere, even between the pillars.

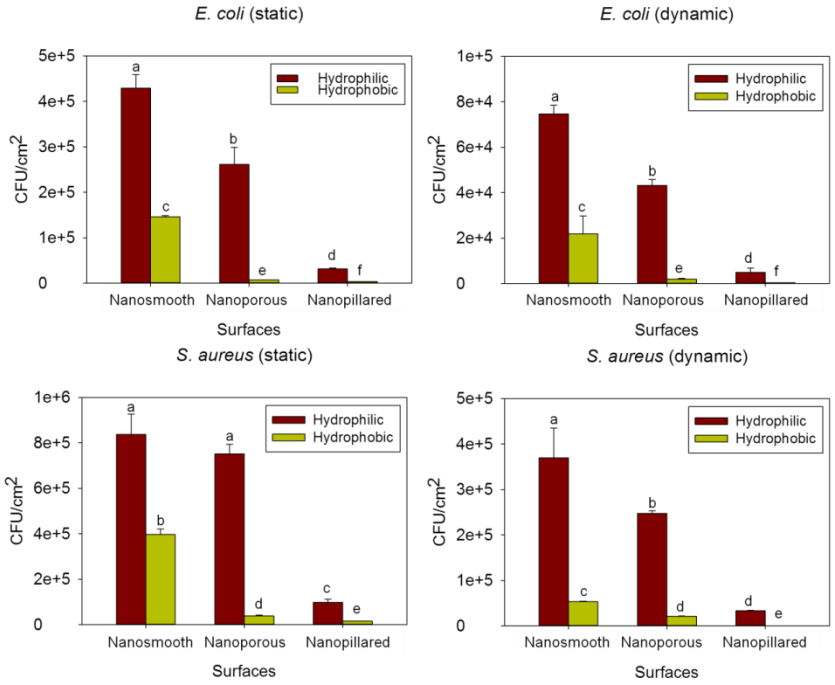

Figure 5.17: Number of adhered bacterial cells to the flat (nanosmooth), nannoporous, and nanopillared surfaces enumerated using aerobic plate count method.

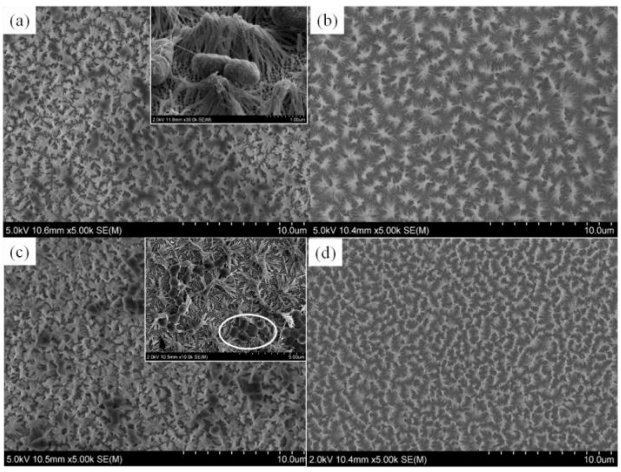

Figure 5.18 FESEM micrograph of nanopillared surfaces after static adhesions (a) superhydrophilic and (b) superhydrophobic surfaces tested with *E. coli*; and (c) superhydrophilic and (b) superhydrophobic surfaces tested with *S.aureus*

Fig 5.18 shows that the bacteria resided in the valleys would not be significantly affected by the developed shear force. On hydrophobic nanopillared surfaces, adherent bacteria cells were not noticeable at the operated FESEM magnification (5000X) in both stagnant and dynamic flow conditions. The superior anti-adhesion ability of the hydrophobic pillared surface related to its superhydrophobicity, where the stable underlying air significantly limited the contact area between the planktonic bacteria cells in the suspension and the substratum; therefore, the bacteria-solid surface interactions (e.g., hydrophobic-hydrophobic type) and other attractive forces, which was effective in both stagnant and dynamic flow conditions. Both hydrophilic and hydrophobic nanoporous surfaces were not as effective as the hydrophobic nanopillared surface in terms of the anti-bacterial adhesion. It was due to the fact that the pore size and the interpore distance were not large enough to establish such cells-substratum barrier seen in hydrophobic nanopillared surfaces. Overall, the adhesion behaviors of *E. coli* on the different surface and flow conditions were similar to those of *S. aureus.* According to the results, the most effective anti-bacterial adhesion behaviors were shown on the superhydrophobic pillared surfaces.

5.5 Effect of Nanoporous Stainless Steel on *Listeria monocytogenes* Attachment (Objective 4)

In general, acid and corrosion resistant stainless steel 316 possesses high mechanical strength, biocompatible, processibility, and reasonable price; therefore, the steel is generally used to fabricate devices in chemical and biomedical fields such as surgical implant material, dental applications, and storage tank for decades. Moreover, the use of the stainless steel is also extended to food applications including food contact surfaces in food processing plant (Latifi *et al*., 2013). Since the topography of the steel is one of the crucial affecting factors in controlling surface-environment phenomena including wettability and biofouling attachment. In order to minimize surface the bacterial attachment and possible subsequent cross-contamination in food processing facilities, the topography of steel surface was modulated using electropolishing and anodization treatments in different acidic electrolytes. As a result, a nanosmooth and two nanoporous with an approxiamate pore diameter of 50 and 80 nm stainless steel 316 specimens were obtained.

Fig. 5.19 shows FESEM micrographs of mechanically polished (finish #8, mirror-like, Fig. 5.19 (a)), electropolished (Fig. 5.19 (b)), and anodized surfaces (Fig 5.19 (c)). As observed in the FESEM images, the surface topographies of the steel were significantly affected by the developed surface treatments. It can be seen that the topography of the as-received stainless steel was highly rough with deep-trench crevices which may accommodate the bacterial cells and would eventually cause surface infection. On the other hands, both electropolished and anodized steels were visually smooth free from scratches and seemed bright and shiny to bare eyes. Interestingly, the inset of Fig. 5.19 (c) confirms that the developed anodization process, 5% vol of perchloric acid in ethylene glycol was used as an electrolyte with applied 40V for 10 m, successfully created a uniform ordered hexagonal nanostructures with the size of 50 nm.

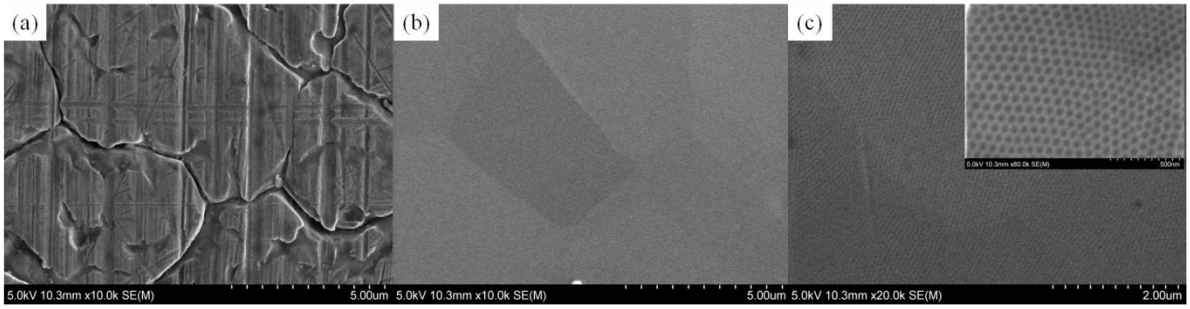

Figure 5.19 FESEM micrograph of stainless steel 316 (a) as-received mirror-like finish, (b) electropolished and (c) anodized stainless steel 316 surfaces.

The electropolishing condition performed using a mixture of phosphoric acid and sulfuric acid (60%:40% vol ratio) with 3.5V for 10 min significantly eliminated the surface irregularities which can was caused by a temperature-enhanced mass transport process on the anode side (steel sample) during electropolishing. The mechanisms of this reaction is not fully understood; however, the reaction is commonly associated with a differential dissociation of peaks and valleys of the steel surface. According to Lee (2000), when the current is continuously applied to the anode and cathode, the oxide layers on the anode side prevents the valleys area from being dissociated by chemical reactions caused by the applied current. This is due to the fact that the lower areas possess high specific gravity, viscosity and insulation. As a result, the higher current rather goes and dissolves the high peaks more rapidly than the lower trench or the valley areas. Finally, the surface of the anode becomes smooth and level. In the case of stainless steel, the dissociated metal ions from the metal surface migrated into the electrolyte are generally clear yellow-to-green in color. The main dissolved metal ions are yellow: Fe^{3+}, Cr(IV), and Cr(VI); and green: Ni^{2+}, Ni^{6+}, and Mo(IV) (Nazneen, *et al*., 2012). Some of these main reactions are shown as follows (Lafiti *et al*., 2013):

$$Fe \rightarrow Fe(III) + 3e^- \quad (5.8)$$

$$Ni \rightarrow Ni(II) + 2e^- \quad (5.9)$$

$$Cr \rightarrow Cr(VI) + 6e^- \quad (5.10)$$

The mass of metal anode that is removed during the electropolishing is described using Faraday's law of electrolysis as follow:

$$W_{loss} = \frac{I'tM'}{n'F'} \tag{5.11}$$

where, *t* and *I'* are time and current consumed during the electropolishing treatment, respectively. *M* 'is the molecular weight of anode. *F'* and *n'* are Faraday's constant and valence of metal ions, respectively.

In the case of anodized sample, the sample contained uniformly regulated hexagonal nanoporous features. The formation of such structure was due to the formation and expansion of an oxide layer formed on the surface of stainless steel during the anodization. The explanation of the self-organization hexagonal nanoporous was given by Jessensky (1998). When the current is applied, the electric field induces the formation of pores on the anode. This reaction is specifically called "field-enhanced oxide dissociation" occurring at the oxide film-anode inteface. Due to the influence of the electric field between the anode and the cathode, the pores tend to grow in perpendicular direction to the anode surface. In the meantime, the migrations of oxygen containing ions such as O^{2-} and OH^{-} from the electrolyte through the oxide layer towards the bottom of the pores occurs. Whilst, metal ions in stainless steel such as Fe^{3+} migrate from the metal-oxide interface to continuously thickens the oxide layer. Since the atomic density of the developed iron and other oxide layers is much lower than that of their metallic states. This density difference causes the expansion of the pores in top-to-bottom direction. During the pore expansion −a formation of oxide layer, the mechanical stress was simultaneously developed. The developed stress eventually causes repulsive forces between neighboring pores throughout the anodization process; as a result, an array of the self-organized hexagonal nanopores were uniformly developed on the surface of anode.

In this research, two different sizes of the nanopore were fabricated and compared. Fig 5.20 shows AFM micrographs of the nanoporous surfaces with the average pore diameters of 50 and 80 nm, respectively. The pore size modulation was achieved by controlling the anodizing

voltage and time. The optimal voltage-time combinations for fabricating both nanoporous surfaces were obtained from factorial experiments based on various anodizing voltages (25, 35, 40, 45, 50 and 55V) and times (1, 2, 3, 5, 10, 15, 20, 25, 30, and 35 min).

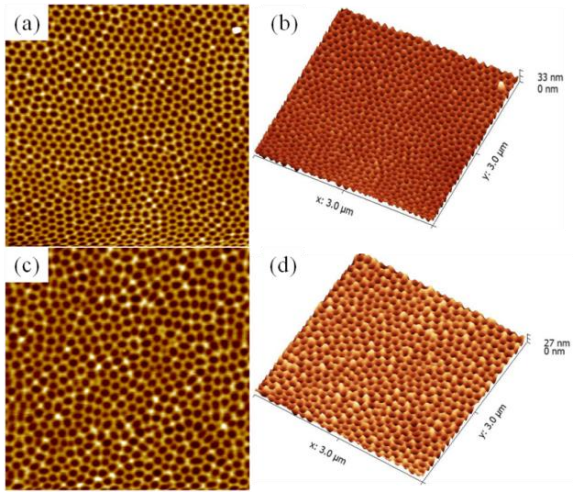

Figure 5.20 AFM micrograph of nanoporous stainless steels (a) 50 nm nanoporous in top view, (b) 50 nm nanoporous in 3D view, and (c) 80 nm nanoporous in top view, (b) 80 nm nanoporous in 3D view.

After the anodizing conditions for both nanoporous surfaces were investigated, both of them were taken to the adhesion test where the biofilm forming health hazardous *L. monocytogenes* was used as a bacterial model. After 4 h of bacterial test, all bacterial cells adhering to all of the test surfaces e.g., nanosmooth (electropolished surface or control), 50 nm nanoporous, and 80 nm nanoporous stainless steel surfaces were enumerated using an aerobic plate count method. It was found that the initial population of the bacteria-PBS suspension was 1.9×10^{8} CFU/mL. The cells were also stained with DAPI and subsequently observed under 400X magnification level using a fluorescence microscope. The fluorescence images of the cells on all the surfaces are shown in Fig. 4.21.

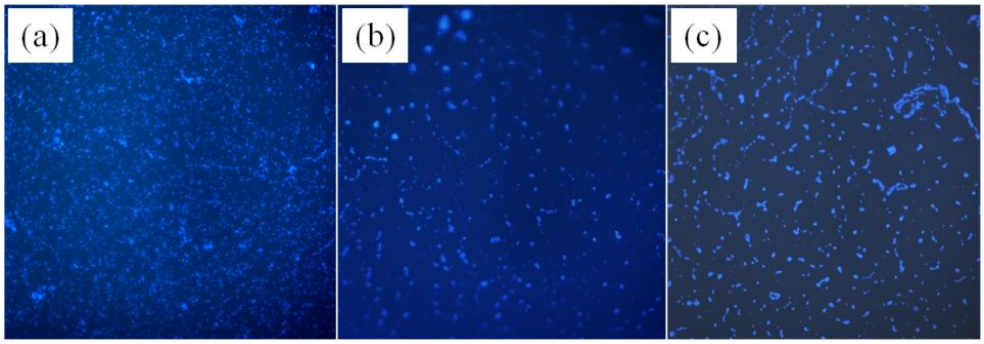

Figure 5.21 Fluorescence image of test surfaces after 4-h stagnant *L. monocytogenes* adhesion test (a) nanosmooth, (b) 50 nm nanoporous, and (c) 80 nm nanoporous surfaces.

It can be observed from the fluorescence images that the bacteria cells were densely adhere to the nanosmooth surface compared to the nanoporous surfaces. Since both of the nanoporous surfaces were fabricated to have three-dimensional porous structures which had the peak to valley distances of 27 to 33 nm, depending on the pore sizes. Therefore, during adhesion test the bacterial cells were limited to contact and interact with only the peak areas of the nanofeatures. As a result, the attractive interactions, which is maximum at the cell-substratum distance of less than 15 nm, between the cells and substratum were limited and some of the cells which were not stably anchor to the surface could possibly remain in a planktonic state in the aqueous suspension.

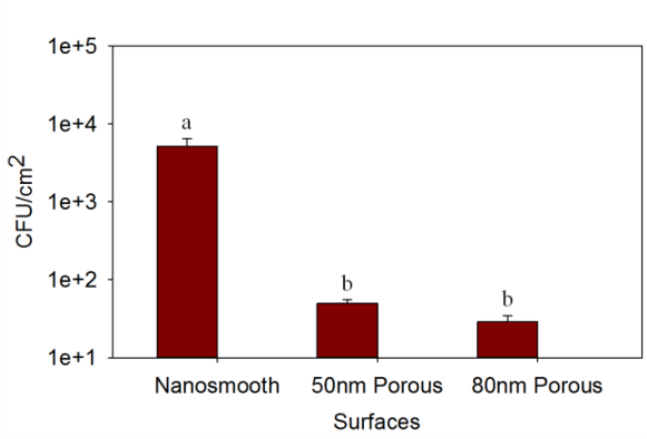

Figure 5.22 Number of bacterial cells adhering to test surfaces

The amounts of bacterial cells adhered to the surfaces enumerated using an aerobic plate counting for the nanosmooth, 50 nm nanoporous, and the 80 nm nanoporous were shown in the Fig. 5.22. The bacterial cells adhering to the nanosmooth (5×10^3 CFU/cm^2) > 50 nm nanoporous (5.0×10^1 CFU/cm^2) > 80 nm nanoporous (2.8×10^1 CFU/cm^2).). The results suggested that regardless of the materials, nonoporous structures on a solid substratum inhibited the adhesion and attachment of *L. monocytogenes* significantly. However, the statistical analysis indicated that the numbers of cells adhering to the 50 nm and the 80 nm nanoporous surfaces were not significantly different. This similarity in number of the cells could be due to the fact that the pore diameter was not only a factor that affected the attachment. Other surface parameters including the height of the peaks and the interpore distance might also play important roles during the adhesion of *L. monocytogenes*.

6. CONCLUSION AND FUTURE STUDY

6.1. Conclusion

Although the surface foulant and bacterial biofilms might be removed by conventional surface cleaning and sanitizing methods such as a traditional cleaning-in-place (CIP) protocol, food manufacturers would confront with additional costs of water, energy, chemicals and frequent process downtimes. It has been estimated that a milk and dairy factory typically wastes approximately 13% of the total energy usage on the CIP. Therefore, this study was aimed to develop various promising surface fabrication approaches for removal and prevention of surface fouling scenarios related to food processing equipment. In summary the outcomes of all performed experiments are as follows:

(1) Superhydrophobic heat exchanger surface was fabricated by annealing a mixture of 5%w/w MWCNTs in Teflon (PTFE) on cleaned and degreased stainless steel plate in a furnace at 360°C for an hour. Hydrophobicity of uncoated steel (control) was switched from hydrophilic (water contact angle or WCA 71.2°) to hydrophobic (WCA 119.6°) and superhydrophobic (WCA 141.1°) regimes after Teflon-only and MWCNTs-Teflon coatings were separately applied. The hydrophobicity of the nanocomposite coating was enabled by the formation of microscale structure including MWCNT fillers in the Teflon matrix. The presence of these rough structures were validated using a field emission scanning electron microscope (FESEM). After continuous milk pasteurization for 5 h, the foulant mass on MWCNTs-Teflon coated heat exchanger surface was 70.3% less than that of the uncoated surface primarily due to a self-cleaning action (lotus effect). Besides the foulant mass, it was also observed after the pasteurization that the developed self cleaning superhydrophobic surface also reduced the total heating energy requirement by 10.2% when compared to the highly fouled control surface. The results suggested that the fabricated superhydrophobic coating will benefit dairy industries by diminishing the unnecessary costs for water and energy.

(2) Quantifications of *E. coli* layers adhered to three different surfaces (e.g., uncoated stainless steel, superhydrophobic MWCNTs-Teflon, and superhydrophilic TiO_2) in stagnant and dynamic adhesion tests were performed and compared. Measured WCAs of the test surfaces were 71.2° (hydrophilic, control), 154.6° (superhydrophobic coated steel), and less than 5° (superhydrophilic coated steel). Measurements of surface topography of all surfaces were completed using filed emission scanning electron microscope (FESEM) and atomic force microscope (AFM). The microbial adhesion tests were performed in a custom designed parallel plate flow channel. Aerobic plate count and fluorescence microscopic imaging used to enumerate the numbers of bacterial cells adhering to the test surfaces appeared to be in good agreement. After all the experiments were performed, the results suggested that microbial adhesion rates on a stainless steel substratum were significantly influenced by the magnitude of developed wall shear rates (or flow conditions), surface morphologies (i.e. surface roughness) as well as wettabilities (i.e. hydrophobicity). The superhydrophobic MWCNTs–PTFE coating showed the lowest amounts of bacteria adhered to the highly sheared surface due to its lotus effect attribute. On the other hand, the maximum anti-adhesion efficiency in a stagnant environment was observed when the superhydrophilic (TiO_2) coating was used. It was typically due to the presence of chemically bound hydration layer. Therefore, it is suggested that a superhydrophobic-superhydrophilic hybrid surface which could exhibit multifunctional anti-adhesion attributes in both stagnant and continuous flow environments as food manufacturers often experience in real production lines. The development of an exceptional hybrid surface containing a significant amount of superhydrophobic areas allocated on the superhydrophilic surface could be an example in consideration.

(3) A SLIPS (i.e. omniphobic surface) was subsequently fabricated to overcome the pitfalls of superhydrophobic and superhydrophobic surfaces which their self-cleaning functions were strongly affected by flow conditions and types of liquid to be repelled. Developed SLIPS consisted of two main components, namely superhydrophobic porous MWCNTs-Teflon and low-surface energy food-grade infusing liquid. The exceptional liquid repelling capability of the SLIPS was validated using multiple liquid foods such as oil and ketchup as well as bacterial biofilms. The findings from this experiment showed that the developed slippery surface was

capable to limit the attractive forces between liquid food droplets, as well as hard-to-remove bacterial biofilms, and the stainless steel substratum; thus, allowing the droplets and biofilms suspensions to apparently slide over the slippery surface when the tilting angles were less than 20°. In particular, the anti-biofilms effects of the SLIPS were effective on both Gram-positive and Gram-negative bacterial strains, even after 7-day storage. The fabrication method shown in this paper can be potentially scaled-up for larger surfaces with a wide variety of substrates including glass, polymers and other metals in order to minimize the costs of surface cleaning as well as risks of food outbreaks caused by cross-contamination.

(4) Nanoporous surfaces with a relatively high solid fraction with a small pore size, the surface wettability did not make a significant difference in bacteria adhesions. Instead, the effect of dynamic flow was significantly able to reduce bacteria adhesions due to the high wall shear flow. On the tall and slender 3D nanopillared surfaces, the effect of dynamic flow was insignificant due to the entrapment of bacteria in the nanoscale valleys. However, the strongest anti-microbial behaviors were found in a hydrophobic condition in both stagnant and dynamic flows. It was attributed to the minimized contact area and accordingly the reduced adhesion force between the bacteria and the nanopillared surface, compared to other surfaces. The anodization technique developed in this study is simple, scalable, and adaptable to various types of materials so that the 3D nanopillared substrates would be of great significance in many anti-microbial applications, such as water supplies, biomaterials, and food processing, where the biofilm formation could be widespread public health problems. For stainless steel, the presences of 50 and 80 nm nanoporous patterns significantly inhibited the adhesion of *L. monocytogenes* by 2.0 to 2.3 log-cycles, depending on the pore diameter. However, an increase in the pore diameter from 50 to 80 nm did not significantly increase the anti-adhesion effect of the nanoporous surface; hence, the 50 nm pore size which required less power consumption and time to fabricate (40V 10 min) was preferable.

6.2. Future Study

In order to extend the understanding of adhesion mechanisms of biofouling to solid substratum with different nanopatterns, further studies on biofouling resistant nanoengineered surfaces should be needed for these following aspects:

(1) Computer simulation: A computational fluid dynamics (CFD) model to elucidate and verify interactions between bacterial cell and substratum surface should be established. The model should govern all the forces involved during the attachment which are exerted in the range of pico to nano Newton. The model should also combine accurate diffusion–reaction equations to simulate substrate diffusion with cellular automation-like criteria to model initial bacterial adhesion process as well as the growth and colonization of biofilm on the surface of solid substratum (Noguera *et al*., 1999). Therefore, the cell-surface interactions e.g., attachment kinetics, effects of surface nanotopography, hydrophobicity, and slipperiness can be determined.

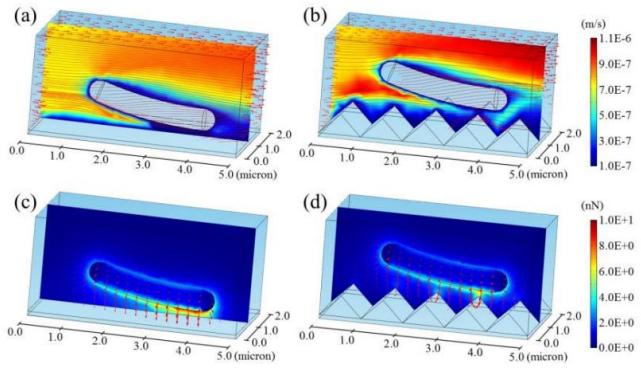

Figure 6.1. Simulation data: (a-b) single bacterial cell attachment and (c-d) potential adhesion force. Left: control, Right: nanopillared surface.

(2). Large-scale surface fabrication: The optimum electropolishing and anodizing conditions for the development of nanopatterns on both aluminum and stainless steel surfaces for small samples were already investigated this research (surface area less than 5 cm^2). For further research activity, the scaling-up protocol of these surface fabrications should be studied and

implemented. Although a set of high capacity equipment such as rectifier, jacketed anodizing chamber, and circulating water bath might be required, the resulting large-scale nanoengineered surface will potentially provide a great benefit to fresh fruit and vegetable industry where the product is generally consumed fresh. Therefore, its processing equipment should be free from bacterial biofilms. A prototype fruit and vegetable washer could be designed for fulfilling such demands. The schematic of a fruit and vegetable washer equipped with a nanoengineered surface at the bottom is shown in Fig. 6.1.

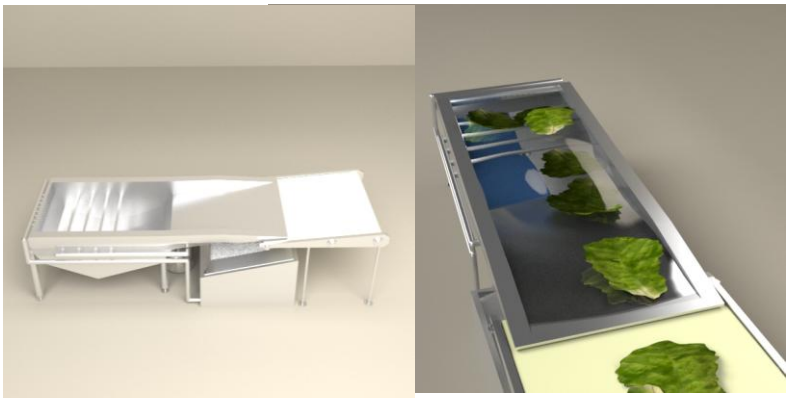

Figure 6.2. Schematic of the pilot-scale washing station for fresh produce.

(3) Modulation of nanopores: By controlling the pore diameter, interpore distance, and the pore depth, the array of nanopores on the anodized metal substrates can be further modified to enable other novel nanoengineered surfaces. For example, the nanopores can be used to hold a lubricating liquid in SLIPS or filled with an anti-microbial agent to achieve an extra biofouling resistance level.

APPENDIX A: PUBLICATIONS

Peer-reviewed Articles

Rungraeng, N., Cho, Y.C., Yoon, S.H., Jun, S. 2012. Polytetrafluoroethylene-based carbon nanotube coating for milk fouling reduction in plate heat exchanger. *Journal of Food Engineering*, 111, 218-224.

Chee, G., Rungraeng, N., Han, J.H., Jun, S. 2014. Electrochemical impedance spectroscopy as an alternative to determine dielectric constant of potatoes at various moisture contents. Journal of Food Science, 79, E195-E201.

Choi, W., Jun, S., Nguyen, L.T., Rungraeng, N., Yi, H., Balasubramanian, S., Puri, V.M., Lee, J. 2012. 3D Milk fouling modeling of plate heat exchangers with different surface finishes using computational fluid dynamics codes. *Journal of Food Process Engineering*, doi: 10.1111/j.1745-4530.2012.00684.x

Yoon, S.H., Rungraeng, N., Song, W., Jun, S. 2014. Superhydrophobic and superhydrophilic nanocomposite coatings for preventing bacterial adhesion on food contact surface. *Journal of Food Engineering*. 131, 135-141.

Hizal, F., Rungraeng, N., Choi, C.H., & Jun, S. (2014). Bacterial adhesion on nanoporous and nanopillared alumina surfaces. *IEEE-NEMS 2014*, HI, USA.

Book Chapter

Rungraeng, N., & Jun, S. 2013. Carbon nanotubes-polytetrafluoroethylene nanocomposite coatings. Chapter 3, In Mittal, V. (Ed.). Polymer Nanocomposite Coating. CRC Press. Boca Raton, FL.

REFFERENCES

Advincula, M.C., Rahemtulla, F.G., Advincula, R.C., Ada, E.T., Lemons, J.E., & Bellis, S.L. (2006). Osteoblast adhesion and matrix mineralization on sol-gel-derived titanium oxide. *Biomaerials*, 27, 2201-2212.

Anand, S., Paxton, A.T., Dhiman, R., Smith, J.D., & Varanasi, K.K. (2012). Enhanced condensation on lubricant-impregnated nanotextured surfaces. *ACS Nano*, 10122-10129.

Balasubramanian, S., & Puri, V. M. (2009a). Reduction of milk fouling in a plate heat exchnager system using food-grade surface coating. *Transaction of the ASABE*, 52, 1603−1610.

Balasubramanian, S., & Puri, V. M. (2009b). Thermal energy savings in pilot-scale plate heat exchanger system during product processing using modified surfaces. *Journal of Food Engineering*, *91,* 608–611.

Bansal, B., & Chen, X. D. (2006). A critical review of milk fouling in heat exchangers. *Comprehensive Reviews in Food Science and Food Safety*, *5*, 27–33.

Bayoudh, S., Othmane, A., Mora, L., & Ouada, H.B. (2009). Assessing bacterial adhesion using DLVO and XDLVO theories and the jet impingement technique. *Colloids and Surfaces B: Biointerfaces*, 73, 1−9.

Berger, C.N., Sodha, S.V., Shaw, R.K., Griffin, P.M., Pink, D., Hand, P., & Frankel, G. (2010). Fresh fruit and vegetables as vehicles for the transmission of human pathogens. *Environmental microbiology*, 9, 2385-2397.

Bermúdez-Aguirre, D., Wemlinger, E., Pedrow, P., Barbosa- Cánovas, G., & Garcia-Perez, M. (2013). Effect of atmospheric pressure cold plasma (APCP) on the inactivation of *Escherichia coli* in fresh produce. *Food Control*, 34, 149-157.

Beuf, M., Rizzo, G., Leuliet, J.C., Müller-Steinhagen, H., Yiantsios, S., Karabelas, A. & Benezech, T. (2003). Fouling and cleaning of modied stainless steel plate heat exchangers processing milk products. In *Proceedings of Heat Exchanger Fouling and Cleaning: Fundamentals and Applications.* New Mexico, USA.

Boinovich, L.B., Emelyanenko, A.M., Ivanov, V.K., Pashinin, A.S. (2013). Durable icephobic coating for stainless steel. *ACS Applied Materials & Interfaces*, 5, 2549-2554.

Bormashenko, E., Pogreb, R., Whyman, G., & Erlich, M. (2007). Cassie-Wenzel wetting transition in vibrating drops deposited on rough surfaces: Is the dynamic Cassie-Wenzel transition a 2D or 1D affair? Langmuir, 23, 6501-6503.

Burris, D. L., Bosel, B., Bourne, G. R., & Sawyer, W.G. (2007). Polymeric nanocomposites for tribological applications. *Macromolecular Materials and Engineering*, *292*, 387–402.

Burton, E., Yakandawala, N., LoVetri, K. (2007). A microplate spectrofluorometric assay for bacterial biofilms. J Ind Microbiol Biotechnol, 34, 1-4.

Busscher, H.J., & van der Mei, H.C. (2006). Microbial adhesion in flow displacement systems. *Clin. Microbiol. Rev.*, 19, 127-141.

Busscher, H.J., & Weerkamp, A.H. (1987). Specifiec and non-specific interactions in bacterial adhesion to solid substrata. *FEMS Microbiology*. 46, 165-173.

Casimiro, T., Shariati, A., Peters, C.J., da Ponte, M.N., Aguiar-Ricardo, A. (2005). Phase behavior studies of perfluoropolyether in high-pressure carbon dioxide. *Fluid Phase Equilibr*, 228-229, 367-371.

Cassie, A.B.D., & Baxter, S. (1944). Wettability of porous surfaces. *Trans Faraday Soc*. 40, 546-551.

Chamielewski, R. A. N., & Frank, J.F. (2003). Biofilm formation and control in food processing facilities. *Compr Rev Food Sci F*. 2(1), 22-32.

Characklis, W.G., & Marshall, K.C. (1990). *Biofilms*. John Wiley, New York, USA.

Chen, W. X., Li, F., Han, G., Xia, J. B., Wang, L. Y., Tu, J. P., & Xu, Z. D. (2003). Tribological behavior of carbon-nanotube-filled PTFE composites. *Tribology Letters, 15,* 275–278.

Chiang, C. K., & Lu, Y. W. (2011). Evaporation phase change processes of water/methanol mixtures on superhydrophobic nanostructured surfaces. *Journal of Micromechanics and Microengineering, 21,* DOI: 10.1088/0960-1317/21/7/075003.

Choi, W., Jun, S., Nguyen, L.T., Rungraeng, N., Yi, H., Balasubramanian, S., Puri, V.M., & Lee, J. (2012). 3-D milk fouling modeling of plate heat exchangers with different surface finishes using computational fluid dynamics codes. *J. Food Process Eng*, 36, 439-779.

Criado, M.T., Suarez, B., Ferreiros, & C.M. (1994). The Importance of bacterial adhesion in the dairy industry. *Food Technol* 48, 123-126

Crick, C.R., Ismail, S., Pratten, J., & Parkin, I.P. (2011). An investigation into bacterial attachment to an elastomeric superhydrophobic surface prepared via aerosol assisted deposition. *Thin Solid Films*, 519, 3722-3727.

de Jong, P. (1997). Impact and control of fouling in milk processing. *Trend in Food Science & Technology*, 8, 401−405

de Jong, P., te Giffel, M. C., Straatsma, H., & Vissers, M. M. (2002). Reduction of fouling and contamination by predictive kinetic models. *International Dairy Journal*, *12,* 285–293.

De Oliveira, R.R.L., Albuquerque, D.A.C., Cruz, T.G.S., Yamaji, F.M., & Leite, F.L. (2012). Measurement of the nanoscale roughness by atomic force microscopy: basic principles and applications, atomic force microscopy - Imaging, measuring and manipulating surfaces at the atomic scale, Bellitto, V. (Ed.), ISBN: 978-953-51-0414-8, InTech, DOI: 10.5772/37583.

Díez-García, M., Capita, R., & Alonso-Calleja, C. (2012). Influence of serotype on the growth kinetics and the ability to form biofilms of *Salmonella* isolates from poultry. *Food Microbiol*, 31, 173-180.

Dong, X., Chen, J., Ma, Y., Wang, J., Chan-Park, M.B., Liu, X., Wawng, L., Huang, W., & Chen, P. (2012). Superhydrophobic and superoleophilic hybrid foam of graphene and carbon nanotube for selective removal of oils or organics solvents from the surface of water. *ChemComm*, 48, 10660-10662.

Dror-Ehre, A., Adin, A., Markovich, G., Mamane, H. (2010). Control of biofilm formation in water using molecular capped silver nanoparticles. *Water Research*, 44, 2601-2609.

Epstein, A.K., Wong, T.S., Belisle, R.A., Boggs, E.M., & Aizenberg, J. (2012). Liquid-infused structured surfaces with exceptional anti-biofouling performance. *PNAS*, 109, 13182-13187.

Erbil, Y. (2006). *Surface chemistry of solid and liquid interfaces*. Blackwell Publishing Inc., MA, USA.

Feng, Y., Zhou, G., Wang, G., Qu, M., & Yu, Z. (2003). Removal of some impurities from carbon nanotubes. *Chemical Physics Letters, 375,* 645–648.

Flemming, H.C., & Ridgway, H. (2008). Biofilms control: conventional and alternative approaches. *Springer Berkin Heidelberg*, 1-15.

Flemming, H.C., & Wingender, J. (2010). The biofilm matrix. *Nature Rev. Microbiol.*, 8, 623-633.

Flint S.H.H., Brooks J.D.D., & Bremer P.J.J.(2000). Properties of the stainless steel substrate, influencing the adhesion of thermo-resistant streptococci. *Journal of Food Engineering*, 43, 235-242.

Gibson, H., Taylor, J.H., Hall, K.E., & Holah, J.T. (1999). Effectiveness of cleaning techniques used in the food industry in terms of the removal of bacterial biofilms. J Appl Microbiol, 87, 41-48.

Gómez-López, V.M., Lannoo, A.S., Gil, M.I., & Allende, A. (2014). Minimum free chlorine residual level required for the inactivation of *Escherichia coli* O157:H7 and trihalomethane generation during dynamic washing of fresh-cut spinach. *Food Control*, 42, 132-138.

Girifalco, L.A., & Good, R.J. (1957). A theory for the estimation of surface and interfacial energies. I. Derivation and application to interfacial tension. *The Journal of Physical Chemistry*, 61, 904-909.

Hall-Stoodley, L., Costerton, J.W., & Stoodley, P. (2004). Bacerterial biofilms: From the natural environment to infectious diseases. *Nat Rev Microbiol.*, 2, 95-108.

Hizal, F., Rungraeng, N., Choi, C.H., & Jun, S. (2014). Bacterial adhesion on nanoporous and nanopillared alumina surfaces. *IEEE-NEMS 2014*, HI, USA.

Horcas, I.,Fernández, R., Gómez-Rodríguez, J.M.,Colchero, J., Gómez-Herrero, J., & Baro, A.M. (2007). WSxM: A software for scanning probe microscopy and a tool for nanotechnology. *Rev. Sci. Instrum.*, 78, 013705.

Hsu, L., Fang, J., Borca-Tasciuc, D.A., Worobo, R.W., Moraru, C.I., (2013). Effect of micro-and nanoscale topography on the adhesion of bacterial cells to solid surfaces. *Applied and Environmental Microbiology*, 79, 2703.

Huang, L., Lau, S. P., Yang, H. Y., Leong, E. S. P., Yu, S. F., & Prawer, S. (2005). Stable superhydrophobic surface via carbon nanotubes coated with a ZnO thin film. *Journal of Physical Chemistry B, 109*, 7746–7748.

Izano, E.A., Amarante, M.A., Kher, W.B., & Kaplan, J.B. (2008). Differential roles of poly-N-acetylglucosamine surface polysaccharide and extracellular DNA in *Staphylococcus aureus* and *Staphylococcus epidermidis* biofilms. *Appl Environ Microbiol*, 74, 470-476.

Jeong, C., & Choi, C.H. (2014). Single-step direct fabrication of pillar-on-pore hybrid nanostructures in anodizing aluminum for superior superhydrophobic efficiency. *ACS Applied Materials & Interfaces*, 4, 842-848.

Jun S, Puri VM. (2005a). 3D Fouling Model of Plate Heat Exchangers using Computational Fluid Dynamics. *International Journal of Dairy Technology*. 58, 214-224.

Jun S, Puri VM. (2005b). Fouling Model for Heat Exchangers in Food Processing: A Review. *Journal of Food Process Engineering*. 28, 1-34.

Jun S, Puri VM. (2006a). A 2D dynamic model for fouling performance of plate heat exchanger. *J. Food Eng*. 75, 364-374.

Jun S, Puri, VM. (2006b). Potential Milk Fouling Area in Plate Heat Exchangers. *Food Engineering Progress*. 10, 6-13.

Jessensky, O., Müller, F., & Gösele, U. (1998). Self-organized formation of hexagonal pore arrays in anodic alumina. *Applied Physics Letters*, 72, 1173-1175.

Kapuscinski, J. (1995). DAPI: a DNA-specific fluorescent probe. *Biotech Histochem*, 70, 220-233.

Kim, P., Wong, T.S., Alvarenga, J., Kreder, M.J., Adorno-Martinez, W.E., & Aizenberg, J. (2012). Liquid-infused nanostructured surfaces with extreme anti-ice and anti-frost performance. *ACS Nano*, 6, 6569-6577.

Klein, R. J., Biesheuvel, R. M., Yu, B. C., Meinhart, C. D., & Lange, F. F. (2003). Producing super-hydrophobic surfaces with nano-silica spheres. *International Journal of Materials Research*, 94, 377–380.

Kobayashi, M., Terayama, Y., Yamaguchi, H., Terada, M., Murakami, D., Ishihara, K., & Takahara, A. (2012). Wettability and antifouling behavior on the surfaces of superhydrophilic polymer brushes. *Langmuir*, 28, 7212-7222.

Kociolek, M.G. (2009). Quorum-sensing inhibitors and biofilms. *Anti-Infective Agents*, 8, 315-326.

Kumar, C.G., & Anand, S.K. (1998). Significance of microbial biofilms in food industry: a review. *International Journal of Food Microbiology*. 42, 9-27.

Kumar, M. & Ando, Y. (2010). Chemical vapor deposition of carbon nanotubes: a review on growth mechanism and mass production. *Journal of Nanoscience and Nanotechnology*, 10, 3739–3758.

Kwok, D. Y., & Neumann, A. W. (1999). Contact angle measurement and contact angle interpretation. *Advances in Colloid and Interface Science*, 81, 167–249.

Lahelin, M., Annala, M., Nykänen, A., Ruokolainen, J., & Seppälä, J. (2011). *In situ* polymerized nanocomposites: Polystyrene/CNT and poly(methyl methacrylate)/CNT composites. *Composites Science and Technology,* 71, 900–907.

Lai, Y., Tang, Y., Gong, J., Gong, D., Chi, L., Lin, C., & Chen, Z. (2012). Transparent superhydrophobic/superhydrophilic TiO_2-based coatings for self-cleaning and anti-fogging. J. *Matter. Chem.*, 22, 7420-7426.

Lapidot, A., Romling, U., & Yaron, S. (2006). Biofilm formation and survival of *Salmonella* Typhimurium on parsley. *International Journal of Food Microbiology*, 109, 229-233.

Latifi, A., Imani, M., Khorasani, M.T., & Joupari, M.D. (2013). Electrochemical and chemical methods for improving surface characteristics of 316L stainless steel for biomedical applications. *Surface and Coatings Technology*, 221, 1-12.

Lau, K. K. S., Bico, J., Teo, K. B. K., Chhowalla, M., Amaratunga, G. A. J., Milne, W. I., McKinley, G. H., & Gleason, K. K. (2003). Superhydrophobic carbon nanotube forests. *Nano Letters*, *3*, 1701–1705.

Lee, E.S. (2000). Machining charateristics of the electropolishing of stainless steel (STS316L). *The International Journal of Advanced Manufacturing Technology, 16*, 591-599.

Leng, Y., Cummings, P.T. (2006). Shear dynamics of hydration layers. *Journal of Chemical Physics*. 125, 104701.

Li, B., & Logan, B.E. (2004). Bacterial adhesion to glass and metal-oxide surfaces. *Colloids Surf., B.*, 36, 81-90.

Li, G., Wang, H., Zheng, H., & Bai, R. (2010). A facile approach for the fabrication of highly stable superhydrophobic cotton fabric with multi-walled carbon nanotubes-azide polymer composites. *Langmuir, 26,* 7529–7534.

Liu, N.T., Lefcourt, A.M., Nou, X., Shelton, D.R., Zhang, G., & Lo, Y.M.(2013) Native microflora in fresh-cut produce processing plants and their potentials for biofilm formation. *Journal of Food Protection*, 5, 744-918.

Liu, N.T., Nou, X., Lefcourt, A.M., Shelton, D.R., & Lo, Y.M. (2014). Dual-species biofilm formation by *Escherichia coli* O157:H7 and environmental bacteria isolated from fresh-cut processing facilities. *International Journal of Food Microbiology*, 171, 15-20.

Lu, L., & Jun, S. (2012). Evaluation of a microwire sensor functionalized to detect *Escherichia coli* bacterial cells. *Biosens. Bioelectron.*, 36, 257-261.

Luo, Z., Zhanga, Z., Wanga, W., Liua, W., & Xuea, Q. (2010). Various curing conditions for controlling PTFE micro/nano-fiber texture of a bionic superhydrophobic coating surface. *Materials Chemistry and Physics, 119,* 40–47.

Ma, W., Higaki, Y., Otsuka, H., & Takahara, A. (2013). Perfluoropolyether-infused nano-texture: a versatile approach to omniphobic coatings with low hysteresis and high transparency. *Chemical Communications*, 49, 597-599.

Ma, Y., Chen, M., Jones, J.E., Ritts, A.C., Yu, Q., & Sun, H. (2012). Inhibition of *Staphylococcus epidermidis* biofilm by trimethylsilane plasma coating. *Antimicrob. Agents. Chemother.*, 56, 5923-5937.

Mamontov, E., Vlcek, L., Wesolowski D.J., Cummings, P.T., Wang, W., Anovitz, L.M., Rosenqvist, J., Brown, C.M., & Sakai, V.G. (2007). Dynamics and structure of hydration

water on rutile and cassiterite nanopowders studied by quasielastic neutron scattering and molecular dynamics simulations. *Journal of Physical Chemistry C*. 111, 4328-4341.

Marshall, K.C., Stout, R., & Mitchell, R. (1971). Mechanisms of the initial events in the sorption of marine bacteria to surfaces. *Journal of General Microbiology*. 68, 337-348.

Men, X., Zhang, Z., Yang, J., Wang, K., & Jiang, W. (2010). Superhydrophobic/superhydrophilic surfaces from a carbon nanotube based composite coating. *Applied Physics A, 98,* 275–280.

Meyyappan, M., Delzeit, L., Cassell, A., & Hash, D. (2003). Carbon nanotube growth by PECVD: A review. *Plasma Sources Science and Technology, 12,* 205–216.

Mitik-Dineva N., Wang J., Stoddart P.R., Crawford R.J., & Ivanova E.P. (2008). Nano-structured surfaces control bacterial attachment, *Int. Conf. Nanosci. Nanotechnol. (ICONN) 2008*, Melbourne, Australia.

Moisala, A., Li, Q., Kinloch, I.A., & Windle, A.H. (2006). Thermal and electrical conductivity of single- and multi-walled carbon nanotube-epoxy composites. *Composites Science and technology,* 66, 1285–1288.

Montville, T.J., & Matthews, K.R. (2008). *Food microbiology: An introduction* (2nd ed., pp. 123-140) ASM Press: Washington, DC.

Murray, B. S., & Deshaires, C. (2000). Monitoring protein fouling of metal surfaces via a quartz crystal microbalance. *Journal of Colloid Interface Science*, 227, 32–41.

Nazneen, F., Galvin, P., Arrigan, D.W.M., Thompson, M., Benvenuto, P., & Herzog, G. (2012). Electropolishing of medical-grade stainless steel in preparation for surface nano-texturing. *Journal of Solid State Electrochemistry,* 16, 1389-1397.

Nečas, D., & Klapetek, P. (2012). Gwyddion: an open-source software for SPM data analysis, *Cent. Eur. J. Phys*. 10, 181-188

Neumann, A.W., David, R., & Zuo, Y.Y. (2010). Applied Surface Thermodynamics, 2nd edit, CRC Press, Boca Raton, FL.

Nishimoto, S., & Bhushan, B. (2013). Bioinspired self-cleaning surfaces with superhydrophobicity, superoleophobicity, and superhydrophilicity. *RSC Adv.*, 3, 671-690.

Noguera, D.R., Pizarro, G., Stahl, D.A., & Rittmann, B.E. (1999). Simulation of multispecies biofilm development in three dimensions. *Water Science and Technology*. 39, 123-130.

Nosonovsky, M., & Bhushan, B. (2007). Biomimetric superhydrophobic surfaces: Multiscale approach. Nano Lett., 7, 2633-2637.

Nosonovsky, M., & Bhushan, B. (2009). Superhydrophobic surfaces and emerging applications: Non-adhesion, energy, green engineering. *Current Opinion in Colloid & Interface Science,* 14, 270-280.

Olaimat, A.N., & Holley, R.A. (2012). Factors influencing the microbial safety of fresh produce: a review. *Food Microbiology*, 32, 1-9.

Ozden, H.O., & Puri, V.M. (2010). Computational analysis of fouling by low energy surfaces. *Journal of Food Engineering.* 99, 250-256.

Pagani, G., Green, M.J., Poulin, P., & Pasquali, M. (2012). Competing mechanisms and scaling laws for carbon nanotube scission by ultrasonication. *Proceedings of the National Academy of Sciences, 109,* 11599–11604.

Patel, P., Choi, C.K., & Meng, D.D. (2010). Superhydrophilic surfaces for antifogging and antifouling microfluidic devices. *Journal of the Association for Laboratory Automation*, 2, 114-119.

Peeters, E., Nelis, H.J., & Coenye, T. (2008). Comparison of multiple methods for quantification of microbial biofilms grown in microtiter plates. *J Microbiol Methods*, 72, 157-165.

Poinern, G.E.J., Ali, N., & Fawcett, D. (2011). Progress in nano-engineered anodic aluminum oxide membrane development. *Materials*, 4, 487-526.

Rosmaninho, R., & Melo, L. F. (2006). Calcium phosphate deposition from simulated milk ultrafiltrate on different stainless steel-based surfaces. *International Dairy Journal*, 16, 81-87.

Rosmaninho, R., Santos, O., Nylander, T., Paulsson, M., Beuf, M., Benezech, T., Yiantsios, S., Andritsos, N., Karabelas, A., Rizzo, G., Müller-Steinhagen, H., & Melo, L.F. (2007). Modified stainless steel surfaces targeted to reduce fouling–evaluation of fouling by milk components. *Journal of Food Engineering, 80,* 1176–1187.

Sandu, C., & Singh, R.K. (1991). Energy increase in operation and cleaning due to heat exchanger fouling in milk pasteurization. *Food Technology*. 32, 84-91.

Santos, O., Nylander, T., Rosmaninho, R., Rizzo, G., Yiantsios, S., Andritsos, N., Karabelas, A., Müller-Steinhagen, H., Melo, L., Boulangé-Petermann, L., Gabet, C., Braem, A., Trägårdh, C., & Paulsson, M. (2004). Modified stainless steel surfaces targeted to reduce fouling–surface characterization. *Journal of Food Engineering*, *64,* 63–79.

Sawyer, W. G., Freudenberg, K. D., Bhimaraj, P., & Schadler, L. S. (2003). A study on the friction and wear behavior of PTFE filled with alumina nanoparticles. *Wear, 254,* 573–580.

Scheuerman T., Camper A., & Hamilton M. (1998). Effects of substratum topography on bacterial adhesion. *Journal of Colloid Interface Science,* 208, 23-33

Shen, G.X., Chen, Y.C., & Lin, C.J. (2005). Corrosion protection of 316 L stainless steel by a TiO_2 nanoparticle coating prepared by sol-gel method. *Thin Solid Films.*, 489, 130-136.

Show, Y., & Takahashi, K. (2009). Stainless steel bipolar plate coated with carbon nanotube (CNT)/polytetrafluoroethylene (PTFE) composite film for proton exchange membrane fuel cell (PEMFC). *Journal of Power Sources, 190,* 322–325.

Song, S., Jing, L., Li, S., Fu, H., & Luan, Y. (2008). Superhydrophilic anatase TiO_2 film with the micro- and nano-scale hierarchical surface structure. *Mater Let.*, 62, 3503-3505.

Srey, S., Jahid, I.K., & Ha, S.D. (2013). Biofilm formation in food industries: A food safety concern. *Food Control,* 31, 572-585.

Su, X.J., Zhao, Q., Wang, S., & Bendavid, A. (2010). Modification of diamond-like carbon coatings with fluorine to reduce biofouling adhesion. *Surf. Coat. Tech.,* 204, 2454-2458.

Takhistov, P. (2004). Electrochemical synthesis and impedance characterization of nano-patterned biosensor substrate. *Biosensors and Bioelectronics*, 19, 1445-1456.

Tavana, H., & Neumann, A. W. (2007). Recent progress in the determination of solid surface tensions from contact angles. *Advances in Colloid and Interface Science, 132,* 1-32.

Tiraferri, A., Kang, Y., Giannelis, E.P., Elimelech, M., (2012). Superhydrophilic thin-filmcomposite forward osmosis membranes for organic fouling control: foulingbehavior and antifouling mechanisms. *Environ. Sci. Technol. Lett.* 46, 11135-11144.

Verran J., Rowe D.L., & Boyd R.D. (2001). The effect of nanometer dimension topographical features on the hygienic status of stainless steel. *Journal of Food Protection*.64, 1183-1187.

Visser, J. (1997). in Fouling of Heat Treatment Equipment, Bulletin of the IDF, 328, Visser, H.J. (ed.) IDF, Brussels.

Visser, J., & Jeurnink, Th.J.M., (1997). Fouling of heat exchangers in the dairy industry. *Experimental Thermal and Fluid Science*, 14, 407−424.

Wang, C.F., Chen, W.Y., Cheng, H.Z., & Fu, S.L. (2010). Pressure-proof superhydrophobic films from flexible carbon nanotube/polymer coatings. *J. Phys. Chem.*, 114, 15607-15611.

Warriner, K., Huber, A., Namvar, A., Fan, W., & Dunfield, K. (2009). Recent advances in the microbial safety of fresh fruits and vegetables. *Adv. Food Nutr. Res*. 57, 155-208.

Wong, T.S., Kang, S.H., Tang, S.K.Y., Smythe, E.J., Hatton, B.D., Grinthal, A., & Aizenberg, J. (2011). Bioinspired self-repairing slippery surfaces with pressure-stable omniphobicity. *Nature*, 477, 443-447.

Woodling S.E., Moraru C.I. (2005). Influence of surface topography on the effectiveness of pulsed light treatment for the inactivation of *Listeria innocua* on stainless-steel surfaces. *Journal of Food Science*.70, m345-m351.

Wu, J., Xia, J., Lei, W., & Wang, B. (2011). A one-step method to fabricate lotus leaves-like ZnO film. *Mater. Lett*., 65, 477-479.

Wu, Z.Y., Li, C., Liang, H.W., Zhang, Y.N., Wang, X., Chen, J.F., & Yu, S.H. (2014). Carbon nanofiber aerogels for emergent cleanup of oil spillage and chemical leakage under harsh conditions. *Sci Rep*, 4, 4079.

Xiao, L., Li, J., Mieszkin, S., Di Fino, A., Clare, A.S., Callow, M.E., Callow, J.A., Grunze, M., Rosenhahn, A., Levkin, P.A. (2013). Slippery liquid-infused porous surfaces showing marine antibiofouling properties. *ACS Applied Materials & Interfaces*, 5, 10074-10080.

Xie, X. L., Mai, Y. W., & Zhou, X. P. (2005). Dispersion and alignment of carbon nanotubes in polymer matrix: A review. *Material Science and Engineering, 49,* 89-112.

Yang, H., & Wang, Y. (2008). Application of atomic force microscopy on rapid determination of microorganisms for food safety. *Journal of Food Science*, 73, N44-N50.

Yao, X., Hu, Y., Grinthal, A., Wong, T.S., Mahadevan, L., & Aizenberg, J. (2013). Adaptive fluid-infused porous films with tunable transparency and wettability. *Nature Materials*, 12, 529-534.

Young, T. (1805). An essay on the cohesion of fluids. *Philosophical Transactions of the Royal Society London, 95,* 65-87.

Zhao, Q., Liu, Y., Wang, C., Wang, S., Peng, N., Jeynes, C. (2008). Reduction of bacterial adhesion on ion-implanted stainless steel surfaces. *Medical Engineering & Physics*. 30, 341-349.

Zhong, G., Warner, J.H., Fouquet, M., Robertson, A.W., Chen, B., & Robertson, J. (2012). Growth of ultrahigh density single walled carbon nanotube forests by improved catalyst design. *ACS Nano*, 6, 2893−2903.